Université de Montréal

The Design of Polymeric Microneedles for the Delivery of Sensors for Real-Time Physiological Monitoring

presented by:

Samuel Babity

Analyse et Formulation des Médicaments

Faculté de Pharmacie

Mémoire présentée à la Faculté de Pharmacie
en vue de l'obtention du grade de Maîtrise en Sciences Pharmaceutiques

Option Technologie Pharmaceutique

Août 2019

Université de Montréal

Axe Analyse et Formulation du Médicament, Faculté de Pharmacie

Ce mémoire intitulé

The Design of Polymeric Microneedles for the Delivery of Sensors for Real-Time Physiological Monitoring

Présenté par

Samuel Babity

A été évalué par un jury composé des personnes suivantes

Xavier Banquy
Président-rapporteur

Davide Brambilla
Directeur de recherche

Gaétan Mayer
Membre du jury

Résumé et Contexte

Ce mémoire de maîtrise porte sur le développement d'un système d'administration de microaiguilles pour livrer des sondes et des capteurs fluorescents dans le contexte du diagnostic et de la surveillance des soins de santé. Bien que parfois négligés en faveur des soins de santé axés sur le traitement, le diagnostic précoce de la maladie et la surveillance préventive des paramètres biologiques peuvent considérablement améliorer les résultats des soins de santé et joueront probablement un rôle plus important dans les années à venir. Cependant, il reste des obstacles importants à cette approche, à savoir le caractère relativement invasif et perturbateur des analyses biologiques. La nécessité de se rendre dans une clinique et de subir un prélèvement de sang (ou de liquide biologique) invasif présente des inconvénients importants par rapport aux traitements classiques, qui consistent souvent de médicaments pouvant être pris à domicile sans douleur.

Une solution à ces problèmes réside dans la mise au point de systèmes minimalement invasifs de diagnostic et de suivi médical, idéalement ceux qui peuvent être utilisés à domicile sans nécessiter de personnel qualifié. À cet égard, les microaiguilles sont une technologie au potentiel énorme, car leur petite taille les rend peu invasives et pratiquement indolores, et leur nature simple à usage unique permet potentiellement une administration à domicile par le patient. Particulièrement prometteuses pour les applications de diagnostic et de surveillance sont les microaiguilles en polymère soluble; fabriquées à partir de polymères synthétiques ou biologiques injectables, ces microaiguilles sont solubilisées après la perforation de la peau, libérant ainsi les composés qu'elles contiennent. Bien que prévu initialement pour la livraison d'agents thérapeutiques, en utilisant ces microaiguilles pour livrer des molécules fluorescentes spécifiquement conçues, il est possible de créer un tatouage médical de diagnostic affichant un signal fluorescent précis. En associant cette technologie à un détecteur de fluorescence portable, la surveillance en temps réel d'un large éventail de paramètres biologiques pourrait devenir accessible en dehors du contexte clinique.

Afin de fournir un contexte pour le développement de cette technologie, cette mémoire commence par une revue des principes et des avancées majeures récentes dans le domaine des applications diagnostiques des microaiguilles (**Chapitre 1**). Par la suite, un tatouage par microaiguille est présenté sous la forme d'un capteur de ROS délivré sur la peau, avec des implications diagnostiques pour le vieillissement et la carcinogenèse de la peau liés aux UV, ainsi que pour des affections inflammatoires telles que le psoriasis, comme validation de concept (**Chapitre 2**). En outre, un autre tatouage par microaiguille est introduit, consistant d'un capteur spécialement adapté ciblant le système lymphatique, permettant la quantification en temps réel du drainage lymphatique, avec des implications pour la détection précoce de plusieurs affections, notamment le lymphœdème (**Chapitre 3**).

Mots-clés: Microaiguilles, diagnostic, ROS, lymphatique, surveillance.

Summary and Context

This Master's thesis concerns the development of a microneedle (MN) delivery system for fluorescent dyes and sensors in the context of diagnostics and healthcare monitoring. While sometimes overlooked in favor of treatment-focused healthcare, early disease diagnosis and preventative monitoring of biological parameters can meaningfully improve healthcare outcomes and will likely play a greater role in coming years. However, significant obstacles to this approach remain, namely the relatively invasive and disruptive nature of biological analyses. The need to travel to a clinic and undergo invasive blood (or biological fluid) sampling presents significant inconveniences relative to common treatments, often consisting of medications that can be taken painlessly at home.

A solution to these problems lies in the development of minimally invasive systems for diagnostics and healthcare monitoring, ideally ones which can be used at home without the need for trained personnel. In this regard, MNs are a technology with tremendous potential, as their small size renders them minimally invasive and virtually painless, and their simple, single-use nature potentially allows for at-home administration by the patient. Showing particular promise for diagnostic and monitoring applications are dissolving polymeric MNs; made from injectable synthetic or biological polymers, these MNs are solubilized after breaching the skin, releasing any compound contained within. Though initially envisioned for the delivery of therapeutic agents, by using these MNs to deliver specifically designed fluorescent molecules, it is possible to create a diagnostic medical *tattoo* displaying a precise fluorescent signal. By pairing this technology with a portable fluorescence detector, real-time monitoring of a wide range of biological parameters could become accessible outside of a clinical setting.

To provide context for the development of this technology, this thesis begins with a review of the principles and major recent advances in the field of diagnostic applications of MNs (**Chapter 1**). Subsequently, a proof-of-concept MN tattoo is introduced in the form of a ROS-sensor delivered to the skin, with diagnostic implications for UV-related skin aging and carcinogenesis, as well as inflammatory conditions such as psoriasis (**Chapter 2**). Further, another MN tattoo is introduced, consisting of a specifically tailored sensor targeting the lymphatic system, allowing the real-time quantification of lymphatic drainage, with implications in the early detection of several conditions, including lymphedema (**Chapter 3**).

Keywords: Microneedles, diagnostics, ROS, lymphatics, monitoring.

Abstract

Microneedles (MNs) are a technology drawing increasing interest for diagnostic applications. Over the past two decades, many MN-based diagnostic systems have been proposed and developed, with some approaching clinical translation in the near future. A particularly novel and interesting diagnostic application of MNs consists of using dissolving polymeric MNs to deliver diagnostic agents directly to the skin, acting as a sort of MN tattoo. By delivering a modified oxidation-sensitive fluorescent dye, these MNs could be used to create a ROS-sensitive tattoo in the skin, relevant for the diagnosis and monitoring of several skin conditions. Alternatively, by delivering a specially designed inert NIR-fluorescent contrast dye, a MN tattoo could be used to selectively monitor lymphatic drainage, particularly important in the context of breast cancer-related lymphedema. Together, these applications suggest that the use of dissolving polymeric MNs for the delivery of fluorescent sensors displays promise for real-time physiological monitoring and warrants further investigation.

Table of Contents

List of Figures

Chapter 1

Chapter 2

Chapter 3

List of Tables

Chapter 1

List of Abbreviations

ACN – Acetonitrile

DCM – Dichloromethane

DIPEA – Diisoprpylethylamine

DMSO – Dimethyl sulfoxide

DNA – Deoxyribonucleic acid

DRIE – Deep reactive ion etching

DSC – Disuccinimydal carbonate

ECG – Electrocardiogram

EDC – 1-Ethyl-3-(3-dimethylaminopropyl)carbodiimide

EEG – Electroencephalogram

ELISA – Enzyme-linked immunosorbent assay

EMG – Electromyography

EU – Endotoxin units

FDA – Food and drug administration

FITC – Fluorescein isothiocyanate

HIV – Human immunodeficiency virus

HPLC – High-performance liquid chromatography

IgG – Immunoglobin G

IL-1α – Interleukin 1-α

ISF – Interstitial fluid

LC-MS – Liquid chromatography-mass spectrometry

MeHA – Methacrylated hyaluronic acid

MeI – Iodomethane

MEMS – Micro-electro-mechanical systems

MN – Microneedle

MPA – Microprojection array

NHS – *N*-Hydroxysuccinimide

NIR – Near-infrared

NMR – Nuclear magnetic resonance

SLMW HA – Super-low molecular weight hyaluronic acid

PDMS – Polydimethylsiloxane

PEG – Poly(ethylene glycol)

PMMA – Poly(methyl methacrylate)

PMS – Polymer matrix solution

PtNP – Platinum nanoparticle

PVA – Poly(vinyl alcohol)

PVDF – Polyvinylidene fluoride

PVME/MA – Poly(methylvinylether-co-maleic anhydride)

PVP – Poly(*N*-vinylpyrrolidone)

ROS – Reactive oxygen species

SEM – Scanning electron microscopy

SPV – Skin potential variation

TB – Tuberculosis

TNF-α – Tumour necrosis factor α

ULMW HA – Ultra-low molecular weight hyaluronic acid

UV – Ultraviolet

Acknowledgements

Thanks to D. Brambilla for advice and guidance throughout the project.

Thanks to F. Couture and A. Polomska for help with *in vivo* tests.

Thanks to A. Melkoumov and R.M. Derbali for showing me around when I first arrived.

Thanks to M. Mailloux and Z. Benkhachan for helping out in the lab.

Thanks to M. Roohnikan, E. Laszlo, C. Penalosa, G. Sala, and P. Delbreil for discussions and making the office less empty.

Thanks to F. Bernard for all the mice.

Chapter 1

The concept of using MNs for diagnostic applications dates back nearly 20 years, to the design of single-MN prototypes for less painful blood sampling. Over the following decade, many examples of MNs were described, primarily consisting of hollow devices made of metal or silicon for the sampling and quantification of blood or dermal interstitial fluid (ISF). While these devices served to highlight the utility of MN-based diagnostics, their potential has been limited by complex and expensive manufacturing procedures, particularly given their single-use nature, and none have translated to commercial products. However, recent years have seen a growing interest in diagnostic MNs made from either swelling or soluble polymers for sampling from and delivery to the dermal ISF, owing to their simpler manufacturing processes, and the elimination of a need for complex built-in sensors. This has led to interest in potential clinical applications of such MNs, with the final section of this chapter providing an overview of preliminary clinical considerations related to the use of polymer MN devices.

Advances in the design of transdermal microneedles for diagnostic and monitoring applications

Samuel Babity[1], *Mahdi Roohnikan*[1], *Davide Brambilla*[1*]

[1]Faculté de Pharmacie, Université de Montréal, C.P. 6128, Succursale Centre-ville, Montréal, Québec H3C 3J7, Canada.

*Corresponding author: davide.brambilla@umontreal.ca

Published in *Small* (**2018**, 14 (49), 1803186)

1.1. Abstract

Due to their intrinsic advantages over classical hypodermic needles, microneedles have received much attention over the last two decades and will likely soon appear in clinics. Although the vast majority of research has been focused on designing microneedles for the painless delivery of drugs, their applications for diagnostic purposes have also provided promising results. In this manuscript we introduce and critically discuss the main advances in the field of microneedles for diagnostic and patient monitoring purposes.

Keywords: diagnostic, microneedles, monitoring, transdermal

1.2. Introduction

The skin is the largest and most easily accessible organ of the human body. It plays a crucial role in maintaining homeostasis, defending against invading microorganisms, and providing protection from environmental attacks such as heat, chemicals, and toxins. It accounts for 16 % of total body weight and is composed of three main layers; namely the epidermis, the dermis, and the hypodermis, with a variable total thickness depending on several factors such as body region, sex, and age.[1] The epidermis is further divided into sub-layers; the most external, the *stratum corneum*, has a thickness of 15 – 20 μm and confers upon the skin its protective barrier function.[1] This quality is mainly imparted by the layer's constituent cells, the corneocytes: skin cells that have undergone apoptosis through the physiological pathway of skin renewal. These cells are filled with keratin and embedded in an extracellular matrix mostly composed of ceramide, cholesterol, and other fatty acids.[2,3]

Underneath the *stratum corneum* is the region usually referred to as the "viable epidermis", a 50 – 100 μm layer of epidermal keratinocytes that serve to continuously renew the *stratum corneum*.[4] Deeper still is the dermis, which is 1 – 2 mm thick and contains rich blood and lymphatic capillary beds.[4] The hypodermis is below the dermis and is mainly composed of adipose tissue. Drugs and diagnostic agents typically need to penetrate through the epidermis to enter systemic circulation. However, the transport of molecules across the epidermis involves diffusion through a tortuous path which is highly restricted. While transdermal patches have been designed for the delivery of low molecular weight, lipophilic molecules, the number of compounds that can be delivered through these means remains limited.[4] Consequently, different chemical and physical strategies have been proposed to increase epidermal permeability.[5]

Among these, microneedles (MNs), miniaturized needles with lengths in the order of hundreds of μm, generally considered as the midpoint between hypodermic injections and transdermal patches, have gained remarkable attention.[6] Indeed, MNs circumvent the pain experienced during hypodermic injection by taking advantage of their size: sufficient to break the *stratum corneum*, but not long enough to reach the pain-sensing neurons found deeper in the tissue.[7] In contrast to transdermal patches, they allow the delivery of a considerably larger variety of molecules to the dermis.[8,9] This concept was first proposed in a patent by Gerstel and Place in 1976,[10] but it was not until late 90's that technological advances allowed the fabrication of MNs suitable for operation in the medical field.[11,12] Since then, the area has seen drastic growth, with research mainly focused on the improvement of MN design, and material refinement for the delivery of drugs and, notably, vaccines, which has led to promising results in nonhuman primates as well as in humans.[1,13,14]

Although much attention has been focused on their use for the delivery of therapeutics, there have also been great advances in MN technology for diagnostic and monitoring applications. Indeed, the skin carries far more health-related information than previously envisioned, and MNs possess key features to help access this information in a non-invasive way.[15] Several variants of MNs have been proposed for diagnostic and monitoring applications, and five main categories can be identified (**Figure 1.1.**): (*i*) MNs for non-invasive

interstitial fluid sampling, (*ii*) MNs for the selective capture of biomarkers, (*iii*) MNs for *in situ* analyte monitoring, (*iv*) MNs for dermal biopotential measurements and, (*v*) MNs for the delivery of diagnostic agents.

The main focus of this review will be to outline and discuss different methodologies that have been developed to take advantage of MNs for diagnostic and physiological monitoring applications. Through representative examples, the most relevant steps in MN design for this purpose will be described. Practical applications will be briefly reviewed, and the advantages/limitations of MNs relative to "traditional" methodologies will be considered. An overview of the challenges relating to clinical translation of the proposed technologies will conclude the article.

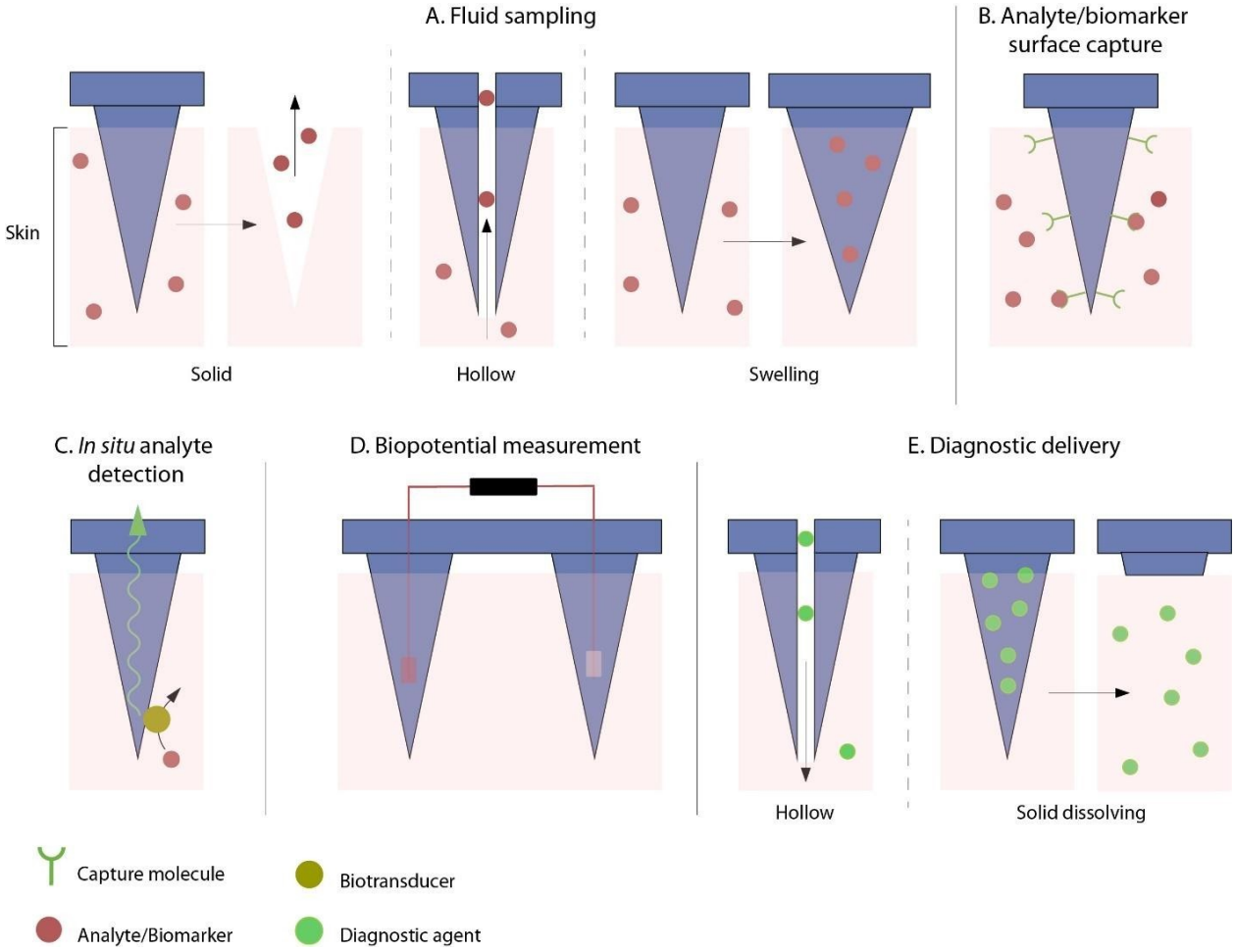

Figure 1.1. *Schematic repr*esentation of the 5 main classes of MNs described for diagnostic and monitoring *applications.*

1.3. MNs for non-invasive interstitial fluid sampling

Many health conditions can be monitored and diagnosed by sampling and measuring different substances found in bodily fluid. Examples include monitoring the concentration of glucose and cholesterol in relation to diabetes and cardiovascular conditions, respectively; as well as the identification of disease-specific biomarkers, such as the N-terminal prohormone of brain natriuretic peptide in relation to heart failure.[16] Traditionally, this information has been accessed by sampling blood using hypodermic needles or lancets,

allowing quantification with external meters. However, such methods have significant disadvantages, including patient discomfort, the need for relatively high sample volume, and the generation of sharp waste.[17] The observation that the population of small molecules, electrolytes, and proteins in the interstitial fluid (ISF) surrounding dermal cells strongly correlates with that of plasma, due to the hydrostatic and osmotic pressures that regulate the outflow of solutes from blood capillaries, has promoted the exploration of innovative strategies for its collection.[18–23] Indeed, the sampling of ISF, rather than blood, has the advantage of a drastic reduction in required penetration depth, from 400 – 900 μm to 50 – 150 μm, potentially resulting in less patient discomfort.[24] Thus, the use of MNs for ISF sampling by disrupting the *stratum corneum,* while avoiding the firing of pain-sensing neurons, is an elegant approach to non-invasively monitor many important health-related parameters. **Table 1.1.** reports the features of the proposed MN-based systems for sampling bodily fluids. Amidst the different information readily available from bodily fluids, glucose concentration arguably represents the most established marker for monitoring diabetes in patients. Thus, unsurprisingly, a great effort has been devoted to the design of MNs for non-invasive sampling and quantification of glucose from both blood and ISF.

1.3.1. Solid MNs

Perhaps the simplest method of ISF extraction consists of puncturing the *stratum corneum* with solid MNs and withdrawing the dermal ISF, *e.g.* with a cloth or vacuum chamber. In a first work, Wang *et al.* repeatedly applied glass MN arrays to the skin, to depths of 1.5 mm, and sampled dermal fluid through vacuum suction for the quantification of ISF glucose.[25] This method allowed the measurement of glucose concentrations at a physiological range (0 – 300 mg/dL), but was accomplished using a commercial glucose meter. Other groups have proposed similar approaches using shorter MN arrays (300 – 500 μm) manufactured from different materials, including polycarbonate [26] and chondroitin sulfate[27], for the quantification of glucose at near physiological ranges (200 – 500 mg/dL[26] and 100 – 400 mg/dL[27]). However, this method bears strong limitations, as skin perspiration was found to disturb analysis, and sampling times of up to 20 minutes were required to withdraw sufficient ISF.[25] Furthermore, all examples of this class of MNs necessitated the use of an external glucose meter for quantification, as well as a means of physically withdrawing ISF, severely limiting their applicability.

Recently, this technique of ISF withdrawal has been proposed by Ito *et al.* as a method of therapeutic drug monitoring, using the same chondroitin sulfate MNs previously studied for glucose measurement. The authors administered the antibiotic vancomycin to rats, pierced their skin using the polymeric MN arrays, and manually extracted dermal ISF with a pipette, allowing drug quantification by LC-MS.[28] While this study suffers the same drawbacks ordinarily associated with solid MNs, it further supports the potential to use MNs for quantifying a wider variety of analytes in the skin. Specifically, this non-invasive monitoring system could be useful if applied to pharmacokinetic drug studies, provided their concentration in ISF is shown to be correlated to their concentration in the blood.

1.3.2. Hollow MNs for ISF sampling

Hollow MNs, usually made of silicon[17,29–32], are MNs with small channels or conduits running from the base to the tip, allowing the passage of fluid (**Figure 1.1.**). In the context of ISF sampling, the base of the MNs are generally connected to a sensing chamber, where analytes from the withdrawn ISF can be quantified instantaneously using a built-in detector.

By mimicking the natural ability of a mosquito to bite and extract blood from human skin, hollow MNs were initially engineered for the sampling of blood by different mechanisms, *e.g.* passive diffusion, capillary force, and vacuum suction, in a nearly pain-free fashion.[29,30,33–37] In a pioneering work, Smart *et al.* fabricated a single in-plane hollow silicon MN with a length of 2 mm and a diameter of 100 µm for superficial blood sampling and glucose quantification.[17,38] The authors used a relatively low-cost microfabrication procedure, consisting of mixed-acid wet etching followed by anodic binding of a thin layer of glass, to create a silicon microcuvette with a volume of 200 nL, sealed with a glass window for the absorbance quantification of glucose, directly integrated into a hollow MN.[38] Once drawn up into the MN through capillary action, glucose was oxidized by the enzyme glucose dehydrogenase, triggering the reduction of a coloured dye and allowing for absorbance ($\lambda = 621$ nm) quantification in the microcuvette. The team was able to identify the most suitable MN dimensions and fabrication techniques to obtain a MN with optimal physical properties — toughness and flexibility — and an internal diameter of 25 µm, providing a strong capillary force and allowing the free passage of red blood cells. The device precisely measured biologically relevant concentrations of glucose (50 – 200 mg/dL) in as little as 200 nL of blood, and a clinical evaluation demonstrated a tangible reduction in perceived pain relative to commonly used lancets.[17] In spite of this, the device never became a marketed product, likely owing to its single-use nature and complex manufacturing process. Lancets, though more painful, are often reused, and the disposable paper test strips used for quantification are simpler than this device. While this early report focused on MNs for blood sampling, few others have investigated this application, likely because the relatively long MNs required for blood sampling do not entirely avoid the pain and inconvenience of traditional sampling methods. Additionally, as such devices rely on similar principles of operation to lancets, requiring the withdrawal of blood, the novelty may not have been sufficient to prompt further investigation.

While other examples of hollow MNs for blood sampling exist[36], more work has been focused on utilizing hollow MNs to sample ISF, owing to the reduction in required penetration depth and the less invasive nature of ISF sampling. Mukerjee *et al.* describe a 20 x 20 array of hollow, out-of-plane, silicon MNs with average lengths of around 250 µm; short enough to access the dermal ISF without breaching the capillaries found deeper in the skin.[29] The array was found to be capable of piercing the skin and withdrawing an unspecified volume of ISF through capillary action into an external reservoir. Though glucose in the withdrawn ISF could be quantified at a normal physiological range, external paper test strips were required, and no integrated detector was proposed for the device.

Around the same time, Zimmerman and Stoeber proposed a similar device for withdrawing ISF using hollow silicon MN arrays.[30] They demonstrated that MNs with lengths of 200 μm could efficiently reach and sample ISF, allowing quantification of glucose without the need to draw blood. Notably, they proposed the incorporation of an enzymatic detector directly into this MN device, which required the development of a new method of enzyme immobilization due to the high temperatures encountered during manufacturing. The temperature required to assemble the glucose sensor (400 °C) through anodic binding of a Pyrex wafer to a silicon platform was significantly higher than the denaturation temperature of glucose oxidase (65 °C). To avoid denaturing the enzyme, it was necessary to immobilize glucose oxidase after the sensor was assembled. Their approach consisted of mixing a solution of glucose oxidase with a water-soluble polymer (poly(vinyl alcohol)-styrylpyridinium) that could be cross-linked under UV light. This mixture was allowed to flow between the two layers, where it was then cross-linked, resulting in enzymatically active glucose oxidase immobilized within the sensing chamber (**Figure 1.2. a**). As ISF flowed into the chamber, glucose oxidase could react with glucose to form gluconic acid and hydrogen peroxide, which would then be oxidized at a platinum electrode, generating an electrical current proportional to the concentration of glucose. This effectively constituted the first example of an electrochemical enzymatic detector incorporated directly into an MN-based sampling device. While this detector represented a significant advancement in glucose monitoring, it only displayed a linear response for glucose concentrations between 0 and 160 mg/dL, below the threshold of hyperglycemia (180 mg/dL).[30]

Of note, a device incorporating similar design principles and detection methods for continuous glucose monitoring underwent a preliminary clinical study in 2014.[39] Using an array of hollow MNs connected to a similar electrochemical enzymatic detector, ISF glucose levels of 10 human volunteers were accurately measured over a 72 hour period, highlighting the viability of such MN-based monitoring devices.

Apart from improvements to the detection method, structural modifications of early MN designs have been explored, to address a common problem observed when using hollow MNs for sampling — the obstruction of the MN channels by skin fragments. This has been achieved by slightly offsetting the flow channel relative to the sharp tip of the MNs, physically separating the fluid conduits from the site of skin puncture, while producing MNs capable of successful skin penetration.[34] A similar MN design was developed and optimized by Mukerjee *et al.*, based on similar observations of MN channel obstruction.[29] Specifically, they determined that placing the channel directly at the peak of the tips resulted in relatively fragile MNs, prone to collapse upon skin puncture, as well as obstruction by skin fragments. Adding a slight tilt to the channel opening, similar to a miniaturized hypodermic needle, resulted in a more stable structure, but did not solve the problem of channel blockage. Similar to other reports[34], they determined that offsetting the channel from the MN tip effectively solved both issues, resulting in stable MNs that were resistant to blockage.

Almost concurrent to the first reports on hollow MNs for fluid sampling, single gel-containing hollow MNs were proposed by a group at the University of Tsukuba in Japan for the monitoring of physiological glucose.[31,40,41] The system, based on a poly-(*N*-isopropylacrylamide) gel exhibiting swelling upon temperature

change, was shown *in vitro* to efficiently and reproducibly take up sub-µL volumes of a glucose solution. Upon contact with a glucose solution at physiological temperature, the volume of the gel decreased, causing the solution to be drawn towards the detector. A built-in electrochemical enzymatic glucose sensor (similar in design to the one described by Zimmerman and Stoeber) allowed the linear quantification of glucose solutions between 0 and 360 mg/dL; a significantly greater range than the previously described devices. However, despite the improved detector performance, these MNs were never proposed for ISF sampling, as their length necessitated the sampling of blood from the deeper dermis. Additionally, all data was collected *in vitro* using glucose solutions, as the physical structure of the MNs was theorized to be too fragile to pierce the skin.

Though hollow MNs have primarily been used for the sampling and quantification of glucose, their principle of operation has been applied to other analytes. In a recent report, single polymeric hollow MNs have been used to sample ISF for the quantification and monitoring of K^+ concentration within the normal physiological range (3 – 6 mM). Consisting of fluid conduits linked to a miniaturized ion-selective electrode made from porous carbon, the device was shown to selectively measure K^+ concentration in extracted ISF, highlighting the potential versatility of this type of monitoring.[42]

The technique of fluid sampling through hollow MNs has also found potential application in the field of disease diagnosis and detection. Based on similar principles to the devices used for glucose quantification, the group of Ganesan *et al.* has developed MNs capable of sensing viral cytokines or immunoglobulins for the detection of globally relevant infections. Examples of this include microfluidics-based MN devices for the detection of biomarkers of HIV[32] and the Ebola[43] virus. For HIV detection, the device consisted of an array of hollow MNs connected to a chamber containing immobilized CD4 T^+ cell antibodies. Upon binding, an electrical current was generated proportional to the number of bound cells, allowing CD4 T^+ cell quantification (a common method of HIV diagnosis). For the detection of Ebola, the device operated in a similar manner, but with antibodies for Ebola capsid glycoproteins. This demonstrates the great impact such MNs may have for future disease diagnosis.

When designing a device to withdraw bodily fluids into a sensing chamber containing electrodes, a significant concern is the adsorption of proteins at the electrode surface, which can gradually reduce their detection sensitivity.[44] This presents an obstacle to longer-term glucose monitoring using hollow MN-based devices, by limiting the lifetime of their detectors. As such, studies have focused on overcoming this phenomenon. The chief strategy has consisted of coating a hollow MN with a poly-Si micro-dialysis membrane, to exclude high molecular weight molecules such as proteins, while allowing small molecule analytes to freely pass through.[45–47] The poly-Si microdialysis membrane consisted of ~150 nm grains of silicon forming a semipermeable membrane and resulting in small pores (15 – 20 nm) between the grains. These nanopores allowed analyte molecules to pass through, but blocked larger proteins, preventing them from coating the sensor, thereby extending the useful lifetime of the device. The authors demonstrated that fluorescein, a small molecule, was able to diffuse out of the MN through the poly-Si membrane, increasing the fluorescence of the surrounding solution; while proteins were excluded. It was proposed that, when used as

part of a continuous glucose monitor, this modification could result in an improved detector response over time, however, this was not further verified in any biological models.

As with solid MNs, recent reports have emerged describing the use of hollow MNs for therapeutic drug monitoring.[48,49] Using a single gold-coated MN with a functionalized inner surface, Ranamukhaarachchi *et al.* showed that it was possible to quantify model analytes (including vancomycin) at low µM concentrations using a built-in ELISA-based detection method. While the device required a complex functionalized gold surface and was only tested *in vitro*, the technique nonetheless represents an example of hollow MNs used for therapeutic drug monitoring, and is the only example of a MN for this purpose with an integrated detection method.

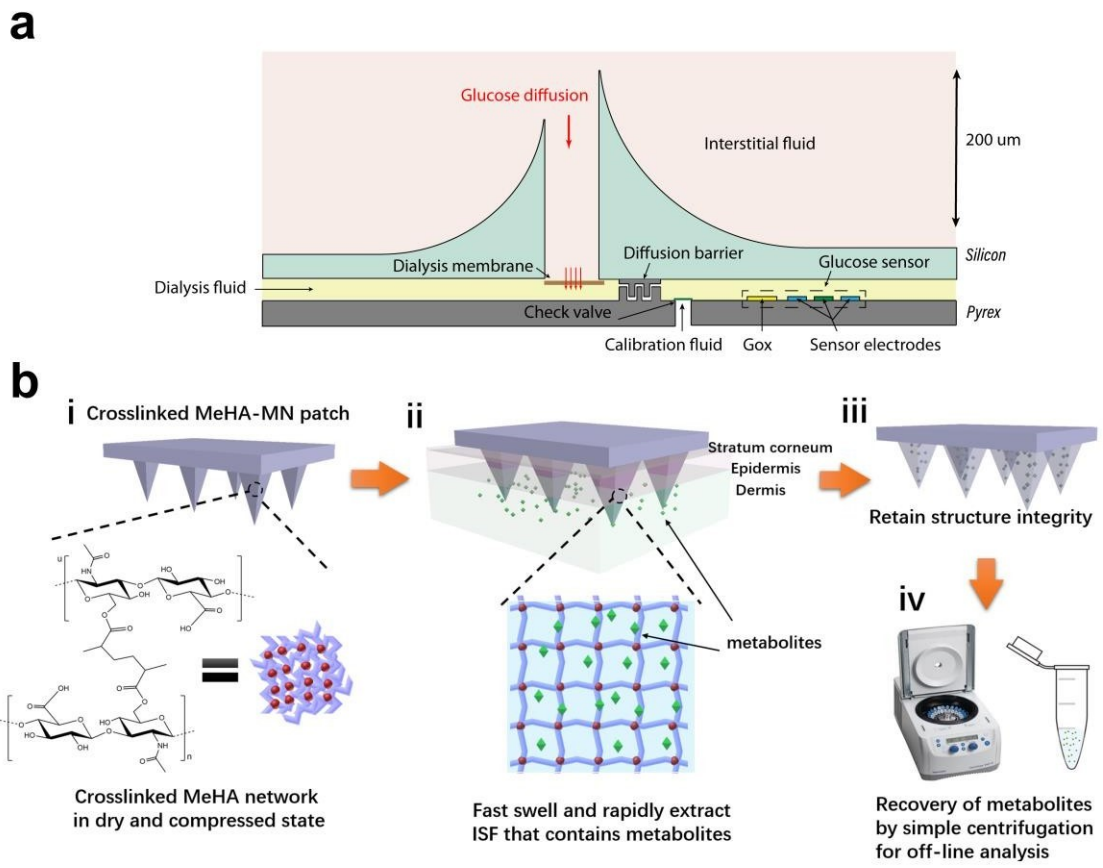

Figure 1.2. Examples of MNs for sampling bodily fluids: **a) disposable hollow MN for continuous glucose monitoring and b) rapid extraction of ISF with crosslinked hydrogel MN patches. Adapted with permission from [30,50].**

1.3.3. Hydrogel forming MNs

While the advances made in the design and implementation of hollow silicon MNs for biological fluid sampling have been significant, these devices require complex manufacturing and analyte quantification, which can be inconvenient for single-use or point-of-care devices. Very recently, another class of MNs has been proposed for ISF extraction, namely swellable hydrogel MN arrays. These MNs are formed from

crosslinked hydrophilic polymers, allowing the absorption of water, while preventing the MNs themselves from dissolving. Furthermore, this class of MNs has the advantage of being self-disabling after use, generating no sharp waste and requiring no specialized disposal, unlike solid and hollow MNs.

Early examples were primarily made using crosslinked mixtures of poly(methylvinylether-co-maleic anhydride) (PVME/MA) and polyethylene glycol.[51,52] Such MNs have been proposed for ISF glucose quantification, as well as therapeutic drug monitoring, with caffeine and theophylline serving as model drugs detectable in ISF. Similarly, fluid extraction using swellable polymeric MNs, followed by external quantification, has been used to monitor levels of administered Li^+ in the context of therapeutic drug monitoring, with potential implications in the management of bipolar disorder treatment.[53] However, in order to extract even small volumes of ISF (< 1 μL), it was necessary to apply MNs to the skin for 1 – 3 hours, which would be impractical from a clinical perspective.

A recent MN device proposed by Chang *et al,* based on UV-crosslinked methacrylated hyaluronic acid (MeHA) (**Figure 1.2. b**), has shown improvements in this regard.[50] These MNs were found to be able to absorb 1.4 μL of ISF within just one minute of application (or 2.3 μL within 10 minutes), owing to the highly hygroscopic nature of MeHA. Following extraction, the ISF could be recovered through centrifugation for further analysis. From this extract, it was possible to accurately quantify variations in glucose and cholesterol levels in ISF using commercially available test kits, proportional to variations observed in blood through commercially available meters. These tests were performed *in vivo*, representing an interesting advance in bodily fluid quantification using MNs, though it should be noted that no integrated detection method was used with this variety of MNs, requiring external processing and quantification of the sampled analytes.

An important consideration when using MNs to sample ISF is the volume collected for analysis, as their small size and the nature of ISF prevent the extraction of large volumes.[54] When using solid MNs, ISF is withdrawn manually, allowing access to relatively larger sample volumes (up to 10 μL) suitable for external analysis (**Table 1.1.**). Hollow MNs typically sample smaller volumes, often < 1 μL, but tend to contain more complex integrated detection systems, suitable for low-volume analyses. On the other hand, swellable hydrogel-based MNs are usually capable of sampling 1 – 2 μL volumes, which must then be extracted and analysed externally. This could present an issue for applications where lower-abundance analytes are quantified, such as in therapeutic drug monitoring, highlighting a potential limitation of this MN class unless integrated detection systems are incorporated, or polymers with larger fluid-absorbing capacities are implemented.

A potential application of such MN-based devices is the integration of a glucose monitoring system and a complementary insulin delivery mechanism onto a single platform, creating a so-called artificial pancreas as a closed-loop diabetes monitoring system.[55] Recently, such a device has been described by Yu *et al.*, consisting of a swellable polymeric MN-based enzymatic glucose detector coupled to a polymeric vesicle-based insulin-release system[56]. The polymeric MNs of this device, made from MeHA, sample the ISF, and

glucose is oxidized by the enzyme glucose oxidase, contained within vesicles inside the MNs. When concentrations are high, this reaction creates a hypoxic environment inside the vesicles, causing them to dissociate and release insulin, thereby regulating blood glucose levels. While this illustrates the utility of a closed-loop delivery system, the complexity of the vesicle-based release, the lack of reversibility, as well as the challenge of quantifying the amount of insulin remaining in the device following initial delivery, highlight potential obstacles to clinical translation. Nonetheless, this remains the first example of integrated detection within a swellable polymeric MN array, an important consideration for point-of-care systems.

Collectively, the various approaches presented here show great potential in terms of fluid sampling for the detection of various analytes and corresponding disease diagnosis and monitoring. The techniques have been under intense research for approximately 20 years, and great advances have been made to improve all components of the developed devices. No product has yet made it to the market, although clinical trials evaluating the potential of MNs for fluid sampling and glucose sensing are in progress,[57] suggesting that viable applications of analyte sensing through ISF sampling can be foreseen.

Table 1.1. Properties of MNs used for sampling bodily fluids.

Type of MN	Design	Manufacturing	Material	Analyte	Quantification Range	Integrated Detection	Extraction Volume	Sensing Method	*In vivo*?	Ref
Solid	7-Array (1.5 mm)	Glass pulling	Glass	Glucose	0 – 300 mg/dL	-	1 – 10 µL	Enzymatic (External)	+	[25]
Solid	305-Array (300 µm)	n.d.	Polycarbonate	Glucose	200 – 500 mg/dL	-	n.d.	Fluorescence (External)	+	[26]
Solid	5×5-Array (475 µm)	Moulding	Chondroitin Sulfate	Glucose	100 – 400 mg/dL	-	10 µL	Enzymatic (External)	+	[27]
Solid	300-Array (500 µm)	Moulding	Chondroitin Sulfate	Vancomycin	n.d.	-	2 µL	LC-MS (External)	+	[28]
Hollow	Single (2 mm)	MEMS	Silicon	Glucose	50 – 200 mg/dL	+	200 nL	Enzymatic (Absorbance)	+	[17]
Hollow	20×20-Array (200 µm)	MEMS	Silicon	Glucose	n.d.	-	n.d.	Enzymatic (External)	+	[29]
Hollow	2×4-Array (200 µm)	MEMS	Silicon	Glucose	0 – 160 mg/dL	+	n.d.	Enzymatic (Electrode)	-	[30]
Hollow	20×10-Array (300 µm)	MEMS	Silicon	Glucose	50 – 250 mg/dL	+	n.d.	Enzymatic (Electrode)	+	[39]

Hollow	Single	Injection	Silicon	Glucose	0 – 360 mg/dL	+	200 nL	Enzymatic (Electrode)	-	[31,40,41]
Hollow	Array (250 µm)	MEMS	Ni-Coated Silicon	CD4 T^+ Cells	n.d.	+	1 µL	Electrical Impedance	-	[32]
Hollow	18-array (n.d.)	MEMS	Ni-Coated Silicon	Ebola Virus	n.d.	+	6 µL	Electrical Impedance	-	[43]
Hollow	Single (450 µm)	Electrodeposition	Au-Coated Nickel	Vancomycin	0.3 – 40 µM	+	0.6 nL	ELISA	-	[48]
Polymer	10×10-Array (800 µm)	Moulding	MeHA*	Glucose Cholesterol	18 – 288 mg/dL 1 – 10 mM	-	2.3 µL	Enzymatic (External)	-	[50]
Polymer	11×11-Array (600 µm)	Moulding	MeHA	Glucose	n.d.	+	n.d.	Enzymatic (External)	+	[56]
Polymer	Single (1 mm)	Laser Etching	Eshell 300**	K^+	10 µM – 10 mM	+	n.d.	Electrochemical	-	[42]
Polymer	19×19-Array (600 µm)	Moulding	PMVE/MA***	Li^+	n.d.	-	n.d.	Spectroscopic (External)	+	[53]

* MeHA = Methacrylated hyaluronic acid

** Eshell 300 = Acrylic Resin + tetrahydrofurfuryl methacrylate + urethane dimethacrylate

*** PVME/MA = Poly(methylvinylether-co-maelic anhydride)

1.4. MNs for the selective capture of biomarkers

The diagnostic potential of the skin for both local and systemic diseases is attributable to the great amount of information that can be readily accessed through it. Indeed, cutaneous protein composition can vary significantly in certain conditions, such as during the activation of inflammatory or immune responses. Of particular interest is the detection of biomarkers, quantifiable indicators of a biological process or state.[58] Biomarkers are often proteins/peptides, and can play a significant role in disease diagnosis, but have traditionally only been accessible through blood sampling, which is invasive and requires significant laboratory processing.

Kendall and co-workers have focused on antibody-coated MNs for the selective capture of dermal proteins, with the goal of allowing easy diagnosis of systemic diseases. To best sample biomarkers of interest, it was found that MNs should have sharp, tapered tips at a high density, in order to maximize the surface area available for antibody capture. In accordance with this, solid silicon MNs with the desired design were fabricated through a combination of anisotropic and Bosch etch processes.[59] Using this procedure, it was possible to produce highly uniform MNs with a tunable tip shape, at a density in excess of 20000 needles per cm^2.

In 2010, they presented an array of 65 μm long gold-coated silicon MNs, functionalized with a PEG layer, onto which capture proteins specific to influenza antibodies were immobilized.[60] These functionalized MNs were able to selectively bind influenza antibodies both *in vitro* and in live mouse models, allowing quantification with an specially designed ELISA assay. This finding was significant, as similar biomarkers had previously only been detectable through conventional blood sampling.[60] However, the antibodies also displayed a low capture efficiency and low sensitivity relative to conventional ELISA assays, hypothesized to be due to either low surface density or poor antibody orientation upon immobilization, performed *via* EDC/NHS coupling. Accordingly, in a subsequent report, it was found that by optimizing the protein immobilization conditions — carrying out the reaction for longer, at 37 °C, and at a slightly acidic pH to favour the coupling reaction — the antibodies' capture efficiency, and the corresponding sensitivity of the assay, could be boosted by 18-fold *in vivo* (**Figure 1.3.**).[61]

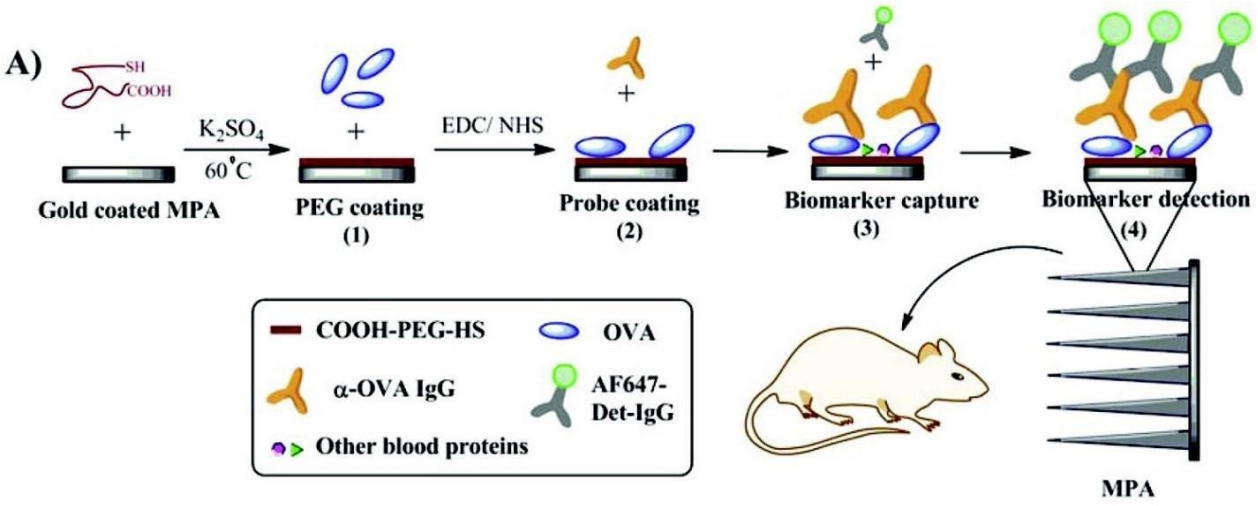

Figure 1.3. Capture by antibody-coated MNs and successive analysis by ELISA of the sampled molecules of interest. Re-used with permission from [61].

While high-abundance biomarkers were successfully captured in the viable epidermis, their concentration is thought to be much higher in the deeper dermis, owing to its closer proximity to capillaries. As a result, MNs piercing deeper into the skin should be exposed to a greater concentration of biomarkers, potentially allowing the detection of lower-abundance biomarkers.[62] With this in mind, it was demonstrated that the capturing capacities of the MNs were directly dependent on their depth of penetration in the skin, as well as application time. Indeed, the capture efficiency was increased 4-fold when sampling from the dermal (153 ± 30 μm) rather than the epidermal layer (27 ± 9 μm). Additionally, it was found that rapid applications of roughly 10 minutes were sufficient for the detection of high-abundance biomarkers. The signal was also found to increase with application time up to 6 hours, at which point sensitivity was comparable to a standard ELISA assay, and was theorized to be appropriate for the detection of low-abundance biomarkers.[62] This study showed that the properties of MNs can be specifically tuned to the properties of the biomarker to be collected. Despite this, the manufacturing process of silicon MNs remains complex, which has generated substantial interest in the development of simpler approaches.

One solution came from the use of polycarbonate MNs fabricated using moulding techniques, followed by chemical modifications of the external polymer chains to immobilize proteins on their surface. Polycarbonate MN arrays were manufactured through a hot embossing process, consisting of heating and compressing polycarbonate into a prefabricated mould, followed by surface modification through nitric acid treatment. This resulted in surface-level nitro groups, which were reduced to yield primary amines, allowing attachment of a functionalized PEG layer. It was then possible to immobilize antibodies at the surface of this layer, allowing the detection of influenza antibodies and resulting in polymeric MNs capable of high abundance biomarker capture (anti-influenza IgG). The polycarbonate MNs were shown to have a capture efficiency comparable to the gold-coated silicon arrays previously described, with the advantage of a simpler and more cost-effective manufacturing process.[63]

While these MN devices represent a novel and efficient strategy for *in vivo* biomarker capture, they have only been proposed as a semi-quantitative method, as the nature and the amount of bodily fluids sampled by the microprojections remains unclear. For this reason, there has been substantial interest in simultaneous quantification of a control biomarker, to determine the relative abundance of the analyte biomarker.

Ng *et al.* focused on this aspect, presenting a blotting method for the successful simultaneous near real-time detections of mouse IL-1α, as well as positive and negative controls (**Table 1.2.**). The method consisted of applying a MN patch to the skin, removing it, and treating the MNs with an HRP-conjugated secondary antibody, as in an ELISA assay. The MNs were then applied to a sheet of paper soaked in an HRP substrate, resulting in coloured spots at the points of contact with the MN tips. This allowed visualisation of biomarkers sampled at a specific depth, dependent on MN length, as only those bound to the tips of the needles would come into contact with the paper and generate a signal. Further, by immobilizing different antibodies on different needles within the array, this method allowed for the simultaneous detection of a positive control and an analyte biomarker. While the method allowed for the detection of biomarkers at the desired depth only, selectively sampling either ISF or blood, a clear signal-concentration relationship was not established, limiting this technique to qualitative analysis until further development.[64]

The Kendall group has also focused on simultaneous biomarker detection, designing multiplexed MN arrays capable of detecting analyte biomarkers alongside positive and negative controls. By dividing the array into three parts and functionalizing each section with a different antibody, it was possible to semiquantitatively detect the protein r*Pf*HRP2 (a structural protein serving as a marker of *Plasmodium falciparum* infection) relative to total IgG concentration, which acted as a positive control.[65] A negative control was also established by functionalizing part of the array with a capture antibody for a protein not expected to be found in the test subjects, namely the Dengue virus structural protein NS1. In subsequent tests, these devices were shown to successfully detect elevated levels of both NS1 and r*Pf*HRP2 *in vivo*, using infected mice, highlighting the practical applications of this technology.[65,66]

MNs of this class show great potential for the detection of further biomarkers, provided they are expressed in dermal tissue at disease-relevant levels. For example, it has recently been discovered that Parkinson's and Alzheimer's diseases display clinical indicators in the skin, likely owing to the common embryonic development of the skin and nervous systems.[67,68] While skin biopsies have been proposed as a relevant diagnostic technique,[69] a MN-based device with the capacity to capture and detect such indicators would present an opportunity to revolutionize diagnosis protocols for both diseases.

Among the challenges of MN-based biomarker capture, the disruption of the local environment is perhaps the most relevant, as it could alter the nature and concentration of proteins in the viable epidermis.[64] Indeed, when MNs breach the *stratum corneum,* they trigger the activation of wound healing processes. Remarkably, these are associated with a local increase in blood flow and increased recruitment of cytokines, thereby altering biomarker concentration in the skin.[70,71] Ng *et al.* (2015) proposed that this phenomenon should be further investigated, to determine its effect on biomarker capture and analysis.[64] In relation to this,

a report by Kendall *et al.* (2016) proposed that the increased protein extravasation to the skin could constitute an advantage for the capture of low-abundance biomarkers, by increasing their local concentration in the ISF upon sampling. They found that when MNs were applied to the skin with pressures between 1 – 10 MPa, capture efficiency of anti-influenza IgG was increased, and required application time was reduced, indicating a potentially beneficial effect of this biomarker recruitment.[72]

Although much data has been collected through *in vitro* and *in vivo* studies, these MN arrays have not yet been clinically evaluated. The field has gained attention in the last few years, as shown by the increasing number of topic-related publications. The challenge will now be to translate the acquired knowledge to clinical applications. Before this can occur, however, some questions need to be addressed.[64] First, the nature of the sampled fluid needs to be identified, to determine whether initial research should focus on systemic or local diseases. Second, the correlation between penetration depth and the target biomarker should be optimized. Additionally, through current methods, it is only possible to sample soluble circulating biomarkers, while intracellular ones — relevant to many other diseases — cannot yet be measured.[73,74] Finally, further work should be done to better understand the relationship between application time and biomarker capture. While the MNs should be applied long enough to allow for adequate binding of circulating biomarkers, the sampling time should also be brief enough to avoid altering the protein composition of the dermal layer through wound healing processes. As such, while MNs display tremendous potential as immunodiagnostic platforms, more research is required before any such devices will be available on the market.

Table 1.2. Properties of MNs for selective biomarker capture.

Type of MN	Design	Material	Analyte	Sensing method	Detection range	Ref.
Solid	Array (65 μm)	Gold-coated silicon	Influenza IgG	MPA-ELISA	n.d.	[60–62]
Solid	Array (65 μm)	Polycarbonate	Influenza IgG	MPA-ELISA	n.d.	[63]
			Human TNF-α			
Solid	Array (1 mm)	Polylactic acid	Mouse IL1-α	Paper Blotting	50 pg/mL –500ng/mL	
			Mouse IL6			[64]
			Influenza IgG			
Solid	Array (250 μm)	Gold-coated silicon	Dengue NS1	MPA-ELISA	n.d.	[65]
			*Pf*HRP2			

1.5. MNs for *in situ* analyte monitoring

While many works have focused on analyte quantification and monitoring through the sampling of bodily fluid, another, related, method has emerged for quantifying analytes within the skin (*in situ*) using MNs. In this technique, the surfaces of MNs are functionalized, often with an immobilized enzyme, allowing a redox reaction to occur at the MN surface upon contact with the analyte of interest (**Table 1.3.**). This allows the surface of the MN to act as an electrode, generating an electrical signal proportional to the concentration of the analyte of interest, that can be read in real-time.

Similar to reports on analyte quantification by ISF sampling, many groups have focused on the application of this technique to glucose monitoring.[75–78] Notably, Chen *et al.* have developed a single, multi-layer MN capable of monitoring glucose across the physiologically useful range (0 – 360 mg/dL) (**Figure 1.4.**).[76] Using a base layer of platinum nanoparticles (PtNPs) to act as an electrode surface, glucose oxide was immobilized around the MN, followed by layers of polyaniline, porous polyvinylidene fluoride (PVDF) and Nafion. Much like membranes proposed for coating hollow MNs, these outer polymer layers served to allow glucose to reach the electrode surface, while excluding larger molecules that could interfere with the electrode.

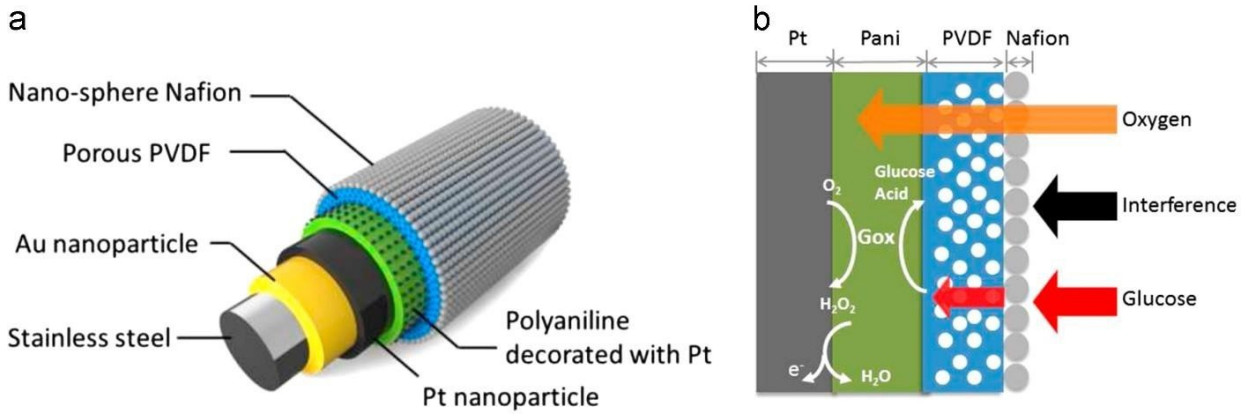

Figure 1.4. Schematic representation of a glucose-sensing MN: a) Layered nanostructures, and b) principle of operation. Re-used with permission from [76].

Additionally, the detection of glucose by this method has been accomplished without the need for immobilized glucose oxidase at the MN surface. A report from 2013 described an array of silicon MNs decorated with carbon nanotubes and PtNPs, able to oxidize glucose through electrical current, without the need for an enzyme, allowing quantification at the physiological range (54 – 360 mg/dL).[75]

Very recently, this type of enzyme-free glucose detection has been accomplished without the need for silicon arrays, which can be expensive and complex to manufacture.[77] Single polymer MNs with lengths of around 2 mm were coated with a layer of silver and used as probes for Raman spectroscopy, augmenting signals used to detect glucose in solution. The MNs were formed by casting melted agarose into a standard micropipette tip and inserting a thin needle with a diameter of 200 μm to form a hollow channel, after which a silver coating was added by chemical deposition, using $AgNO_3$ and glucose. The authors were able to

demonstrate that biologically relevant concentrations of glucose (90 – 2700 mg/dL) could be accurately quantified *in vitro* and *ex vivo* through Raman spectroscopy.[77] While this class of MNs has the advantage of using relatively inexpensive materials and simple manufacturing, the use of Raman spectroscopy for quantification could limit the clinical translation. However, by performing measurements within the skin, and without using enzymes, these technologies could lead towards the development of a continuous glucose monitor, by overcoming the short lifetimes associated with other sampling techniques.

Aside from glucose analysis, this class of MNs has been shown to be useful in the monitoring of other physiologically relevant analytes, such as glutamate[79] and lactic acid.[78,80] The devices used for detecting these analytes are largely similar to those used to detect glucose, consisting of solid MNs coupled to oxidative enzymatic detectors. In these cases, the enzymes were dispersed in a carbon paste matrix serving as an electrode, generating a signal used for analyte quantification. The strategy has also been proposed for continuously monitoring blood alcohol level, following the findings that ISF ethanol concentration is strongly correlated with ethanol concentration in the blood.[81]

Reactive oxygen species (ROS) are oxygen species containing unpaired radical electrons, and are known to cause DNA and tissue damage. As such, their detection and quantification is of great interest. A recent study has demonstrated the detection of H_2O_2 (a common ROS) using a single MN, coated with platinum nanoparticles (PtNPs) and a thin layer of molybdenum sulfide (MoS_2).[82] The PtNPs triggered the reduction of H_2O_2 at the MN surface, allowing the *in vitro* quantification of ROS through differential pulse voltammetry. Together, these devices serve to highlight the wide variety of analytes that can be detected using MNs, demonstrating their broad diagnostic utility.

Table 1.3. Properties of MNs designed for in situ analyte detection.

Type of MN	Design	Manufacturing	Material	Analyte	Range	Sensing Method	*In vivo*	Ref.
Solid	Single (coated)	Deposition	Steel	Glucose	0 – 360 mg/dL	Enzymatic (Electrode)	+	[76]
Solid	15×15 Array (380 µm)	MEMS	Silicon	Glucose	54 – 360 mg/dL	Electrode	-	[75]
Polymer	Single (2 mm)	Moulding	Agarose	Glucose	0 – 2700 mg/dL	Spectroscopic	+	[77]
Hollow	Array (1.4 mm)	Injection Moulding	Eshell 200*	Glutamate	0 – 140 µM	Enzymatic (Electrode)	-	[79]
Hollow	Array (1.5 mm)	Injection Moulding	Eshell 200*	Lactate	0 – 8 mM	Enzymatic (Electrode)	-	[80]
Hollow	Array (length not specified)	Stereo-lithography	Eshell 300**	Glucose, Lactate, pH	0 – 216 mg/dL, 2 – 12 mM, 5.0 – 8.0	Enzymatic (Electrode)	-	[78]
Solid	Single (length not specified)	Deposition	Steel	H_2O_2	1 – 100 µM	Electrochemical	-	[82]
Hollow	Array (800 µm)	Injection Moulding	n.d.	Ethanol	0 – 80 mM	Enzymatic (Electrode)	-	[81]

***** Eshell 200 = Urethane dimethacrylate + neopentyl glycol propoxylate diacrylate

****** Eshell 300 = Acrylic Resin + tetrahydrofurfuryl methacrylate + urethane dimethacrylate

1.6. MNs for dermal biopotential measurements

Owing to the high electrical capacity of the lipophilic matrix in which corneocytes are embedded, the *stratum corneum* is conferred dielectric properties, resulting in the skin impedance: the force opposing the passage of electrical charge through the skin.[83] Electrolytes present in the ISF of the viable epidermis, on the other hand, account for an electric potential, connected to the activity of electrically-driven tissues, such the heart and muscles. The measurement of this electric potential allows for the monitoring of biosignals, including ECGs, EMGs, and EEGs; relevant when monitoring cardiovascular disease, muscular dysfunction, and epilepsy, among other disorders.[84,85] This electrical activity is typically measured using wet or dry electrodes to detect signals from the viable epidermis, across the *stratum corneum*. These methods have limitations however, as wet electrodes require skin abrasion and/or the application of a conductive gel, both of which can irritate the skin; while dry electrodes suffer from the interference of the skin impedence, due to their inability to breach the *stratum corneum*. Because of their ability to painlessly pierce the *stratum corneum*, MN-based electrodes could mitigate the disadvantages of other classes of electrodes, and have emerged as an alternative means of measuring biopotentials.

The use of MNs for biopotential measurement displays great advantages over the currently-used methods of wet and dry electrodes.[86] The main advantage is direct contact with the electrically-active viable epidermis, eliminating the need for conductive gels or skin abrasion.[86] Indeed, the former can cause swelling and allergies, and evaporate over time, preventing their use for continuous monitoring; whereas the latter is time-consuming and uncomfortable for the patient.[86] Moreover, electrodes comprised of MNs are much smaller, and therefore require far less skin surface area for application.[87] Owing to their rapid application, ease of use, and lack of requirement for specialized personnel, MNs could serve as a promising point-of-care platform for continuous biosignal monitoring. Though this field of research remains in its infancy, some findings show great potential and deserve to be reported.

For the past 15 years, researchers have worked primarily with solid MNs engineered to allow for biopotential measurements. The field was pioneered by the group of Prof. Stemme at the Royal Institute of Technology in Stockholm, and their work on MN-based electrodes coated with electrolyte-conducting layers.[88] Consisting of an array of 100 – 200 μm long silicon MNs, coated first with a layer of silver, followed by a deposited layer of silver chloride, the manufactured electrodes were shown to be capable of accurately measuring biopotentials without the need for skin preparation. The Ag/AgCl coating on the MNs was also shown to reduce impedence between the electrode and the viable epidermis, while preventing polarization of the electrode surface.

When measuring biopotentials, it is important that the electrodes remain in place, to avoid signal interference. To this end, further work by the Stemme group focused on optimizing the design of the MNs to increase their displacement force — the force needed to remove the MNs from the skin after piercing — to allow them to be used for continuous monitoring.[89] Specifically, the tips of the MNs were modified to create a barbed shape, similar to an arrowhead, to improve their ability to remain in the skin (**Figure 1.5.**). This resulted in an increased average displacement force (320 mN) relative to non-barbed MNs (100 mN), suggesting that such designs could be important for the clinical translations of such devices.

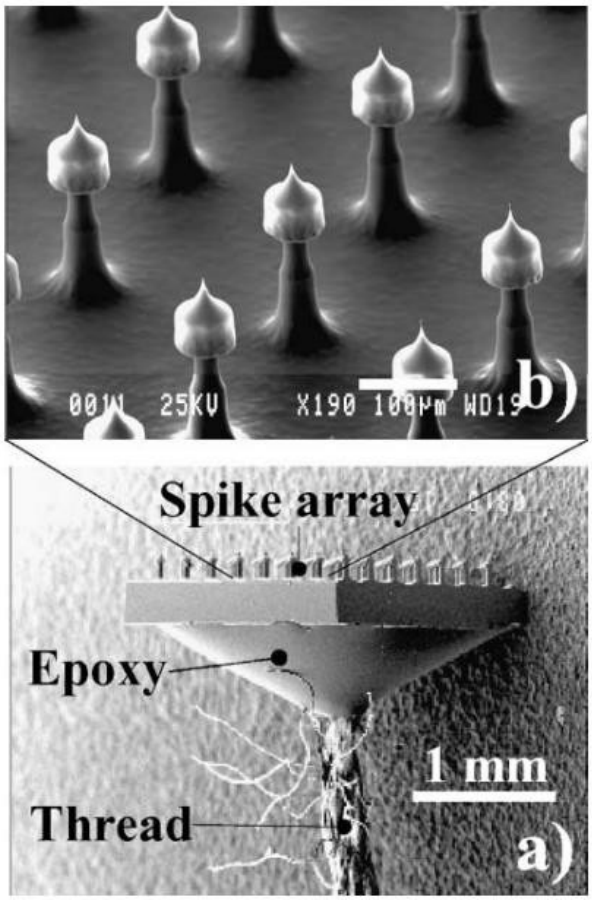

Figure 1.5. MN-based miniaturized electrode for biopotential measurement: a) SEM of a chip containing an array of barbed spikes. A thread is glued to the chip by means of epoxy and (b) A magnified view of the spike array. Re-used with permission from [89]

However, the production of such MNs is laborious, which could limit their potential for clinical translation. Consequently, alternative designs have been proposed. One such example can be seen in the work of Hsu *et al*., in the design of barbed MNs resembling fish hooks, which showed an acceptable displacement force as well as a cost-effective preparation protocol.[90] While the maximum displacement

force was lower than earlier examples (85 mN), the barbs were formed using a relatively simple KOH-based wet etching process, in contrast to the deep reactive ion etching (DRIE) required for previous designs.[89,90] In another report, the Ag/AgCl coating on the MNs was substituted with heavily doped silicon, which was able to serve as both the electrode and the material composing the MNs.[91] This modification served to simplify the manufacturing process of the electrodes by eliminating the need for a silver deposition step following the silicon etching.

Nonetheless, the manufacturing process of silicon MNs requires cleanrooms and complex manufacturing techniques, which has generated interest in simpler and less expensive alternatives.[92] This has resulted in the development of polymeric MNs, with polymethyl methacrylate (PMMA) having been proposed as a material, owing to its biocompatibility and high mechanical strength.[87,93] Examples of polyurethane MNs have also been seen.[94] In all cases, the electrodes are coated with a layer of metal (either Pd/Au or Ag/AgCl) to allow for electrical conductivity, and have displayed comparable performances *in vivo* to their silicon counterparts. However, while some of the costs and complexity associated with silicon micromachining have been avoided, polymeric MNs still require expensive metal deposition steps to generate the electrodes, which could offset this benefit.

In addition to silicon and polymeric MNs, hollow MNs have also been considered for *in situ* biopotential measurements, due to their ability to create a continuous link between the ISF and the electrode located in the back reservoir of the MN array.[95,96] Rather than using the inserted MNs themselves as electrodes, these devices house their electrodes in a rear chamber, towards which the ISF is drained through hollow channels in the MNs. An advantage of this method is the reduction of protein adsorption onto the electrode, as it is only exposed to a small amount of drained ISF, rather than the entirety of the circulating fluid. This could serve to prolong the effective life of the devices, greatly increasing their potential for at-home monitoring use.

Another advantage offered by MN-based biopotential electrodes is their ability to neglect the skin-potential variation (SPV). The SPV consists of small changes in the skin potential that occur when mechanical pressure is applied to the *stratum corneum*, such as upon the insertion of an electrode.[97] While this can usually be corrected for in a clinical setting, it remains an obstacle in the development of continuous-use monitoring systems, as small pressure differences resulting from regular motion can result in meaningful changes of SPV. Recently, Pei *et al.* have developed a MN-based electrode system capable of neglecting these small changes in SPV. In this system, the portion of the MNs in contact with the *stratum corneum* was coated with an insulating layer, leaving only the tips exposed deeper in the tissue.[97] As such,

the electrodes are unaffected by the slight mechanical pressures caused by regular motion, potentially paving the way for continuous-use biopotential monitoring systems.

Other groups have taken advantage of MN-based electrodes to quantify intercellular swelling, as a means of monitoring edema.[98] Using swellable polymeric MN-based electrodes, they were able to monitor and observe changes in the electrical resistance of the skin. In the study, subjects remained seated for 70 minutes to induce edema in the legs, which was found to reduced skin resistance by 20 kΩ, which corresponded to a change in leg circumference of roughly 0.4 cm. Upon standing, both leg circumference and skin resistance were found to return to normal levels, as edema decreased. This suggests a potential new point-of-care approach to easily monitor and diagnose edema in humans.

However, no commercial product based on MNs has yet been approved for this application. The main limitations of the herein presented devices are their high manufacturing costs,[99] which likely account for delays in their commercial translation.

1.7. MNs for delivery of diagnostic agents

Similar to their primary use for the delivery of drugs, MNs are well-suited for the selective and painless delivery of diagnostic agents. For this purpose, hollow, coated, and dissolving MNs have been investigated for the delivery of different agents, including fluorescent contrast dyes for imaging, and allergens for non-invasive allergy tests. The delivery of imaging agents through the skin could be useful both for the detection/monitoring of skin-related disorders, as well as for any application involving the quantification of systemic biomarkers present in the ISF. Although only a few reports have focused on this approach thus far, initial results have been promising, suggesting the possibility of further development in the field.[100]

Dermal ISF is drained by the lymphatic system, which is responsible for the homeostasis of peripheral tissue by taking up substances and draining them back into venous circulation. In recent years, it has become clear that disparate pathological conditions, including lymphedema, chronic inflammation, as well as tumour growth and metastasis, are associated with alterations to this system;[101] and the assessment of the structure and function of its vessels for diagnostic purposes has thus attracted increasing attention.[102] As their size specifically targets the ISF, MNs are well-suited for the delivery of compounds, including diagnostic agents, to the lymphatic system. For instance, fluorescence microlymphography, based on the administration of a fluorescent FITC-dextran (MW 150,000) conjugate using a single hollow MN (0.2 mm outer diameter), has allowed imaging of the architecture of lymphatic vessels, providing promising results for the diagnosis and stratification of lymphatic dysfunctions such as Milroy’s lymphedema, systemic sclerosis, and Fabry's disease in humans.[103,104] The conjugation to dextran increases the MW and

hydrophilicity of the probe, thus improving the selectivity of drainage by the lymphatic system versus the bloodstream, providing a greater spatial resolution. Nevertheless, the relatively low wavelength of FITC (λ_{exc} ~ 490 nm; λ_{em} ~ 520 nm) results in a significant background signal from surrounding tissues, including the skin, necessitating relatively high doses and reducing the sensitivity of the imaging procedure. A drastic improvement could come from the use of probes fluorescent in the near-infrared region (> 750 nm). At this range of wavelengths, photons are minimally scattered and absorbed by biological tissues, offering excellent spatial resolution for superficial imaging.

A recent report by Brambilla *et al.* demonstrated the feasibility of using dissolving polymeric MNs arrays to deliver Indocyanine green (ICG), the only FDA-approved injectable NIR probe, to the dermis as a simple and painless point-of-care diagnostic method (**Figure 1.6.**) for monitoring lymphatic function.[100] These MNs consisted of a solid dispersion of ICG within a low molecular weight polyvinylpyrrolidone (PVP) matrix, meant to rapidly dissolve (~5 minutes) after successful penetration of the skin. Though only a limited amount of ICG could be delivered, leading to reduced structural observation compared to standard hypodermic needles, the authors demonstrated that the drainage kinetics of the resulting non-invasive *tattoo* correlated with lymphatic drainage, offering the possibility of non-invasively monitoring lymphatic function, potentially using a simple fluorescence detector. Unlike many of the previously described MNs, the ones used in this study were made entirely of FDA-approved materials, offering the possibility for a rapid clinical translation for the early stage identification of lymphedema, a serious condition characterized by the swelling of a limb due to insufficient lymphatic drainage. This condition appears in roughly 20% of patients having undergone lymph node dissection in the context of breast cancer surgery, and urgently lacks an early and quantitative monitoring method. Unlike standard hypodermic needles, these patches do not require special training to administer, and could be used by patients for self-monitoring of lymphatic function. Moreover, this dissolution-based delivery approach prevents the increase in interstitial hydraulic pressure resulting from hypodermic injection, which could alter the drainage and lead to erroneous results. Nevertheless, despite being approved and generally considered safe, ICG suffers from some limitations, such as low quantum yield, poor chemical stability, and limited selectivity for lymphatic drainage, which could drastically limit the sensitivity of the system. Thus, a great improvement could come from the use of recently described highly fluorescent and lymphatic-selective fluorescently-labelled polymers or nanoparticles.[105,106]

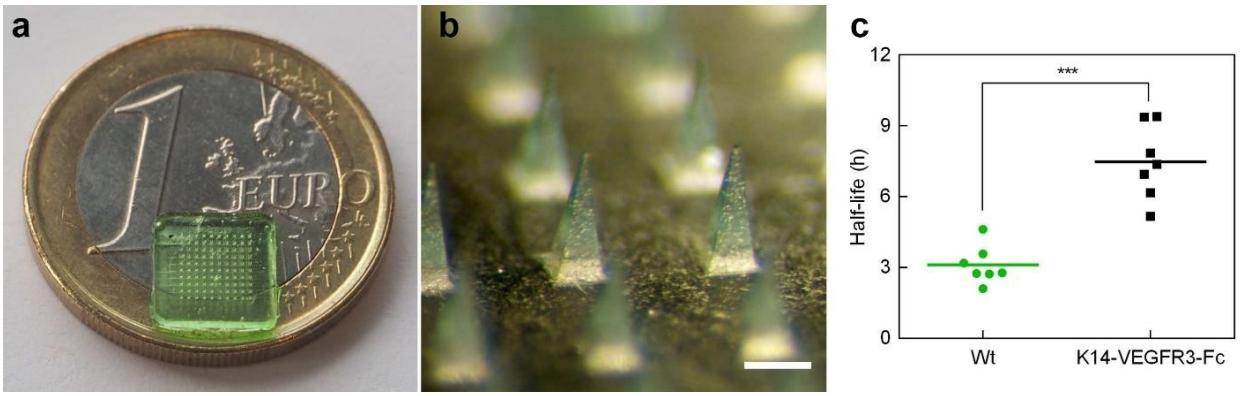

Figure 1.6. Dissolving polymeric MNs for the functional imaging of dermal lymphatic drainage: a) Whole MNs patch on a one-Euro coin, b) stereomicroscopic views of ICG-containing MNs (Scale bar: 200 μm) and c) clearance half-life in wt and transgenic animals lacking dermal lymphatic drainage (K14-VEGFR3-Fc) after application of ICG-loaded PVP MNs on the ear. Adapted with permission from [100].

The skin is composed of different cell types, including specialized immune cells known as Langerhans cells, which are responsible for antigen presentation.[107] Consequently, several groups have proposed the use of MNs for allergy testing.[108–110] Currently, the most common methods of allergy testing consist of lightly puncturing the skin followed by the application of an allergen solution, or the delivery of an allergen solution through dermal needles.[111] Application of MNs containing, or coated with, a protein allergen solution could eliminate the pain associated with traditional methods by selectively targeting the epidermis and avoiding contact with the dermis. Early reports primarily described silicon MN arrays, which could be coated with an allergen solution, and administered to the skin similar to a skin prick test.[108,109] While these devices showed comparable performance to conventional allergy tests, with the advantage of reduced skin irritation and patient discomfort, the high cost of manufacturing silicon MNs could prevent the wider adoption of this testing method. More recent works have described dissolving polymeric MNs, made of PVP or dextran, into which protein allergens could be loaded.[110,112] Though these MNs were not tested *in vivo*, fluorescence tests in excised skin indicate that allergens could successfully be delivered by this method, potentially offering a more cost-effective method of MN-based allergy diagnosis.

Similarly, dissolving MNs composed of chitin and loaded with tuberculosis (TB) antigens have been prepared and have shown promising *in vivo* results, opening the way for potential point-of-care tuberculosis diagnosis.[113] Though effective, current methods of TB diagnosis (consisting of intradermal injections of TB antigens) require specialized personnel to perform, and involve the careful manipulation of hypodermic needles to reach a specific depth in the skin. This can cause discomfort for the patient, as well as skin irritation, which could interfere with results. Because of this, an MN-based diagnostic device,

with lengths that could be tuned to the specific skin depth required for antigen delivery, could present a simpler, pain-free diagnostic platform.

A potential consideration regarding the delivery of diagnostic agents using dissolving MNs is the deposition of small amounts of polymeric material within the dermis. This consideration is actually shared with MNs used for the delivery of therapeutic agents, which have been more extensively investigated. A recent work evaluated the impact of a promising polymeric formulation used for the fabrication of MNs, based on PVME/MA, by means of *in vitro* (EpiSkin, reconstructed human epidermis) and *in vivo* models. The data demonstrated that the co-polymer, at concentrations comparable to (or higher than) those delivered by MNs, did not affect cell viability and did not promote the release of IL-1α — a proinflammatory marker — after 60 minutes of exposure. More importantly, the application of the dissolving MN arrays for 24 hours caused no irritation *in vivo*. Interestingly, the authors calculated that the dissolving MNs used in the study would deposit approximately 5 – 10 mg of polymer per cm^2 in the skin per application, which would correspond to a dose of 50 – 100 mg of polymer deposited by a patch with a size of 10 cm^2. [114,115] While this would not constitute a major hazard for single or limited number of applications, this aspect becomes very relevant in the context of repeat applications, such as in the case of chronic monitoring, potentially resulting in exposure to a significant dose of exogenous materials and related compatibility issues (polymer accumulation and irritation). To begin investigating this open question, the impact of repeated applications (up to 6 times over 6 weeks) of dissolving (Gantrez® S-97 BF/PVP) and hydrogel-forming (Gantrez® S-97 BF/PEG) MNs arrays was recently assessed in living immunocompetent mice. The study showed that the skin appearance and barrier function were not measurably altered throughout the experiments, and no infection, immunity, or inflammation biomarker alterations were observed.[116] Although more systematic research is needed to specifically examine the clearance, excretion, and compatibility problems of dermally delivered polymers, the final outcome would strongly depend on the nature of the material. While low MW non-degradable polymers would likely be drained by the lymphatic system and excreted renally (*e.g.* PVP), biodegradable polymers could be degraded *in situ* or after drainage.[117] For instance, fluorescently-labelled hydrophilic polymers of comparable MW to those used in dissolving MNs were recently demonstrated to be selectively drained by the lymphatic system and routed to the blood circulation, suggesting that MN polymers may experience a similar fate.[105] Nonetheless, this aspect represents an important line of investigation to be addressed before the effective clinical use of dissolving polymeric MNs for repeated administrations can be achieved.

Lymphatic and immune system assessment are only some of the various diagnostic applications of MNs. The examples reported here focus primarily on local diseases, or the stimulation of local responses. To our knowledge, no report has yet focused on the delivery of diagnostic agents for systemic distribution,

conceivable considering the use of MNs for systemic insulin delivery in diabetes management. However, future studies may focus on this application, benefitting from the knowledge gained through the study of MNs for drug delivery, opening the way for further needle-free diagnostic methods.

1.8. Translational Considerations

Though recent years have seen many advances in MN-based technology for diagnostic applications, these successes have not yet resulted in the development of clinically approved MN-based products, as mentioned previously. While this is to be expected as part of the development process of a novel technology, several key factors can be identified, which will need to be addressed before a consumer product can be envisioned. These aspects have primarily been considered in the context of MNs for the delivery of pharmaceutical products ([115] for an exhaustive discussion) but could, at least partially, be extended to the previously described monitoring applications.

Chief among these considerations is the scalability of current MN manufacturing procedures, and the ensuing costs of manufacturing these devices on a commercial scale. This is most apparent when considering silicon-based MNs, such as the hollow silicon MNs often used for fluid sampling, and the solid silicon MNs used for measuring biopotentials.[29-41,83-91] The micromachining process used to create such MNs requires cleanrooms, and high manufacturing costs are often cited as reasons for the introduction of new manufacturing protocols. With this in mind, alternatives to solid silicon MNs such as, polycarbonate and PMMA MNs have been both proposed, depending on the target application.[63,87,93] The use of alternative materials could also have an impact on the large-scale production of MNs. For example, a recent article has suggested a method of manufacturing hollow MNs from a thermoplastic polymer through a soft-embossing technique using heated metal plates to press the polymer into a premade mould.[118] Besides requiring less expensive materials and equipment than silicon-etching methods, this procedure could also facilitate the manufacturing of hollow MN-based devices on a commercial scale. Swellable hydrogel-based MNs have gained much attention recently, in part due to their simplicity relative to more complex silicon-based devices.[50] Despite this advantage, the fabrication of these MNs could nonetheless pose difficulties for commercial-scale translation, due to the high initial costs of the centrifuges used in their manufacture and the time required for their drying and crosslinking. As such, alternative production methods have been recently suggested, including roller-based manufacturing for larger-scale production[119] and microwave-assisted curing for faster drying and crosslinking.[120]

Another consideration relates to the mechanism of action of MNs, namely the fact that they pierce the *stratum corneum* to access the dermal ISF. This layer acts as the skin's protective barrier, and great care must be taken to avoid introducing microbes beneath it, where they could cause infection.[121] As such, it

can be expected that MNs will need to be sterilized for any clinical application. Though no specific guidelines currently exist, due to the novelty of MN-based technologies, based on FDA guidelines for medical devices which are in direct contact with lymphatic tissues, the endotoxin content in MNs should be <20 EU/device.[122] While fully aseptic preparation would ensure sterility, this could dramatically increase manufacturing costs, thereby generating interest in terminal sterilization methods, including heat and irradiation. Heat-sterilization would likely be suitable for some MNs, including solid metal and silicon arrays, but would be incompatible with dissolving polymer, hydrogel, or complex hollow MNs devices.[121] For such devices, gamma radiation has been explored as an alternative sterilization method. While the MNs themselves have been shown to be structurally unaffected by this sterilization method, the model protein contained within (ovalbumin) was found to be substantially degraded[121], suggesting that this technique could be poorly suited for MN devices containing protein-based detectors or sensitive diagnostic agents. Furthermore, an assessment has been conducted using swellable hydrogel-based MNs, demonstrating their resistance to microbial growth during storage.[123] This observation, coupled with data suggesting that microbes were unable to penetrate the epidermis of excised skin through MN channels, indicates that this class of MNs could mitigate the need for further sterilization measures.[123]

Finally, if these MNs are intended to serve as point-of-care devices, potentially for at-home use, it is important that they can be reliably inserted by untrained users. Reports from several groups have focused on this issue, with varying results. The earliest reports indicated that volunteers were able to reliably insert relatively longer MNs (> 550 μm) by hand, while shorter ones (~ 300 μm) required the use of a spring-loaded applicator.[124,125] Further studies have appeared to confirm that while manual pressure is sufficient to insert most MNs, better reproducibility is achieved using applicators.[126,127] Despite their reliability, the inclusion of an applicator device with each MN array could greatly increase the cost of commercial translation. To overcome this issue, novel methods have been explored for improving the reproducibility of the manual insertion of MNs, notably through the inclusion of a pressure-sensitive film on the back of each MN array.[128] By attaching this membrane, which displays a colour-change when pressure sufficient to breach the *stratum corneum* is applied to the MNs, a visual assurance is provided to users that the MNs have been correctly inserted. This, coupled with recent results showing that volunteers following written instructions were capable of reliably applying MN patches of variable sizes, suggests that manual insertion could be a viable technique upon clinical translation, for both drug delivery and diagnostic applications of MN technologies.[129,130]

The systematic evaluation of these translational aspects for each selected application and device, aside from their technological advances, will be of crucial importance for the actual involvement of the

MedTech industry in the commercial and clinical translation of MN-based diagnostic and monitoring devices.

1.9. Conclusions & Outlook

Recent advancements in MNs research as minimally invasive devices for diagnosing of systemic and local diseases, have taken developing point-of-care/lab-on-chip diagnostic methods to a new level. Time-consuming and invasive monitoring methods for systemic diseases, such as glucose measurement in diabetic patients and immunodiagnostics for infectious diseases can be potentially replaced by MN-based diagnostic devices and provide quality-of-life improvements for patients suffering from many health issues. The design of MNs can vary based on the targeted diagnostic application, for instance, hollow MNs fit a design that involves collecting considerable amounts of interstitial fluid, while hydrogel and dissolving MNs are suitable for the delivery of diagnostic agents. However, an ideal design is not necessarily linked to an easy and cost-effective manufacturing process. In this article, we reported the most important works on the development of MNs for diagnostic purposes and provided an in-depth comparison of the improvements offered by these designs, as well as the flaws they may present. Aside from this, MNs likely represent an ideal technology to non-invasively provide a link between the human body and rapidly developing new technologies for precise, real-time physiological monitoring. This could eventually allow for the early detection and recognition of health-related issues, as well as providing useful physiological information to inform lifestyle choice, leading to improved disease prevention.

1.10. Acknowledgements

The authors kindly acknowledge Dr. V. Agostoni for proof-reading and revising the manuscript. S.B., M.R. and D.B. gratefully acknowledge financial support from the Faculty of Pharmacy at the Université de Montréal, the Fonds de Recherche du Québec (Audace program), and the Canadian Generic Pharmaceutical Association and Biosimilars Canada, respectively.

1.11. References

[1] K. van der Maaden, W. Jiskoot, J. Bouwstra, *J. Control. Release* **2012**, *161*, 645.

[2] L. Eckhart, S. Lippens, E. Tschachler, W. Declercq, *Biochim. Biophys. Acta* **2013**, *1833*, 3471.

[3] C. Schoellhammer, D. Blankschtein, R. Langer, *Expert Opin. Drug Deliv.* **2014**, *11*, 393.

[4] M. R. Prausnitz, R. Langer, *Nat. Biotechnol.* **2008**, *26*, 1261.

[5] M. R. Prausnitz, *Diabetes Technol. Ther.* **2001**, *3*, 233.

[6] S. P. Davis, B. J. Landis, Z. H. Adams, M. G. Allen, M. R. Prausnitz, *J. Biomech.* **2004**, *37*, 1155.

[7] S. Hirobe, H. Azukizawa, K. Matsuo, Y. Zhai, Y.-S. Quan, F. Kamiyama, H. Suzuki, I. Katayama, N. Okada, S. Nakagawa, *Pharm. Res.* **2013**, *30*, 2664.

[8] A. L. Teo, C. Shearwood, K. C. Ng, J. Lu, S. Moochhala, *Mater. Sci. Eng. B* **2006**, *132*, 151.

[9] M. B. R. Pierre, F. C. Rossetti, *Curr. Drug Targets* **2014**, *15*, 281.

[10] T.-M. Tuan-Mahmood, M. T. C. McCrudden, B. M. Torrisi, E. McAlister, M. J. Garland, T. R. R. Singh, R. F. Donnelly, *Eur. J. Pharm. Sci.* **2013**, *50*, 623.

[11] S. Henry, D. V McAllister, M. G. Allen, M. R. Prausnitz, *J. Pharm. Sci.* **1998**, *87*, 922.

[12] L. Kulinsky, M. J. Madou, in *MEMs for Biomedical Applications* (Eds: S. Bhansali, A. Vasudev), Woodward Publishing Limited, Cambridge, UK, **2012**, pp. 218–268.

[13] N. G. Rouphael, M. Paine, R. Mosley, S. Henry, D. V. McAllister, H. Kalluri, W. Pewin, P. M. Frew, T. Yu, N. J. Thornburg, S. Kabbani, L. Lai, E. V. Vassilieva, I. Skountzou, R. W. Compans, M. J. Mulligan, M. R. Prausnitz, *Lancet* **2017**, *390*, 649.

[14] K. Ita, *Pharmaceutics* **2015**, *7*, 90.

[15] X. Liu, P. Kruger, H. Maibach, P. B. Colditz, M. S. Roberts, *Adv. Drug Deliv. Rev.* **2014**, *77*, 40.

[16] S. Sokhanvar, M. Shekhi, S. Mazlomzadeh, Z. Golmohammadi, *J. Cardiovasc. Thorac. Res.* **2011**, *3*, 57.

[17] W. H. Smart, K. Subramanian, *Diabetes Technol. Ther.* **2000**, *2*, 549.

[18] B. M. Koeppen, B. A. Stanton, in *Renal Physiology*, Mosby, Maryland Heights, US, **2013**, pp. 1-14.

[19] J. P. Bantle, W. Thomas, *J. Lab. Clin. Med.* **1997**, *130*, 436.

[20] F. J. Service, P. C. O'Brien, S. D. Wise, S. Ness, S. M. Leblanc, *Diabetes Care* **1997**, *20*, 1426.

[21] K. Rebrin, G. M. Steil, *Diabetes Technol. Ther.* **2000**, *2*, 461.

[22] P. J. Stout, N. Peled, B. J. Erickson, M. E. Hilgers, J. R. Racchini, T. B. Hoegh, *Diabetes Technol. Ther.* **2001**, *3*, 81.

[23] B. Q. Tran, P. R. Miller, R. M. Taylor, G. Boyd, P. M. Mach, C. N. Rosenzweig, J. T. Baca, R. Polsky, T. Glaros, *J. Proteome Res.* **2017**, *17*, 479.

[24] P. Khanna, J. A. Strom, J. I. Malone, S. Bhansali, *J. Diabetes Sci. Technol.* **2008**, *2*, 1122.

[25] P. M. Wang, M. Cornwell, M. R. Prausnitz, *Diabetes Technol. Ther.* **2005**, *7*, 131.

[26] T. Sato, S. Okada, K. Hagino, Y. Asakura, Y. Kikkawa, J. Kojima, T. Watanabe, Y. Maekawa, K. Isobe, R. Koike, H. Nakajima, K. Asano, *Diabetes Technol. Ther.* **2011**, *13*, 1194.

[27] Y. Ito, M. Taniguchi, A. Hayashi, M. Anai, S. Morita, E. Ko, N. Yoshimoto, Y. Yoshii, S. Kobuchi, T. Sakaeda, K. Takada, *Biol. Pharm. Bull.* **2014**, *37*, 1776.

[28] Y. Ito, Y. Inagaki, S. Kobuchi, K. Takada, T. Sakaeda, *Int. J. Med. Sci.* **2016**, *13*, 271.

[29] E. V. Mukerjee, S. D. Collins, R. R. Isseroff, R. L. Smith, *Sens. Actuators A Phys.* **2004**, *114*, 267.

[30] S. Zimmermann, D. Fienbork, B. Stoeber, A. W. Flounders, D. Liepmann, *12th International Conference on Solid-State Sensors, Actuators, and Microsystems* **2003**, pp 92-102.

[31] K. Kobayashi, H. Suzuki, *Sens. Actuators B Chem.* **2001**, *80*, 1.

[32] A. V. Ganesan, D. K. Kumar, A. Banerjee, S. Swaminathan, *13th International Conference on Nanotechnology* **2013**, pp. 557–560.

[33] T. R. R. Singh, H. McMillan, K. Mooney, A. Z. Alkilani, R. F. Donnelly, in *Microfluidic Devices for Biomedical Applications* (Eds: X. Li, Y. Zhou), Woodhead Publishing, Cambridge, UK, **2013**, pp. 185-230

[34] H. J. G. E. Gardeniers, R. Luttge, E. J. W. Berenschot, M. J. de Boer, S. Y. Yeshurun, M. Hefetz, R. van't Oever, A. van den Berg, *J. Microelectromech. Syst.* **2003**, *12*, 855.

[35] S.-J. Paik, S. Byun, J.-M. Lim, Y. Park, A. Lee, S. Chung, J. Chang, K. Chun, D. Cho, *Sens. Actuators A Phys.* **2004**, *114*, 276.

[36] R. Liu, X. H. Wang, F. Tang, Y. Y. Feng, Z. Y. Zhou, *13th International Conference on Solid-State Sensors, Actuators, and Microsystems* **2005**, pp. 1517–1520.

[37] L. M. Strambini, A. Longo, A. Diligenti, G. Barillaro, *Lab Chip* **2012**, *12*, 3370.

[38] W. H. Smart, K. Subramanian, US005801057A, **1998**.

[39] A. Jina, M. J. Tierney, J. A. Tamada, S. McGill, S. Desai, B. Chua, A. Chang, M. Christiansen, *J. Diabetes Sci. Technol.* **2014**, *8*, 483.

[40] H. Suzuki, T. Tokuda, K. Kobayashi, *Sens. Actuators B Chem.* **2002**, *83*, 53.

[41] H. Suzuki, T. Tokuda, T. Miyagishi, H. Yoshida, N. Honda, *Sens. Actuators B Chem.* **2004**, *97*,90.

[42] P. R. Miller, X. Xiao, I. Brener, D. B. Burckel, R. Narayan, R. Polsky, *Adv. Healthc. Mater.* **2014**, *3*, 876.

[43] A. V. Ganesan, *ASME 2013 International Mechanical Engineering Congress and Exposition* **2013**, pp. 1-5.

[44] S. E. Moulton, J. N. Barisci, A. Bath, R. Stella, G. G. Wallace, *J. Colloid Interface Sci.* **2003**, *261*, 312.

[45] J. D. Zahn, D. Trebotich, D. Liepmann, *1st Annual International IEEE-EMBS Special Topic Conference on Microtechnologies in Medicine & Biology* **2000**, pp. 1-6.

[46] J. D. Zahn, D. Trebotich, D. Liepmann, *Biomed. Microdevices* **2005**, *7*, 59.

[47] J. D. Zahn, Y.-C. Hsieh, M. Yang, *Diabetes Technol. Ther.* **2005**, *7*, 536.

[48] S. A. Ranamukhaarachchi, C. Padeste, M. Dübner, U. O. Häfeli, B. Stoeber, V. J. Cadarso, *Sci. Rep.* **2016**, *6*, 1.

[49] S. A. Ranamukhaarachchi, C. Padeste, U. O. Häfeli, B. Stoeber, V. J. Cadarso, *J. Micromech. Microeng.* **2018**, *28*.

[50] H. Chang, M. Zheng, X. Yu, A. Than, R. Z. Seeni, R. Kang, J. Tian, D. P. Khanh, L. Liu, P. Chen, C. Xu, *Adv. Mater.* **2017**, *29*.

[51] A. V. Romanyuk, V. N. Zvezdin, P. Samant, M. I. Grenader, M. Zemlyanova, M. R. Prausnitz, *Anal. Chem.* **2014**, *86*, 10520.

[52] E. Caffarel-Salvador, A. J. Brady, E. Eltayib, T. Meng, A. Alonso-Vicente, P. Gonzalez-Vazquez, B. M. Torrisi, E. M. Vicente-Perez, K. Mooney, D. S. Jones, S. E. J. Bell, C. P. McCoy, H. O. McCarthy, J. C. McElnay, R. F. Donnelly, *PLoS One* **2015**, *10*.

[53] E. Eltayib, A. J. Brady, E. Caffarel-Salvador, P. Gonzalez-Vazquez, A. Z. Alkilani, H. O. McCarthy, J. C. McElnay, R. F. Donnelly, *Eur. J. Pharm. Biopharm.* **2016**, *102*, 123.

[54] P. P. Samant, M. R. Prausnitz, *Proc. Natl. Acad. Sci. U. S. A.* **2018**, *115*, 4583.

[55] R. Hovorka, *Nat. Rev. Endocrinol.* **2011**, *7*, 385.

[56] J. Yu, Y. Zhang, Y. Ye, R. DiSanto, W. Sun, D. Ranson, F. S. Ligler, J. B. Buse, Z. Gu, *Proc. Natl. Acad. Sci. U. S. A.* **2015**, *112*, 8260.

[57] Imperial College London, Clinical Assessment of a Novel Microprobe Array Continuous Glucose

Monitor for Type 1 Diabetes, NCT01908530, https://clinicaltrials.gov/ct2/show/NCT01908530.

[58] K. Strimbu, J. A. Tavel, *Curr. Opin. HIV AIDS* **2010**, *5*, 463.

[59] D. Jenkins, S. Corrie, C. Flaim, M. Kendall, *RSC Adv.* **2012**, *2*, 3490.

[60] S. R. Corrie, G. J. P. Fernando, M. L. Crichton, M. E. G. Brunck, C. D. Anderson, M. A. F. Kendall, *Lab Chip* **2010**, *10*, 2655.

[61] A. Bhargav, D. A. Muller, M. A. F. Kendall, S. R. Corrie, *ACS Appl. Mater. Interfaces* **2012**, *4*, 2483.

[62] J. W. Coffey, S. R. Corrie, M. A. F. Kendall, *Biomaterials* **2013**, *34*, 9572.

[63] B. Yeow, J. W. Coffey, D. A. Muller, L. Grøndahl, M. A. F. Kendall, S. R. Corrie, *Anal. Chem.* **2013**, *85*, 10196.

[64] K. W. Ng, W. M. Lau, A. C. Williams, *Drug Deliv. Transl. Res.* **2015**, *5*, 387.

[65] K. T. Lee, D. A. Muller, J. W. Coffey, K. J. Robinson, J. S. McCarthy, M. A. F. Kendall, S. R. Corrie, *Anal. Chem.* **2014**, *86*, 10474.

[66] D. A. Muller, S. R. Corrie, J. Coffey, P. R. Young, M. A. Kendall, *Anal. Chem.* **2012**, *84*, 3262.

[67] American Academy of Neurology, Skin Test May Shed New Light on Alzheimer's and Parkinson's Diseases, https://www.aan.com/PressRoom/Home/PressRelease/1346, July, 2018.

[68] S. Paliwal, B. H. Hwang, K. Y. Tsai, S. Mitragotri, *Eur. J. Pharm. Sci.* **2013**, *50*, 546.

[69] F. A. Ellis, *J. Invest. Dermatol.* **1949**, *13*, 265.

[70] P. Martin, *Science* **1997**, *276*, 75.

[71] J. Gupta, H. S. Gill, S. N. Andrews, M. R. Prausnitz, *J. Control. Release* **2011**, *154*, 148.

[72] J. W. Coffey, S. C. Meliga, S. R. Corrie, M. A. F. Kendall, *Biomaterials* **2016**, *84*, 130.

[73] J. B. Haun, N. K. Devaraj, B. S. Marinelli, H. Lee, R. Weissleder, *ACS Nano* **2011**, *5*, 3204.

[74] A. A. Heikal, *Biomark. Med.* **2010**, *4*, 241.

[75] Y. Yoon, G. S. Lee, K. Yoo, J.-B. Lee, *Sensors*, **2013**, *13*, 16672.

[76] D. Chen, C. Wang, W. Chen, Y. Chen, J. X. J. Zhang, *Biosens. Bioelectron.* **2015**, *74*, 1047.

[77] C. Yuen, Q. Liu, *J. Biomed. Opt.* **2015**, *20*, 61102.

[78] P. R. Miller, S. A. Skoog, T. L. Edwards, D. M. Lopez, D. R. Wheeler, D. C. Arango, X. Xiao, S. M. Brozik, J. Wang, R. Polsky, R. J. Narayan, *Talanta* **2012**, *88*, 739.

[79] J. R. Windmiller, G. Valdés-Ramírez, N. Zhou, M. Zhou, P. R. Miller, C. Jin, S. M. Brozik, R. Polsky, E. Katz, R. Narayan, J. Wang, *Electroanalysis* **2011**, *23*, 2302.

[80] J. R. Windmiller, N. Zhou, M.-C. Chuang, G. Valdés-Ramírez, P. Santhosh, P. R. Miller, R. Narayan, J. Wang, *Analyst* **2011**, *136*, 1846.

[81] A. M. V. Mohan, J. R. Windmiller, R. K. Mishra, J. Wang, *Biosens. Bioelectron.* **2017**, *91*, 574.

[82] J.-X. Zhou, L.-N. Tang, F. Yang, F.-X. Liang, H. Wang, Y.-T. Li, G.-J. Zhang, *Analyst* **2017**, *142*, 4322.

[83] J. C. Lawler, M. J. Davis, E. C. Griffith, *J. Invest. Dermatol.* **1960**, *34*, 301.

[84] National Heart, Lung and Blood Institute, What is an Electrocardiogram?, https://www.nhlbi.nih.gov/health-topics/electrocardiogram, accessed: July, 2018.

[85] World Health Organization, The Top 10 Causes of Death, http://www.who.int/news-room/fact-sheets/detail/the-top-10-causes-of-death, accessed: July, 2018.

[86] E. Forvi, M. Bedoni, R. Carabalona, M. Soncini, P. Mazzoleni, F. Rizzo, C. O'Mahony, C. Morasso, D. G. Cassarà, F. Gramatica, *Sens. Actuators A Phys.* **2012**, *180*, 177.

[87] S. Rajaraman, J. A. Bragg, J. D. Ross, M. G. Allen, *J. Micromech. Microeng.* **2011**, *21*.

[88] P. Griss, P. Enoksson, H. K. Tolvanen-Laakso, P. Meriläinen, S. Ollmar, G. Stemme, *J. Microelectromech. Syst.* **2001**, *10*, 10.

[89] P. Griss, P. Enoksson, G. Stemme, *Sens. Actuators, A Phys.* **2002**, *95*, 94.

[90] L.-S. Hsu, S.-W. Tung, C.-H. Kuo, Y.-J. Yang, *Sensors* **2014**, *14*, 12370.

[91] D. G. Guo, F. E. H. Tay, L. Xu, L. M. Yu, M. N. Nyan, F. W. Chong, K. L. Yap, B. Xu, *6th International Workshop on Wearable and Implantable Body Sensor Networks* **2009**, pp. 125-130.

[92] S. H. Bariya, M. C. Gohel, T. A. Mehta, O. P. Sharma, *J. Pharm. Pharmacol.* **2012**, *64*, 11.

[93] F. Gramatica, R. Carabalona, M. Casella, C. Cepek, E. di Fabrizio, M. di Rienzo, L. Gavioli, M. Matteucci, F. Rizzo, M. Sancrotti, *3rd IEEE-EMBS International Summer School and Symposium on Medical Devices and Biosensors* **2006**, pp. 69-72.

[94] W. C. Ng, H. L. Seet, K. S. Lee, N. Ning, W. X. Tai, M. Sutedja, J. Y. H. Fuh, X. P. Li, *J. Mater. Process. Technol.* **2009**, *209*, 4434.

[95] L. M. Yu, F. E. H. Tay, D. G. Guo, L. Xu, M. N. Nyan, F. W. Chong, K. L. Yap, B. Xu, *The 7th IEEE Conference on Sensors* **2008**, pp. 1068–1071.

[96] C. O'Mahony, F. Pini, K. G. McCarthy, *Procedia Eng.* **2011**, *25*, 992.

[97] W. Pei, H. Zhang, Y. Wang, X. Guo, X. Xing, Y. Huang, Y. Xie, X. Yang, H. Chen, *IEEE Trans. Biomed. Eng.* **2017**, *64*, 463.

[98] K. Nagamine, J. Kubota, H. Kai, Y. Ono, M. Nishizawa, *Biomed. Microdevices* **2017**, *19*, 68.

[99] P. Griss, H. K. Tolvanen-Laakso, P. Meriläinen, G. Stemme, *IEEE Trans. Biomed. Eng.* **2002**, *49*, 597.

[100] D. Brambilla, S. T. Proulx, P. Marschalkova, M. Detmar, J.-C. Leroux, *Small* **2016**, *12*, 1053.

[101] K. Alitalo, *Nat. Med.* **2011**, *17*, 1371.

[102] E. M. Sevick-Muraca, S. Kwon, J. C. Rasmussen, *J. Clin. Invest.* **2014**, *124*, 905.

[103] A. Bollinger, K. Jäger, F. Sgier, J. Seglias, *Circulation* **1981**, *64*, 1195.

[104] A. Bollinger, B. R. Amann-Vesti, *Lymphology* **2007**, *40*, 52.

[105] S. T. Proulx, P. Luciani, A. Christiansen, S. Karaman, K. S. Blum, M. Rinderknecht, J.-C. Leroux, M. Detmar, *Biomaterials* **2013**, *34*, 5128.

[106] N. Kosaka, M. Ogawa, N. Sato, P. L. Choyke, H. Kobayashi, *J. Invest. Dermatol.* **2009**, *129*, 2818.

[107] B. Z. Igyártó, D. H. Kaplan, *Curr. Opin. Immunol.* **2013**, *25*, 115.

[108] S. Tokumoto, T. Matsudo, T. Kuwahara, US20100030100A1, **1998**.

[109] A. Trautmann, F. Heuck, R. Denfeld, P. Ruther, O. Paul, *19th IEEE International Conference on Microelectromechanical Systems* **2006**, pp. 434–437.

[110] W. Sun, Z. Araci, M. Inayathullah, S. Manickam, X. Zhang, M. A. Bruce, M. P. Marinkovich, A. T. Lane, C. Milla, J. Rajadas, M. J. Butte, *Acta Biomater.* **2013**, *9*, 7767.

[111] D. J. Unsworth, R. J. Lock, in *Advances in Clinical Chemistry, Vol. 65* (Ed: G. S. Makowski), Elsevier, Amsterdam, Netherlands, **2014**, pp. 173-198.

[112] Y. Ito, K. Matsumoto, N. Osakama, R. Yoshioka, S. Kobuchi, T. Sakaeda, K. Takada, *Biol. Pharm. Bull.* **2017**, *40*, 531.

[113] J. Jin, V. Reese, R. Coler, D. Carter, M. Rolandi, *Adv. Healthc. Mater.* **2014**, *3*, 349.

[114] M. T. C. McCrudden, A. Z. Alkilani, C. M. McCrudden, E. McAlister, H. O. McCarthy, A. D. Woolfson, R. F. Donnelly, *J. Control. Release* **2014**, *180*, 71.

[115] R. F. Donnelly, in *Microneedles for Drug and Vaccine Delivery and Patient Monitoring* (Eds: R. F. Donnelly, T. R. R. Singh, E. Larrañeta, M. T. C. McCrudden), Wiley, Hoboken, New Jersey, **2018**, pp. 307-322.

[116] E. M. Vincente-Pérez, E. Larrañeta, M. T. C. McCrudden, A. Kissenpfennig, S. Hegarty, H. O. McCarthy, R. F. Donnelly, *Eur. J. Pharm. Biopharm.* **2017**, *117*, 400.

[117] L. Arisz, B. P. Hazenberg, A. van Zanten, E. Mandema, *Acta Med. Scand.* **1969**, *186*, 393.

[118] Z. F. Rad, R. E. Nordon, C. J. Anthony, L. Bilston, P. D. Prewett, J.-Y. Arns, C. H. Arns, L. Zhang, G. J. Davies, *Microsyst. Nanoeng.* **2017**, *3*.

[119] R. E. M. Lutton, E. Larrañeta, M.-C. Kearney, P. Boyd, A. D. Woolfson, R. F. Donnelly, *Int. J. Pharm.* **2015**, *494*, 417.

[120] E. Larrañeta, R. E. M. Lutton, A. J. Brady, E. M. Vincente-Pérez, A. D. Woolfson, R. R. S. Thakur, R. F. Donnelly, *Macromol. Mater. Eng.* **2015**, *300*, 586.

[121] M. T. C. McCrudden, A. Z. Alkilani, A. J. Courtenay, C. M. McCrudden, B. McCloskey, C. Walker, *N.* Alshraiedeh, R. E. M. Lutton, B. F. Gilmore, A. D. Woolfson, R. F. Donnelly, *Drug Deliv. Transl. Res.* **2015**, *5*, 3.

[122] M. Leone, J. Mönkäre, J. A. Bouwstra, G. Kersten, *Pharm. Res.* **2017**, *34*, 2223.

[123] R. F. Donnelly, T. R. R. Singh, A. Z. Alkilani, M. T. C. McCrudden, S. O'Neill, C. O'Mahony, K. Armstrong, N. McLoone, P. Kole, A. D. Woolfson, *Int. J. Pharm.* **2013**, *451*, 76.

[124] F. J. Verbaan, S. M. Bal, D. J. van den Berg, W. H. H. Groenink, H. Verpoorten, R. Lüttge, J. A. Bouwstra, *J. Control. Release*, **2007**, *117*, 238.

[125] F. J. Verbaan, S. M. Bal, D. J. van den Berg, J. A. Dijksman, M. van Hecke, H. Verpoorten, A. van den Berg, R. Lüttge, J. A. Bouwstra, *J. Control. Release*, **2008**, *128*, 80.

[126] J. J. Norman, J. M. Arya, M. A. McClain, P. M. Frew, M. I. Meltzer, M. R. Prausnitz, *Vaccine*, **2014**, *32*, 1856.

[127] K. van der Maaden, E. Sekerdag, W. Jiskoot, J. Bouwstra, *AAPS J.*, **2014**, *16*, 681.

[128] E. M. Vincente-Pérez, H. L. Quinn, E. McAlister, S. O'Neill, L.-A. Hanna, J. G. Barry, R. F. Donnelly, *Pharm. Res.* **2016**, *33*, 3072.

[129] R. F. Donnelly, K. Moffatt, A. Z. Alkilani, E. M. Vincente-Pérez, J. Barry, M. T. C. McCrudden, A. D. Woolfson, *Pharm. Res.* **2014**, *31*, 1989.

[130] A. Ripolin, J. Quinn, E. Larrañeta, E. M. Vincente-Pérez, J. Barry, R. F. Donnelly, *Int. J. Pharm.* **2017**, *521*, 92.

Hypothesis and Research Objectives

Hypothesis

As evidenced in the preceding chapter (**Chapter 1**), microneedles (MNs) have attracted a great deal of attention for their potential diagnostic applications, in addition to their more well-known applications for the delivery of therapeutics. Among these, dissolving polymeric MNs represent a relatively novel approach for the delivery of diagnostic agents, with much opportunity for further development and investigation. With this in mind, my research hypothesis is as follows:

Dissolving polymeric microneedles can be used to deliver specially designed fluorescent probes to the skin, creating a sort of fluorescent microneedle *tattoo* capable of providing health-related information.

Research Objectives

To demonstrate the above hypothesis, I pursued the following research objectives:

1. Develop dissolving polymeric MNs for delivery of a functional sensor to skin, capable of generating a fluorescent signal in response to the presence of reactive oxygen species (ROS).

This objective is focused on a relatively novel concept, which will involve the synthesis of a fluorescent ROS-sensor suitable for use in the skin, optimization of a MN formulation compatible with this sensor, and detection of ROS with a tattoo delivered by the resulting MNs. Work undertaken towards this objective is outlined in **Chapter 2**

2. Optimize a MN-based system for delivering a fluorescent tracer to monitor normal and impaired lymphatic drainage.

This objective is focused on optimizing and improving a recently developed MN system for delivering a fluorescent dye for imaging and monitoring lymphatic drainage. This will consist of the synthesis of an appropriate and selective fluorescent tracer and improving the MN system used for dermal delivery of the tracer. Work undertaken towards this objective is outlined in **Chapter 3**.

Chapter 2

The use of MNs for the delivery of diagnostic agents to the skin is quite novel, and previous examples have largely been limited to the delivery of inert fluorescence contrast agents. If this technology could be expanded to allow for the delivery of functional fluorescent sensors, the impact could be significant, allowing real-time non-invasive monitoring of a vast array of physiological parameters. The detection of reactive oxygen species (ROS) through the delivery of an oxidation sensitive fluorescent dye could serve as a useful proof-of-concept, as many oxidation-sensitive dyes have been described, and ROS are known to be present in the skin under certain pathological conditions. A ROS-sensor (H-Cy5-PEG) was synthesized and characterized, and displayed promising ROS-sensing capabilities suitable for use in the skin. A dissolving polymeric MN delivery system was optimized for use with H-Cy5-PEG, to avoid oxidizing the sensitive probe during the manufacturing process. This system allowed for the delivery of H-Cy5-PEG as a ROS-sensitive MN tattoo, with the probe remaining active after incorporation into the system and subsequent delivery to skin-simulating gels. Ultimately, functionality of the system *ex vivo* or *in vivo* was held back by instrument sensitivity and the relatively low fluorescence recovery of H-Cy5-PEG after fabrication and delivery.

A microneedle tattoo for real-time ROS monitoring in inflammatory skin conditions

Samuel Babity[1] *and Davide Brambilla*[1,*]

[1]Faculté de Pharmacie, Université de Montréal, C.P. 6128, Succursale Centre-ville, Montréal, Québec H3C 3J7, Canada.

*Corresponding author: davide.brambilla@umontreal.ca

2.1. Abstract

The field of precision health monitoring could be greatly helped by the development of real-time, non-invasive sensing and detection methods for various physiological analytes. A promising approach consists of using dissolving polymeric microneedles (MNs) to deliver an active fluorescent sensor directly to the skin for real-time monitoring *in situ* — effectively a medical tattoo. Reactive oxygen species (ROS) — oxygen species containing unpaired radical electrons — are associated with various pathological conditions and are known to be present in the skin. As such, they present an interesting and relevant analyte to detect using this MN tattoo system. In this work, we present a proof-of-concept MN-delivered tattoo capable of sensing reactive oxygen species (ROS) in skin-simulating agarose gels.

Keywords: diagnostic, microneedles, monitoring, tattoo, ROS

2.2. Introduction

In recent years, there has been a growing interest in precision health monitoring, particularly in the context of early disease detection and preventative medicine. Although most medical diagnosis takes place after the presentation of symptoms, earlier detection and preventative monitoring could allow for more effective treatment.[1] While this sort of preventative monitoring is an attractive concept, its utility has historically been limited by the invasive nature of implantable devices or blood sampling. In recent years, this has led to research into less invasive forms of biosensing, with many examples proposing optical, fluorescence-based techniques for direct *in vivo* imaging.[2,3] To this end, other monitoring targets have also been proposed, notably dermal interstitial fluid (ISF): the extracellular fluid surrounding cells in the dermal and epidermal layers of the skin. Recent studies have suggested that there is an overlap of roughly 93% between the proteomes expressed in plasma and in the ISF.[4] Additionally, similar populations of small molecules and ions have been observed, with alterations in plasma levels rapidly reflected in the ISF, suggesting that this fluid could provide an alternative to blood-based monitoring for many biological analytes.[5,6] Among the advantages of ISF-based monitoring is ease-of-access; owing to its proximity to the surface of the skin, beginning at depths of less than 50 μm (directly beneath the *stratum corneum*), it could be reached using relatively non-invasive techniques. One such technique involves the use of microneedles (MNs): miniaturized needles with lengths below 1 mm, often organized into an array.[7] Short enough to avoid activating pain-sensing neurons found deeper in the dermis, MNs can nonetheless easily breach the *stratum corneum*, providing a means of accessing the ISF. Studies have attempted to exploit this feature, using hollow or swellable polymer MNs to withdraw ISF through the skin for external analysis.[8,9] However, this method has shown significant limitations, including the high cost of hollow MN-based devices, and the low volumes extracted using swellable polymers.[10] This has led to interest in an alternative approach, namely the use of dissolving polymeric MNs for the delivery of sensors directly to the dermis, allowing instantaneous *in situ* analysis. These soluble MNs, often made from polysaccharides or other biocompatible polymers, have the advantages of simple, solvent-casting-based manufacturing from inexpensive, readily-available materials, and generating no sharp waste after use.[11] An early example of this approach has been seen in the context of the imaging and quantification of lymphatic drainage. By delivering an inert NIR-fluorescent dye it is possible to non-invasively image the lymphatic vessels in real-time, important in the context of detection of structural modification involved in several diseases such as cancer, inflammation and lymphedema.[12,13] While this approach highlighted the use of MNs for the delivery of diagnostics, only an inert probe was delivered; by instead delivering an active fluorescent sensor, the scope of this biosensing technique could be greatly increased. Examples of specific, sensitive, and bright fluorescent probes exist for a variety of physiological analytes; by delivering these sensors directly to the dermis, MNs could be used to create a sort of *medical tattoo*, which could then be read with a fluorescence detector, permitting

real-time monitoring. While similar concepts have been proposed, using sweat-based analysis[14] or the subcutaneous implantation of cells[15], MNs could present an ideal delivery system, potentially allowing non-invasive monitoring of a broad range of analytes.

Reactive oxygen species (ROS) are highly reactive oxygen compounds which occur *in vivo*, often containing unpaired radical electrons, and are involved in signaling mechanisms and other biological processes.[16] ROS are also associated with disease, and elevated levels can lead to oxidative stress, resulting in DNA damage, cell death, and the development of a variety of pathological conditions, including disorders of the skin; specifically, exposure to UV radiation has been demonstrated to induce the production of dermal ROS.[17] The oxidative stress caused by these ROS can lead to the production of proinflammatory cytokines, associated with psoriasis[18] and skin aging,[19,20] as well as DNA damage associated with carcinogenesis.[21] In light of this, there has been interest in the monitoring of ROS in the skin to better understand these conditions and to potentially evaluate their progression and treatment.[22] ROS also present an attractive target for fluorescent sensing, as a variety of molecules exist which display little to no fluorescence in their reduced states, but display bright fluorescence in their oxidized forms, allowing them to act as specific fluorescent ROS sensors. Among these, hydrocyanines are a class of bright, easily prepared dyes displaying specific sensitivity to superoxide and hydroxyl radicals, two of the most biologically relevant ROS.[23] Probes based on this class of sensor have been applied for a variety of uses, ranging from the optimization of ELISA assays to the *in vivo* imaging of inflammation or tumours.[24-26] Further, examples of hydrocyanines exist with fluorescence at red and near-infrared (NIR) wavelengths, which could allow better imaging *in vivo*, as the skin displays far less background interference at these higher wavelengths.[27] Potential applications in the skin have been limited, however, by their relatively poor water-solubility and small size, rendering them prone to cellular uptake. By developing PEGylated hydrocyanine derivatives, we have addressed both of these issues, effectively creating a soluble extracellular ROS probe.[28] In this work, we have developed a dissolving polymeric MN-based delivery system for PEGylated hydrocyanines, capable of detecting and imaging in skin-simulating agarose gels.

2.3. Experimental

2.3.1. Materials

Poly(vinyl alcohol) (10 kDa) (PVA), Dextran (from Leuconostoc spp. Mr ~ 6,000 Da), diisopropylethylamine (DIPEA), dimethyl sulfoxide (DMSO), *N,N'*-diphenylformamidine, disuccinimydal carbonate (DSC), iodomethane (MeI), malondialdehyde bis(phenylimine) monohydrochloride, nitromethane (CH_3NO_2), and 2,3,3-trimethylindolenine were purchased from Sigma-Aldrich (St. Louis, MO). Acetic anhydride (Ac_2O), acetonitrile (ACN), dichloromethane (DCM), diethyl ether (Et_2O), ethyl

acetate (EtOAc), hydrochloric acid (HCl, 37 wt%, aq), hydrogen peroxide (30% v/v), methanol (MeOH), sodium chloride (NaCl), sodium sulfate (Na_2SO_4, anhydrous), potassium iodide (KI), and pyridine were purchased from Fisher Scientific (Waltham, MA). 6-bromohexanoic acid and iron sulfate heptahydrate ($FeSO_4 \cdot 7H_2O$) were purchased from Acros Organics (Fair Lawn, NJ). Sephadex G-15 was purchased from GE Life Sciences (Pittsburgh, PA). Ultra-low molecular weight hyaluronic acid (< 6 kDa) (ULMW HA) and super-low molecular weight hyaluronic acid (< 50 kDa) were purchased from Lotioncrafter (Eastsound, WA). Poly(*N*-vinylpyrrolidone) (3.5 – 7 kDa) (PVP K-12) was generously provided by BASF (Ludwigshafen, Germany). 230 – 400 mesh silica columns were purchased from SiliCycle Inc. (Québec, QC) and chromatographic separations were performed using a CombiFlash Rf 150 (Teledyne Isco Inc., Lincoln, NE). Samples were concentrated *in vacuo* on the Rotavapor R-100 and heated using the B-100 heating bath (Büchi, Uster, Switzerland). ^{1}H-NMR spectra were recorded on a Varian MR400 NMR (Varian Inc., Palo Alto, CA). Chemical shifts are expressed in parts per million (ppm) and coupling constants are reported in hertz (Hz). Splitting patterns are indicated as: br = broad; s = singlet; d = doublet; dd = doublet of doublets; t = triplet; m = multiplet. LC-MS analyses were performed on a 6120 Quadrupole LC/MS provided by Agilent Technologies (Santa Clara, CA). Square pyramidal female MN moulds of room temperature vulcanizing silicone, 10 × 10 or 15 × 15 array, 250 µm × 250 µm × 800/600/500 µm (W × L × H) were purchased from Micropoint Technologies Pte. Ltd. (Singapore).

2.3.2. Synthesis of Cy5

*2.3.2.1. 1,2,3,3-Tetramethyl-3H-indol-1-ium iodide (**S1**)*

S1 was synthesized using a previously described procedure.[29] Briefly, 2,3,3-Trimethylindolenine (2.52 mL, 15.7 mmol, 1 eq) was diluted in 9 mL nitromethane (CH_3NO_2). Iodomethane (MeI) (1.95 mL, 31.4 mmol, 2 eq) was added dropwise and the reaction mixture was stirred at room temperature for 20 h. The crude product was precipitated using 60 mL of Et_2O, and the resulting purple solid was collected by vacuum filtration and washed 3× with 15 mL of Et_2O. A pale purple solid was obtained (4.17 g, 13.8 mmol, 88% yield). (**Figure 2.S1**). **^{1}H NMR** (Varian, 400 MHz, DMSO): δ = 7.91 – 7.88 (m, 1H), 7.82 – 7.80 (m, 1H), 7.63 – 7.57 (m, 2H), 3.96 (s, 3H), 2.75 (s, 3H), 1.51 (s, 6H);

*2.3.2.2. 1-(5-Carboxylpentyl)-2,3,3-trimethyl-3H-indol-1-ium iodide (**S2**)*

S2 was synthesized by adapting a previously described procedure.[30] Briefly, 2,3,3-Trimethylindolenine (1.60 mL, 10 mmol, 1 eq) and 6-bromohexanoic acid (1.95 g, 10 mmol, 1 eq) were dissolved in 6 mL acetonitrile (ACN). Potassium iodide (KI) (1.66 g, 10 mmol, 1 eq) was added and the reaction mixture was refluxed at 85 °C for 16 h. The mixture was filtered, concentrated under reduced pressure, and the crude product was precipitated using 40 mL of 1:1 ethyl acetate/DCM at -20 °C. The

resulting pink solid was collected by vacuum filtration and washed 3× with 5 mL of 1:1 ethyl acetate/DCM. A light purple solid was obtained (2.38 g, 5.9 mmol, 59% yield). (**Figure 2.S2**). **^{1}H NMR** (Varian, 400 MHz, DMSO): δ = 12.00 (br. s, 1H), 7.99 – 7.94 (m, 1H), 7.85 – 7.81 (m, 1H), 7.63 – 7.58 (m, 2H), 4.44 (t, *J* = 7.8 Hz, 2H), 2.84 (s, 3H), 2.21 (t, *J* = 7.2 Hz, 2H), 1.83 (m, 2H), 1.58 – 1.50 (m, 8H), 1.45 – 1.39 (m, 2H);

2.3.2.3. Cyanine-5 (Cy5)

Cy5 was synthesized by adapting a previously described procedure.[29] Briefly, **S2** (648 mg, 1.8 mmol, 1 eq) and malondialdehyde bis(phenylimine) monohydrochloride (521 mg, 2.0 mmol, 1.1 eq) were dissolved in 6 mL of acetic anhydride (Ac_2O) and the mixture was refluxed at 120 °C for 30 min. **S1** (660 mg, 2.2 mmol, 1.2 eq) was suspended in 6 mL of dry pyridine and added to the reaction mixture. The reaction was stirred for 18 h at room temperature in the dark. The solvents were removed under reduced pressure at 60 °C. The blue solid was dissolved in 10 mL DCM and washed 4× with 40 mL dH_2O, 1× with 40 mL of 1 M $HCl_{(aq)}$, and 1× with 40 mL of sat. NaCl. The organic layer was dried over Na_2SO_4 and concentrated under reduced pressure. The crude mixture was purified by column chromatography, eluting with ethyl acetate, followed by a gradient of 0 – 10% MeOH in DCM. Cy5 was obtained as a metallic red-blue solid (486 mg, 0.93 mmol, 51% yield). (**Figure 2.S3**). **^{1}H NMR** (Varian, 400 MHz, DMSO): δ = 12.04 (br. s, 1H), 8.32 (t, *J* = 13.1 Hz, 2H), 7.60 (d, *J* = 7.4 Hz, 2H), 7.41 – 7.35 (m, 4H), 7.26 – 7.19 (m, 2H), 6.55 (t, *J* = 12.3 Hz, 1H), 6.27 (dd, *J* = 16.8 Hz, 14.1 Hz, 2H), 4.07 (t, *J* = 7.0 Hz, 2H), 3.58 (s, 3H), 2.28 (t, *J* = 7.2 Hz, 1H), 2.18 (t, *J* = 7.2 Hz, 1H), 1.76 – 1.61 (m, 14H), 1.58 – 1.49 (m, 2H), 1.40 – 1.32 (m, 2H);

2.3.3. Synthesis of Cy5-PEG

2.3.3.1. Cyanine-5 N-hydroxysuccinimide ester (Cy5-NHS)

Cy5 was activated as Cy5-NHS by adapting a previously described procedure.[29] Briefly, Cy5 (486 mg, 0.93 mmol, 1 eq) was dissolved in 10 mL of dry DCM. Diisopropylethylamine (DIPEA) (326 µL, 1.87 mmol, 2 eq) and disuccinimydal carbonate (DSC) (536 mg, 2.06 mmol, 2.2 eq) were added and the reaction was stirred for 24 h at room temperature in the dark. The mixture was diluted with 10 mL DCM and washed 4× with 40 mL dH_2O, 1× with 40 mL of 1 M $HCl_{(aq)}$, and 1× with 40 mL of sat. NaCl. The organic layer was dried over Na_2SO_4 and dried under reduced pressure to give Cy5-NHS as a metallic red-blue solid (544 mg, 0.88 mmol, 95% yield). The purity of the product was confirmed by HPLC-MS analysis. (**Figure 2.S4**).

2.3.3.2. Cyanine-5-PEG (Cy5-PEG)

Cy5-PEG was synthesized by adapting a previously described procedure.[28] Briefly, Cy5-NHS (7.4 mg, 12 µmol, 2 eq) and MeO-PEG-NH_2 (MW = 5,000 g/mol) (30 mg, 6 µmol, 1 eq) were dissolved in 1 mL of anhydrous DMSO, and the mixture was stirred for 18 h in the dark. Then, the mixture was diluted in

20 mL of milli-Q H_2O and lyophilized. The resulting residue was dissolved in 1 mL of 180 mM NaCl and purified on G-15 Sephadex. The resulting fractions were combined and lyophilized, giving Cy5-PEG as a blue solid (28 mg, 5.6 µmol, 86% yield). The purity of the product was confirmed by HPLC-MS analysis.

2.3.4. Synthesis of Cy3-PEG

2.3.4.1. Cyanine-3 (Cy3)

Cy3 was synthesized by adapting a previously described procedure.[29] Briefly, **S3** (734 mg, 1.8 mmol, 1 eq) and *N,N'*-Diphenylformamidine (395 mg, 2.0 mmol, 1.1 eq) were dissolved in 5 mL of acetic anhydride (Ac_2O) and the mixture was refluxed at 130 °C for 30 min. **S1** (660 mg, 2.2 mmol, 1.2 eq) was suspended in 5 mL of dry pyridine and added to the reaction mixture. The reaction was stirred for 16 h at room temperature in the dark. The solvents were removed under reduced pressure at 60 °C. The pink solid was dissolved in 10 mL DCM and washed 4× with 40 mL dH_2O, 1× with 40 mL of 1 M $HCl_{(aq)}$, and 1× with 40 mL of sat. NaCl. The organic layer was dried over Na_2SO_4 and concentrated under reduced pressure. The crude mixture was purified by column chromatography, eluting with ethyl acetate, followed by a gradient of 0 – 10% MeOH in DCM. Cy3 was obtained as a metallic green-gold solid (479 mg, 0.99 mmol, 54% yield). (**Figure 2.S5**). **^{1}H NMR** (Varian, 400 MHz, DMSO): δ = 12.05 (br. s, 1H), 8.33 (t, *J* = 13.5 Hz, 1H), 7.62 (d, *J* = 7.4 Hz, 2H), 7.45 – 7.41 (m, 4H), 7.31 – 7.25 (m, 2H), 6.49 (dd, *J* = 13.3 Hz, 4.3 Hz, 2H), 4.09 (t, *J* = 7.4 Hz, 2H), 3.64 (s, 3H), 2.20 (t, *J* = 7.2 Hz, 2H), 1.73 – 1.67 (m, 14H), 1.58=9 – 1.52 (m, 2H), 1.45 – 1.39 (m, 2H);

2.3.4.2. Cyanine-3 N-Hydroxysuccinimide ester (Cy3-NHS)

Cy3 was activated as Cy3-NHS by adapting a previously described procedure.[29] Briefly, Cy3 (479 mg, 0.99 mmol, 1 eq) was dissolved in 10 mL of dry DCM. Diisopropylethylamine (DIPEA) (345 µL, 1.98 mmol, 2 eq) and disuccinimydal carbonate (DSC) (567 mg, 2.18 mmol, 2.2 eq) were added and the reaction was stirred for 24 h at room temperature in the dark. The mixture was diluted with 10 mL DCM and washed 4× with 40 mL dH_2O, 1× with 40 mL of 1 M $HCl_{(aq)}$, and 1× with 40 mL of sat. NaCl. The organic layer was dried over Na_2SO_4 and dried under reduced pressure to give Cy3-NHS as a metallic green-gold solid (554 mg, 0.94 mmol, 95% yield). The purity of the product was confirmed by HPLC-MS analysis. (**Figure 2.S6**).

2.3.4.3. Cyanine-3-PEG (Cy3-PEG)

Cy3-PEG was synthesized by adapting a previously described procedure.[28] Briefly, Cy3-NHS (7.1 mg, 12 µmol, 2 eq) and MeO-PEG-NH_2 (MW = 5,000 g/mol) (30 mg, 6 µmol, 1 eq) were dissolved in 1 mL of anhydrous DMSO, and the mixture was stirred for 18 – 24 h in the dark. Then, the mixture was diluted in 20 mL of milli-Q H_2O and lyophilized. The resulting residue was dissolved in 1 mL of 180 mM

NaCl and purified on G-15 Sephadex. The resulting fractions were combined and lyophilized, giving Cy3-PEG as a pink solid (30 mg, 5.9 μmol, 92% yield). The purity of the product was confirmed by HPLC-MS analysis.

2.3.5. Reduction of the cyanine dye (H-Cy5, H-Cy5-PEG)

Cy5 and Cy5-PEG were converted to their reduced forms (H-Cy5 and H-Cy5-PEG) using a previously described procedure.[29] Unconjugated Cy5 (1 mg, 1.93 μmol, 1 eq) was dissolved in 300 μL of MeOH and 500 μL of a 1 mg/mL solution of $NaBH_4$ in MeOH (13.2 μmol, 6.8 eq) was added. Cy5-PEG (5.3 mg, 0.96 μmol, 1 eq) was dissolved in 150 μL of 1:1 MeOH/degassed H_2O, and 250 μL of a 1 mg/mL solution of $NaBH_4$ in MeOH (7.9 μmol, 8 eq) was added. The loss of blue colour indicated that the reaction had occurred, yielding H-Cy5 or H-Cy5-PEG. The fluorescence intensity was measured using a Spark® multimode fluorescence microplate reader (Tecan Group, Ltd., Männedorf, Switzerland), and the reduction was considered complete if the value obtained was < 500 (λ_{ex} = 630 nm, λ_{em} = 675 nm, gain 125).

2.3.6. Re-oxidation with Fenton's Reagent in solution

The re-oxidation of H-Cy5 and H-Cy5-PEG was carried out by adapting a previously described procedure.[29] A 10 μM solution of H-Cy5 or H-Cy5-PEG was prepared in H_2O. $FeSO_4$ and H_2O_2 were added, yielding final concentrations of 5 μM – 100 μM and 50 μM – 1 mM respectively. The fluorescence (λ_{ex} = 630 nm, λ_{em} = 675 nm) intensity was monitored over 1 h at 23 °C in a black 96-well plate (Brand GMBH & Co., Wertheim, Germany) using a Spark® multimode fluorescence microplate reader (Tecan Group Ltd., Männedorf, Switzerland).

2.3.7. Stability of H-Cy5 and H-Cy5-PEG in polymer solutions

The stability of H-Cy5 or H-Cy5-PEG in common MN polymers was determined by mixing the dyes with concentrated solutions of the polymers and observing the fluorescence over time. Solutions of polymer were prepared in 5mL H_2O at the appropriate concentrations (250 mg/mL for PVP K-12, Dextran, ULMW HA, and (8:1) ULMW HA/Dex; 167 mg/mL for PVA; and 51.4 mg/mL for SLMW HA). H-Cy5 or H-Cy5-PEG-5k was added to each solution for a final concentration of 10 μM. These solutions were stored in the dark, samples were periodically taken over a 24 h period, and their fluorescence (λ_{ex} = 630 nm, λ_{em} = 675 nm) was monitored at 23 °C in a black 96-well plate (Brand GMBH & Co., Wertheim, Germany) using a Spark® multimode fluorescence microplate reader (Tecan Group Ltd., Männedorf, Switzerland).

2.3.8. Preparation of H-Cy5/Cy3-loaded MNs

MNs were manufactured by adapting a previously described solvent casting method.[12] Briefly, to 2 mL of distilled H_2O, ULMW Hyaluronic Acid (1.917 g, 319.5 µmol) and dextran (0.234 g, 39 µmol) were added and mixed thoroughly. The mixture was heated for 30 mins in a 75 °C oven and centrifuged (Sorvall ST 16R, ThermoFisher Scientific, Waltham, MA) for 5 mins at 4700 *g*. H-Cy5 and Cy3 (or H-Cy5-PEG and Cy3-PEG) were added, resulting in concentrations of 250 µM (H-Cy5) and 10 µM (Cy3) respectively. Using a 1 mL syringe, roughly 100 µL of this solution was cast into PDMS moulds (Micropoint Technologies Pte. Ltd., Singapore) and these molds were secured with tape in 6-well cell culture plates (Sarstedt AG & Co., Nümbrecht, Germany). The plates were covered, secured with parafilm, and centrifuged for 5 mins at 2300 *g*. After centrifugation, polymer solution was re-applied, and the plates were rotated 180° and centrifuged again. This process was repeated a total of four times. After the final centrifugation, any excess polymer solution was removed from the molds using a spatula, and they were placed in a vacuum chamber at 150 mbar for 30 minutes. Roughly 100 µL of dye-free polymer solution was added to each mold, and they were allowed to dry for 18 – 24 h at 25 °C and 60 % humidity, after which the MNs were removed from the moulds (**Figure 2.S7**).

2.3.9. Characterization of mechanical properties of MNs

The failure force of the MNs was evaluated using a TA.XT-Plus Texture Analyser (Stable Micro Systems, Surrey, UK) in compression mode. MNs were prepared as previously described, without addition of dye, and with or without addition of 5 % w/w of PEG-NH_2 (5 kDa). MNs were placed on an aluminum plate and a cylindrical stainless-steel probe (6 mm diameter) was moved towards the MNs. The probe moved at 1.2 $mm \cdot s^{-1}$, with a maximum travel distance of 300 µm (sufficient to induce MN deflection). The MN failure force was measured as the maximum of the force-time curve.[31]

2.3.10. Determination of logP of PEGylated cyanines

The logP values of Cy5-PEG and Cy3-PEG were experimentally determined using the established shake-flask method.[32] A 5 mg/mL solution of either Cy5-PEG or Cy3-PEG was prepared in DMSO, and a 20 µL sample was diluted using 480 µL of water-saturated *n*-octanol. The samples were stirred on a Vortemp 56 (Labnet, Edison, NJ) for 5 minutes at 500 rpm, then centrifuged for 5 minutes at 2000 rpm (Mikro 120, Hettich, Tuttlingen, Germany). Five hundred µL of phosphate buffer (pH = 6.8) was added, and samples were stirred for 24 – 48 hours, then centrifuged for 5 minutes at 2000 rpm. Fifty µL of the organic phase was diluted in 450 µL of acetone and 500 µL of a 1:1 mixture of acetonitrile (ACN) and H_2O; and 50 µL of the aqueous phase was diluted in 450 µL of a 1:1 mixture of ACN and H_2O. The

fluorescence intensity (λ_{ex} = 630 nm, λ_{em} = 675 nm for Cy5-PEG; λ_{ex} = 530 nm, λ_{em} = 575 nm for Cy3-PEG) was monitored at 23 °C in a black 96-well plate (Brand GMBH & Co., Wertheim, Germany) using a Spark® multimode fluorescence microplate reader (Tecan Group Ltd., Männedorf, Switzerland).

2.3.11. Re-oxidation with Fenton's Reagent in agarose gels

A 3 % w/w solution of agarose in water was prepared using a standard microwave, and 5 mL portions were dispensed into the wells of a 12-well cell culture plate (Sarstedt AG & Co., Nümbrecht, Germany). Immediately, $FeSO_4$ and H_2O_2 (or an equivalent volume of H_2O) were added, yielding final concentrations of 5 µM – 50 µM and 50 µM – 500 µM respectively. The wells were mixed thoroughly using a glass rod and allowed to cool and solidify for 2 – 3 h. Using a commercially available spring-loaded applicator generating an impact rate of 2 $m \cdot s^{-1}$, an impact force of 1.6 N, and with a spring constant of 1 $N \cdot mm^{-1}$ (values provided by the manufacturer, Micropoint Technologies Pte. Ltd., Singapore), dye-loaded MNs were applied to the gels for approximately 90 seconds using a spring-loaded applicator, until the tips had fully dissolved. The fluorescence (λ_{ex} = 630 nm, λ_{em} = 675 nm) of the gels was then monitored on a Spark® multimode fluorescence microplate reader.

2.3.12. Application of dye-loaded MNs to rat skin

A deceased rat was obtained, and the skin of its back was shaved using a manual blade razor. The skin was then treated with depilatory cream for 5 minutes to remove any remaining hair. Dye-loaded MNs were applied for 2 minutes using a commercially available spring-loaded applicator generating an impact rate of 2 $m \cdot s^{-1}$, an impact force of 1.6 N, and with a spring constant of 1 $N \cdot mm^{-1}$ (values provided by the manufacturer, Micropoint Technologies Pte. Ltd., Singapore). The skin sections were examined using a fluorescence stereomicroscope (AxioZoom.V16, Zeiss, Oberkochen, Germany) equipped with NIR settings (Excelitas Technologies X-Cite® Xylis light source; Photometrics® Prime™ 95B camera) using a Cy5 filter set (λ_{ex} = 630 nm, λ_{em} = 675 nm).

2.4. Results & Discussion

2.4.1. Synthesis and characterization of H-Cy5-PEG

For preliminary investigation, the dye Cyanine-5 (Cy5) was selected, owing to its relatively simple synthesis and high wavelength fluorescence (λ_{em} = 662 nm). While the reduced hydrocyanine form of this dye (H-Cy5) had previously been described for *in vitro* and *in vivo* ROS sensing, its poor water solubility and small size leads to the formation of aggregates, quenching its fluorescence, and uptake by cells of the dermis, where it would be unable to sense ROS in the extracellular ISF. To address this issue, Cy5 was

PEGylated by first converting the carboxyl group to an activated *N*-hydroxysuccinimide (NHS) ester, then conjugating a 5 kDa polyethylene glycol (PEG) polymer through amine coupling, resulting in a water-soluble Cy5 derivative (Cy5-PEG) too large and hydrophilic to be taken up into cells (**Figure 2.1. A**). Using sodium borohydride, the reduced hydrocyanine forms of Cy5 and Cy5-PEG were prepared (H-Cy5 and H-Cy5-PEG). The reduction was confirmed by a colour change from the characteristic blue colour of Cy5 to a pale orange, and the disappearance of the fluorescence emission peak around 662 nm (**Figure 2.1. C**). As ROS-sensors are known to readily revert to their oxidized state due to light and environmental oxidants, the stability of both H-Cy5 and H-Cy5-PEG was assessed by diluting them in aqueous solutions (10 µM).[23] While H-Cy5 displayed no significant increase in fluorescence over the course of 4 hours, H-Cy5-PEG was found to rapidly regain fluorescence, displaying a 20-fold increase within the same period of time (**Figure 2.1. B**). This was likely due to radical oxygen impurities commonly present in commercially available PEG polymers, resulting in rapid auto-oxidation of the sensor.[33] Using a previously described method for peroxide removal, the PEG was purified by lyophilization and used to prepare new H-Cy5-PEG, which displayed greatly improved stability in aqueous solutions, comparable to that of the unconjugated H-Cy5 (**Figure 1B**). The excitation and emission spectra of the oxidized Cy5 and Cy5-PEG were also evaluated and found to be no shifts were observed in either the excitation or emission spectra, suggesting that PEGylation causes minimal interference with the fluorescent ROS-sensing moiety of the dye (**Figure 2.1. C**).

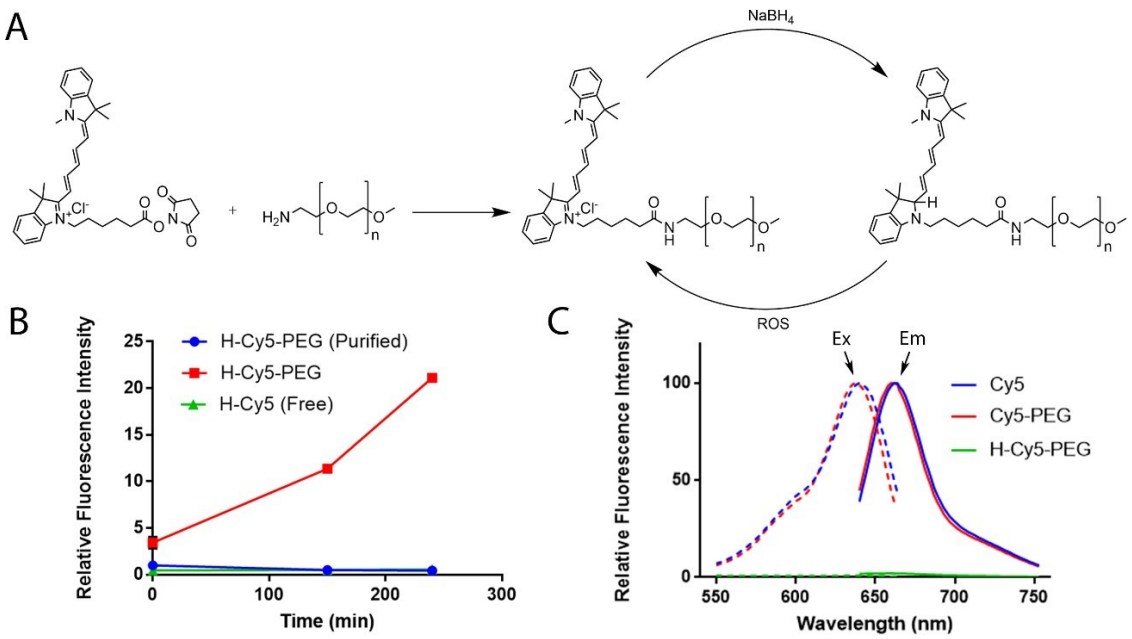

Figure 2.1. Synthesis and characterization of PEGylated Cy5: A) Preparation, reduction and oxidation of Cy5-PEG; B) Stability in aqueous solutions (10 µM) of free Cy5, and Cy5-PEG made from purified and non-purified PEG-NH_2; C) Excitation and emission spectra of Cy5, Cy5-PEG and H-Cy5-PEG. Mean ± SD (n = 3).

The ROS sensitivities of H-Cy5 and H-Cy5-PEG were evaluated by mixing dilute solutions of each sensor (10 µM) with increasing concentrations of Fenton's reagent (a mixture of H_2O_2 and $FeSO_4$, and a source of hydroxyl radicals in solution).[34,35] After mixing, the fluorescence of H-Cy5 exposed to Fenton's reagent was found to increase up to 80-fold relative to a solution of the sensor in water, while H-Cy5-PEG displayed a maximum increase of approximately 60-fold (**Figure 2.2. A, B**). These values are relatively consistent with previously reported data showing increases in fluorescence intensity between 80 and 100-fold, depending on the hydrocyanine used.[36] The signal intensity appeared to be dependent on the concentration of Fenton's reagent used, with optimal sensing occurring between 20 µM: 200 µM ($FeSO_4$:H_2O_2) and 50 µM: 500 µM. Concentrations below this range were likely below the detection limit of H-Cy5, while higher concentrations are known to promote the degradation re-oxidized Cy5, explaining the decreased signal.[36] This re-oxidation appeared to occur nearly instantaneously, with the strongest signal observed immediately after mixing, followed by a gradual decay, with roughly 80% of the initial signal remaining after 1 hour for H-Cy5, and roughly 60% remaining for H-Cy5-PEG (**Figure 2.2. C**). This is also likely due to the previously described gradual degradation of Cy5 following re-oxidation.[36]

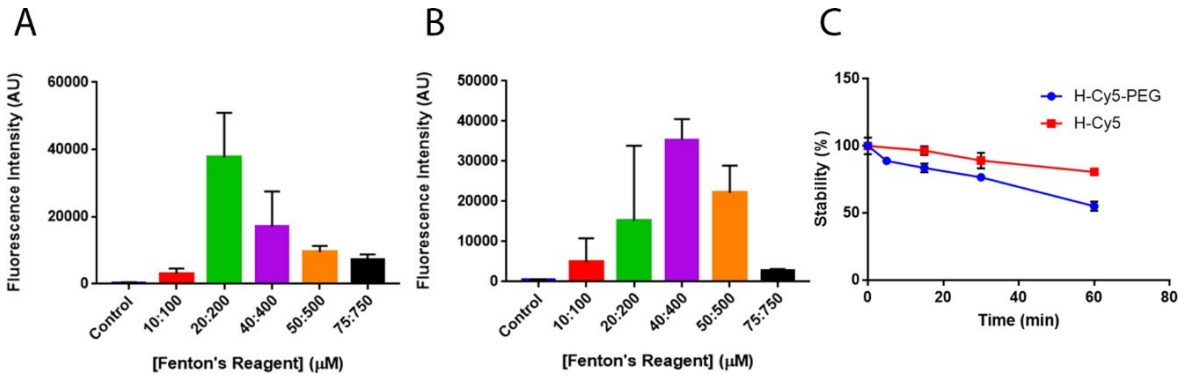

Figure 2.2. ROS-sensing properties of free and PEGylated H-Cy5: A) Sensitivity of free H-Cy5 in solution (10 µM); B) Sensitivity of H-Cy5-PEG in solution (10 µM); C) Stability of signal of re-oxidized probe in aqueous solution (10 µM) over time. Mean ± SD (n = 9).

2.4.2. Selection and characterization of MN polymers

Following confirmation of the ability of the free and PEGylated sensors to detect ROS, their compatibility with a range of previously described MN polymers was assessed, in order to select the optimal material for MN fabrication. Some commonly used MN polymers (such as poly(*N*-vinylpyrrolidone) (M_w = 3,500 – 7,000 Da) (PVP K-12) and poly(vinyl alcohol) (M_w = 10,000 Da) (PVA)) are known to contain radical oxidant impurities and were thus considered unlikely candidates relative to other materials.[37,38] To test this, sensors were diluted (10 μM) in concentrated solutions of each polymer and stored overnight. As expected, both H-Cy5 and H-Cy5-PEG were rapidly oxidized in the presence of PVP K-12 and PVA, with H-Cy5 displaying up to 100-fold greater fluorescence relative to a solution in water (**Figure 2.3. A**). Notably, while H-Cy5-PEG appeared to be oxidized by both PVP and PVA, the effect was much less pronounced than with H-Cy5, with only a 5-to-10-fold increase in fluorescence observed (**Figure 2.3. B**). This could be due to the solubilization effects of PVP and PVA on the poorly soluble H-Cy5, increasing the apparent fluorescence of the solution, while H-Cy5-PEG was already fully solubilized.[39,40]

Other polymers showed more promising results, with ultra-low molecular weight hyaluronic acid (M_w < 6,000 Da) (ULMW HA) and super-low molecular weight hyaluronic acid (M_w < 50,000 Da) (SLMW HA) displaying no oxidizing effect. A carbohydrate-based biopolymer, HA is an important component of the extracellular matrix (ECM) of the skin and has previously been used to prepare dissolving polymeric MNs.[41] Specifically, an 8:1 blend of ULMW HA and dextran (another carbohydrate biopolymer) were found to produce MNs with sharp tips and excellent mechanical properties. This blend of polymers was also tested with H-Cy5 and H-Cy5-PEG and was found to have no oxidizing effect (**Figure 2.3. A, B**).

To ensure that the formulation was suitable for piercing the skin, MNs were prepared from an 8:1 blend of ULMW HA and dextran, and their mechanical properties were assessed. The resulting MNs were found to have an average failure force of 16.7 ± 1.5 N, sufficient to pierce human skin without deformation — previous studies have found that insertion forces between 0.1 N and 3 N are required to do so (**Figure 2.S8**).[42] To determine whether the incorporation of a PEGylated sensor would affect the mechanical strength, MNs were prepared from the same polymer blend with the addition of 5% w/w of 5 kDa PEG-NH_2, double the highest concentration of H-Cy5-PEG tested in this study. The average failure force of the resulting MNs was found to be 16.4 ± 1.3 N, not significantly different from those made without PEG, indicating that the inclusion of (even relatively large amounts of) H-Cy5-PEG within the solid MN structure would not compromise the ability of the MNs to pierce skin.

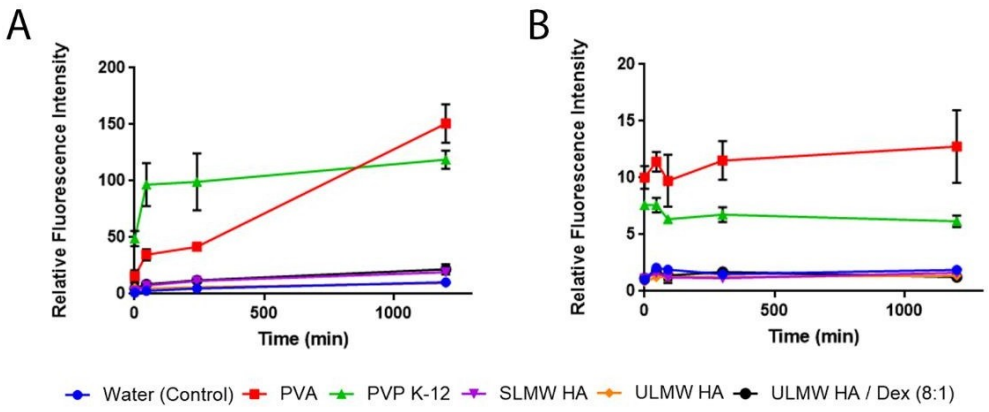

Figure 2.3. Stability of the generated ROS sensors in common MN polymers: A) Free H-Cy5 (10 µM), and B) H-Cy5-PEG. Mean ± SD (n = 6).

2.4.3. Characterization of dissolving polymeric MNs

Based on their compatibility with H-Cy5 and H-Cy5-PEG, as well as their suitable mechanical properties, MNs were prepared from an 8:1 blend of ULMW and dextran through a solvent casting method in PDMS moulds (**Figure 2.S6**). Using bright-field microscopy, the resulting MNs were shown to form a 10 x 10 array of uniform pyramidal projections, with lengths of 604 ± 17 µm and widths of 249 ± 7 µm × 249 ± 7 µm at the base (**Figure 2.4. A**). While the measured base width was in agreement with the dimensions of the moulds (250 µm × 250 µm), the lengths were significantly lower than the stated lengths of the moulds (800 µm). This was likely due to contraction of the polymer due to water loss during the drying process. Further examination using scanning electron microscopy (SEM) revealed that the MNs consistently formed sharp tips with diameters significantly below 10 µm (**Figure 2.4. B**).

When delivering a compound to the skin using MNs, only the tips dissolve and release their loaded compound into the skin. As such, any sensor loaded into the backing layer of the MNs is not delivered and is thus wasted. To mitigate this, the MN manufacturing process was modified to allow dye to be incorporated only in the tips of the MNs, while the backing layer is composed of dye-free polymer. This was accomplished by preparing two polymer matrix solutions (PMS), one with H-Cy5-PEG, and one without. The dye-containing PMS was used for the initial centrifugation steps, after which any excess PMS not localized in the tips of the MN molds was removed, at which point a backing layer of dye-free polymer could be applied, resulting in MNs with H-Cy5-PEG contained exclusively within the tips. When MNs were prepared with this method, containing oxidized Cy5 or Cy5-PEG, fluorescence was only observed in the tips of the MNs, with no dye appearing to diffuse into the backing layer (**Figure 2.4. C**).

To ensure their ability to deliver sensors to the skin, MNs containing oxidized Cy5-PEG were applied to the shaved skin of a deceased rat using a spring-loaded applicator. After 2 minutes of application,

a fluorescent tattoo could clearly be observed at the location of application using fluorescence stereomicroscopy, indicating successful skin penetration and release of dye (**Figure 2.4. D**). Diffusion of the dye could also be observed, highlighting the solubility of Cy5-PEG relative to free Cy5, which did not appear to significantly diffuse from the application site.

0

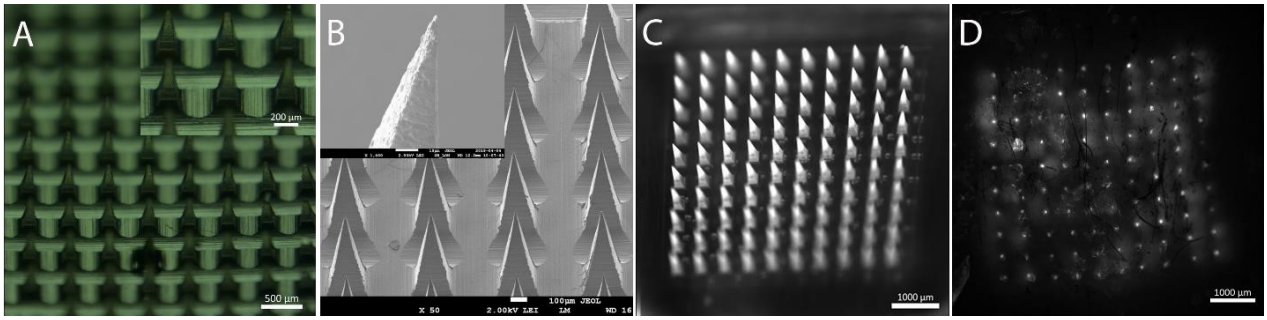

Figure 2.4. Characterization of generated polymeric MNs: A) Brightfield image of MNs made from ULMW HA/Dextran (8:1); B) SEM of ULMW HA/Dextran MNs; C) Fluorescent image of Cy5-PEG contained within MN tips; D) Tattoo of Cy5-PEG delivered to mouse skin using MNs.

2.4.4. Validation of H-Cy5-PEG activity after drying in MNs

After validating the ability of MNs to deliver a PEGylated dye to the skin, it was necessary to ensure that the sensor (H-Cy5-PEG) remained active after drying within the polymer matrix of the MNs. To test this, H-Cy5-PEG MNs prepared from ULMW HA and dextran were dissolved in increasing concentrations of Fenton's reagent. No increase in fluorescence was observed, which was observed to be due to interactions between the Fe^{2+} ions from the Fenton's reagent and the dissolved hyaluronic acid polymer. This notion was supported by subsequent tests, where H-Cy5-PEG-containing MNs were dissolved instead in increasing concentrations of H_2O_2 (another ROS) alone, and a fluorescence increase of approximately 5-fold was observed (**Figure 2.5. A**). The significantly smaller increase in fluorescence observed in this test can be explained by two factors. First, during preparation and drying of the MNs, H-Cy5-PEG was observed to become partially oxidized, likely due to remaining in aqueous solution and exposure to atmospheric oxygen. Additionally, H-Cy5-PEG was observed to be less sensitive to H_2O_2 alone, with a roughly 20-fold increase in fluorescence observed in solution, whereas the increase was between 60 and 80-fold for Fenton's reagent (**Figure 2.S9**). Nonetheless, the concentration-dependent fluorescence increase observed demonstrated that the sensing activity of H-Cy5-PEG was retained after drying.

2.4.5. Selection and validation of reference dye (Cy3-PEG)

When delivering compounds to the skin through MNs, differences in application time and force, as well as topographic variability of the skin, can have an effect on the total yield of compound delivered.[43,44] In the context of a fluorescent sensor, this is of critical importance, as the final concentration of dye has a significant effect of the intensity of the fluorescent signal. A solution to this issue is to incorporate a reference dye into the MNs to act as an internal standard, accounting for the variability in the amount of dye delivered. The dye selected for this purpose was Cyanine-3 (Cy3) — another cyanine dye related to Cy5. Cy3 was chosen due to its simple synthesis and structural similarity to Cy5, allowing PEGylation at the same site, for a sensor with similar physicochemical properties to Cy5-PEG. This was validated by experimentally determining the logP values of Cy5-PEG and Cy3-PEG, which were found to be -1.22 ± 0.03 and -1.04 ± 0.04 respectively, indicating dyes of similar hydrophilicity as well as size.

Further, Cy3-PEG was found to have good stability when exposed to ROS, retaining over 75 % of its signal at 50 µM/500 µM concentrations of $FeSO_4$:H_2O_2 (**Figure 2.5. B**). This constitutes a marked improvement over free Cy3, which retained only 40 % of its initial signal when exposed to this level of ROS. The re-oxidation of H-Cy5-PEG was also investigated in the presence of Cy3-PEG, to ensure that it did not interfere with the reaction. It was found that the re-oxidation proceeded as normal, with H-Cy5-PEG reaching comparable fluorescence intensity values as when no Cy3-PEG was present, highlighting the suitability of Cy3-PEG as a reference dye (**Figure 2.5. C**).

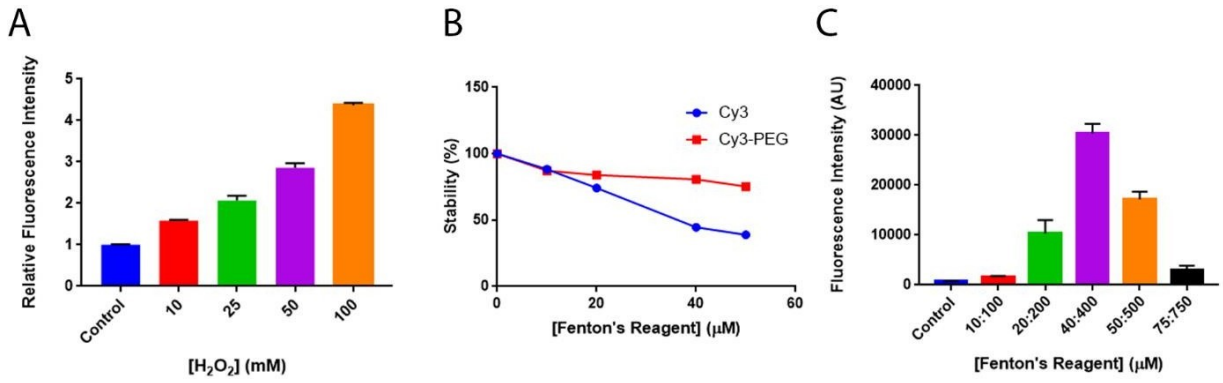

Figure 2.5. Functionality of the generated sensors after loading in MNs: A) Sensitivity ofH-Cy5-PEG MNs after re-dissolution (using H_2O_2 as oxidant); B) Stability of Cy3 and Cy3-PEG in the presence of ROS (Fenton's reagent, $FeSO_4/H_2O_2$); C) Sensitivity of H-Cy5-PEG in the presence of Cy3-PEG (10 µM). Mean ± SD (n = 3).

As Cy3 is added to the MNs in its oxidized fluorescent form, it should generate a consistent fluorescent signal, independent of the presence of ROS, allowing more accurate quantification. The ability of Cy3 to correct for the amount of sensor delivered was supported by tests conducted in agarose gels. MNs containing both oxidized Cy5-PEG and Cy3-PEG were prepared and applied to the gels, and the resulting fluorescent signal was quantified. Another set of MNs was prepared identically, but with half of the tips removed before application, resulting in the delivery of roughly half the total amount of dye. While the total fluorescent signal from the application of the latter set of MNs was significantly lower than the former, this difference is corrected by examining the ratio of Cy5-PEG fluorescence to that of Cy3-PEG (**Figure 2.5. B**). Examination by fluorescence stereomicroscopy also clearly showed the presence of both dyes in the tips of the MNs and in the resulting tattoo after their application to rat skin, highlighting that both dyes display similar incorporation and delivery behaviour (**Figure 2.6.**).

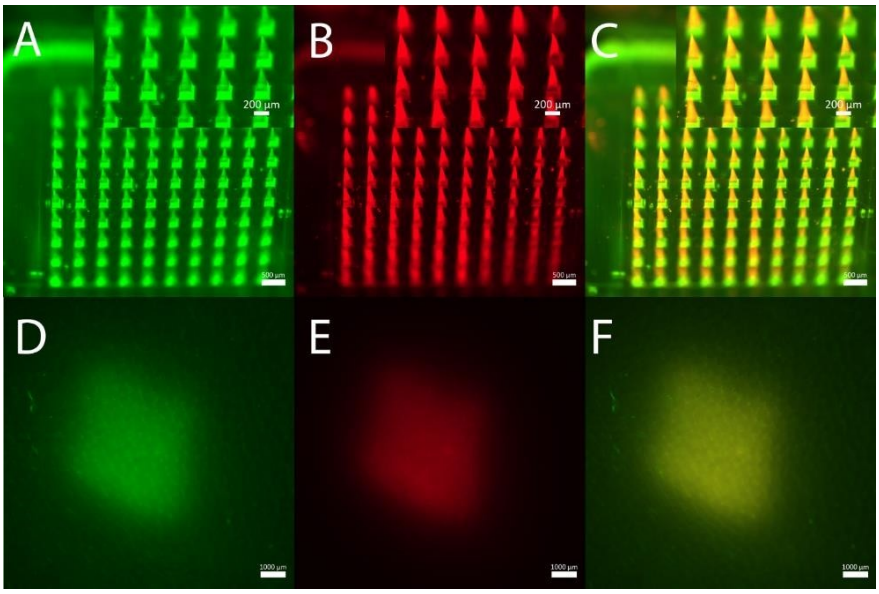

Figure 2.6. Double dye-loaded polymeric MNs: Localization of A) Cy3-PEG, and B) Cy5-PEG in the tips of MNs, and C) an overlaid image showing the fluorescence of both dyes. The *tattoo* in rat skin of D) Cy3-PEG, E) Cy5-PEG, and F) both dyes overlaid.

2.4.6. ROS-sensing ability of dye-loaded MNs in skin-simulating gels

The ability of H-Cy5-PEG-loaded MNs to produce a ROS-sensitive *tattoo* was first investigated in agarose gels, which have previously been used as a skin-simulating medium when studying the application

of MNs.[45,46] These gels, made of a 3% w/w solution of agarose, were chosen based on their viscoelastic properties (comparable to human skin) and the ability to easily control the concentrations of ROS present (by adjusting the concentration of Fenton's reagent within the gels), unlike actual skin. MNs containing either free H-Cy5 and Cy3, or H-Cy5-PEG and Cy3-PEG were prepared and applied to the gels, and their fluorescence was quantified. Clear signals at both wavelengths could be observed, and when examining the ratio of H-Cy5 to Cy3 signal, an increase in fluorescence intensity between 3-fold and 4-fold could be observed (**Figure 2.7. A, B**). This demonstrates the ability of MNs made from ULMW HA and dextran to produce an ROS-sensitive MN *tattoo*.

Notably, the relative increase in fluorescence observed in agarose gels for the MN *tattoo* was much lower than in solution. The primary reasons for this are likely the oxidation of H-Cy5-PEG during MN preparation and the relatively low amount of dye delivered by the MNs. It has been observed that H-Cy5-PEG is relatively sensitive to oxidation by factors other than ROS, notably atmospheric oxygen and light, particularly when stored at high concentrations in aqueous solution. As such, despite care being taken during MN preparation, such as limiting exposure of the solutions to air, and working in the dark, a certain amount of oxidation cannot be avoided by the time the MNs have dried. This, coupled with the relatively small amount of dye delivered by the MN tips, could contribute to the markedly reduced sensitivity observed in gels relative to in solution.

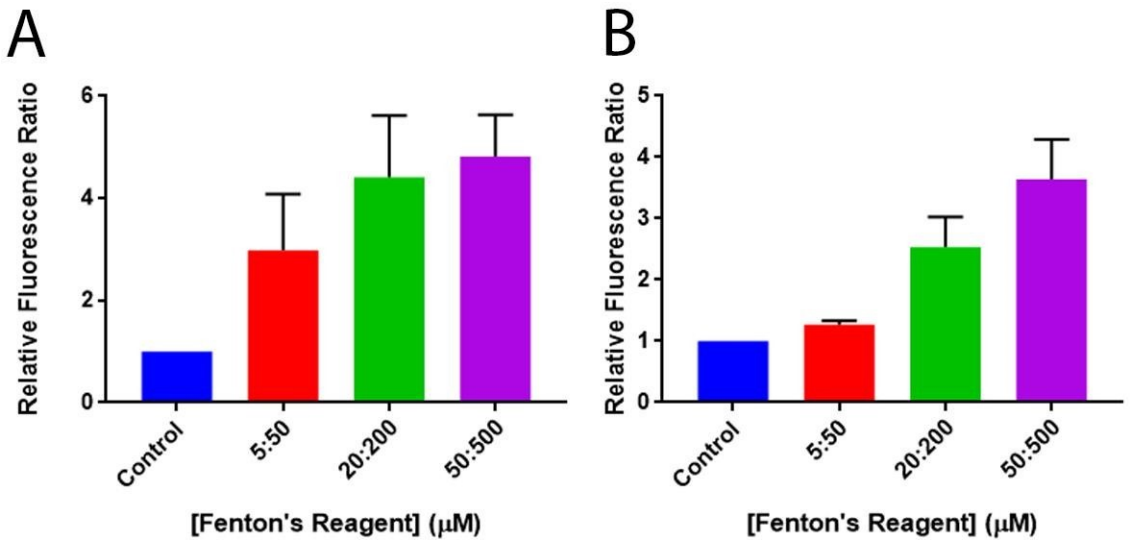

Figure 2.7. Sensitivity of free and PEGylated H-Cy5 delivered to agarose gels using MNs: A) Sensitivity (Cy5/Cy3 ratio) of free H-Cy5 in skin-simulating agarose gels; B) Sensitivity (Cy5/Cy3 ratio) of H-Cy5-PEG in skin-simulating agarose gels. Mean ± SD (n = 6).

2.5. Conclusions & Outlook

The delivery of functional sensors to the dermis for physiological monitoring is a burgeoning field of study with a wide variety of potential medical applications. This study sought to demonstrate, as a proof-of-concept, that an active ROS-sensor could be delivered to the dermis using MNs, acting as a *functional medical tattoo* and indicating the presence of dermal ROS. It was found that by selecting an appropriate dye, and optimizing a compatible polymer formulation, it was possible to retain sensing ability after the formation and drying of the MNs. Further, it was demonstrated that the tattoo delivered by H-Cy5-PEG-loaded MNs displayed a significant increase in fluorescence when delivered to a gel-based skin-simulating environment. The need for inclusion of a reference dye (Cy3), delivered alongside the functional sensor, was also evidenced by the variability in the fluorescent signal of the tattoo depending on the geometry of the MN array.

Nonetheless, this technique currently suffers from certain limitations. ROS-sensing dyes, by their nature, are prone to oxidation by environmental factors, resulting in decreased sensitivity over time following their preparation when stored in solution. Additionally, the amount of sensor delivered by the MNs remains relatively low, resulting in quantification difficulties, particularly *in vivo*. While re-oxidation of H-Cy5-PEG could clearly be seen in skin-simulating gels using the fluorescence plate reader, comparable results were not observed using the fluorescence stereomicroscope, owing the reduced quantitative sensitivity of the instrument. As skin (*ex vivo* or *in vivo*) could not be used with the fluorescence plate reader, this issue of sensitivity prevented the further development of the technique.

In spite of this, the concept of a MN-delivered *functional medical tattoo* remains an exciting prospect for precision health monitoring. Many of the challenges faced by the system described in this article are specific to ROS-sensing, namely the tendency of H-Cy5-PEG to be oxidized during MN preparation, and the relatively low brightness of the re-oxidized sensor limiting quantification in the skin. By selecting appropriate sensors, with high brightness and stability, the potential of this system could be more fully realized.

2.6. Acknowledgements

The authors kindly acknowledge Maya Mailloux and Kivilcim Öztürk-Atar. S.B., and D.B. gratefully acknowledge financial support from the Faculty of Pharmacy at the Université de Montréal, the Natural Sciences and Engineering Research Council of Canada (Discovery program), and the Canadian Generic Pharmaceutical Association and Biosimilars Canada, respectively.

2.7. References

1. Gambhir, S.S.;Ge, T.J.; Vermesh, O.; Spitler, R. Toward achieving precision health. *Sci. Transl. Med.* **2018**, *10*, eaao3612. doi:10.1126/scitranslmed.aao3612
2. Cambronne, X.A.; Stewart, M.L.; Kin, D.; Jones-Brunette, A.M.; Morgan, R.K.; Farrens, D.L.; Cohen, M.S.; Goodman, R.H. NAD^+ biosensor reveals multiple sources for mitochondrial NAD^+. *Science*. **2016**, *352*, 1474-1477. doi:10.1126/science.aad5168
3. Williams, R.M.; Lee, C.; Galassi, T.V.; Harevy, J.D.; Leicher, R.; Sirenko, M; Dorso, M.A.; Shah, J.; Olvera, N.; Dao, F.; Levine, D.A.; Heller, D.A. Noninvasive ovarian cancer biomarker detection via an optical nanosensor implant. *Sci. Adv.* **2018**, *4*, eaaq1090. doi:10.1126/sciadv.aaq1090
4. Tran, B.Q.; Miller, P.R.; Taylor, R.M.; Boyd, G.; Mach, P.M.; Rosenzweig, C.N.; Baca, J.T.; Polsky, R.; Glaros, T. Proteomic characterization of dermal interstitial fluid extracted using a novel microneedle-assisted technique. *J. Proteome Res.* **2018**, *17*, 479-485. doi:10.1021/acs.jproteome.7b00642
5. Thennadil, S.N.; Rennert, J.L.; Wenzel, B.J.; Hazen, K.H.; Ruchti, T.L.; Block, M.B. Comparison of glucose concentration in interstitial fluid, and capillary and venous blood during rapid changes in blood glucose levels. *Diabetes Technol. Ther.* **2001**, *3*, 357-365. doi:10.1089/15209150152607132
6. Fogh-Andersen, N.; Altura, B.M.; Altura, B.T.; Siggaard-Andersen, O. Composition of interstitial fluid. *Clin. Chem.* **1995**, *41*, 1522-1525. doi:
7. Babity, S.; Roohnikan, M.; Brambilla, D. Advances in the design of transdermal microneedles for diagnostic and monitoring applications. *Small*. **2018**, *14*, 1803186. doi:10.1002/smll.201803186
8. Chang, H.; Zheng, M.; Yu, X.; Than, A.; Seeni, R.Z.; Kang, R.; Tian, J.; Khanh, D.P.; Liu, L.; Chen, P.; Xu, C. A swellable microneedle patch to rapidly extract skin interstitial fluid for timely metabolic analysis. *Adv. Mater.* **2017**, *29*, 1702243. doi:10.1002/adma.201702243
9. Miller, P.R.; Skoog, S.A.; Edwards, T.L.; Wheeler, D.R.; Xiao, X.; Brozik, S.M.; Polsky, R.; Narayan, R.J. Hollow microneedle-based sensor for multiplexed transdermal electrochemical sensing. *J. Vis. Exp.* **2012**, *1*, e4067. doi:10.3791/4067
10. Samant, P.P; Prausnitz, M.R. Mechanisms of sampling interstitial fluid from skin using a microneedle patch. *Proc. Natl. Acad. Sci. USA.* **2018**, *115*, 4583-4588. doi:10.1073/pnas.1716772115
11. Wang, M.; Hu, L.; Xu, C. Recent advances in the design of polymeric microneedles for transdermal drug delivery and biosensing. *Lab Chip*. **2017**, *17*, 1373-1387. doi: 10.1039/c7lc00016b

12. Brambilla, D.; Proulx, S.T.; Marschalkova, P.; Detmar, M.; Leroux, J-C. Microneedles for the noninvasive structural and functional assessment of dermal lymphatic vessels. *Small*. **2016**, *12*, 1053-1061. doi:10.1002/smll.201503093
13. Polomska, A.K.; Proulx, S.T.; Brambilla, D.; Fehr, D.; Bonmarin, M.; Brändli, S.; Meboldt, M.; Steuer, C.; Vasileva, T.; Reinke, N.; Leroux, J.-C.; Detmar, M. Minimally invasive method for the point-of-care quantification of lymphatic vessel function. *JCI Insight.* **2019**, *4*, 126515. doi:10.1172/jci.insight.126515
14. Jia, W.; Bandodkar, A.J.; Valdés-Ramírez, G.; Windmiller, J.R.; Yang, Z.; Ramírez, J.; Chan, G.; Wang, J. Electrochemical tattoo biosensors for real-time noninvasive lactate monitoring in human perspiration. *Anal. Chem.* **2013**, *85*, 6553-6560. doi: 10.1021/ac401573r
15. Tastanova, A.; Folcher, M.; Müller, M.; Camenisch, G.; Ponti, A.; Horn, T.; Tikhomirova, M.S.; Fussenegger, M. Synthetic biology-based cellular biomedical tattoo for detection of hypercalcemia associated with cancer. *Sci. Transl. Med.* **2018**, *10*, eaap8562. doi:10.1126/scitranslmed.aap8562
16. Apel, K.; Hirt, H. Reactive oxygen species: metabolism, oxidative stress, and signal transduction. *Annu. Rev. Plant Biol.* **2004**, *55*, 373-399. doi:10.1146/annurev.arplant.55.031903.141701
17. Sakurai, H.; Yasui, H.; Yamada, Y.; Nishimura, H; Shigemoto, M. Detection of reactive oxygen species in the skin of live mice and rats exposed to UVA light: a research review on chemiluminescence and trials for UVA protection. *Photochem. Photobiol. Sci.* **2005**, *4*, 715-720. doi:10.1039/b417319h
18. Young, C.N.; Koepke, J.I.; Terlecky, L.J.; Borkin, M.S.; Boyd, S.L.; Terlecky, S.R. Reactive oxygen species in tumor necrosis factor-α-activated primary human keratinocytes: implications for psoriasis and inflammatory skin disease. *J. Investig. Dermatol.* **2008**, *128*, 2606-2614. doi:10.1038/jid.2008.122
19. Carbonare, M.D.; Pathak, M.A. Skin photosensitizing agents and the role of reactive oxygen species in photoaging. *J. Photochem. Photobiol. B. Biol.* **1992**, *14*, 105-124. doi:10.1016/1011-1344(92)85086-A
20. Pillai, S.; Oresajo, C.; Hayward, J. Ultraviolet radiation and skin aging: roles of reactive oxygen species, inflammation and protease activation, and strategies for prevention of inflammation-induced matrix degradation – a review. *Int. J. Cosmet. Sci.* **2005**, *27*, 17-34. doi:10.1111/j.1467-2494.2004.00241.x.
21. Nishigori, C.; Hattori, Y.; Toyokuni, S. Role of reactive oxygen species in skin carcinogenesis. *Antioxid. Redox Signal.* **2004**, *6*, 561-570. doi:10.1089/152308604773934314
22. Wolf, A.M.; Nishimaki, K.; Kamimura, N.; Ohta, S. Real-time monitoring of oxidative stress in live mouse-skin. *J. Investig. Dermatol.* **2014**, *134*, 1701-1709. doi:10.1038/jid.2013.428

23. Kundu, K.; Knight, S.F.; Willett, N.; Lee, S.; Taylor, W.R.; Murthy, N. Hydrocyanines: a class of fluorescent sensors that can image reactive oxygen species in cell culture, tissue, and in vivo. *Angew Chem. Int. Ed. Engl.* **2009**, *48*, 299-303. doi:10.1002/anie.200804851
24. Acharya, A.P.; Nafisi, P.M.; Gardner, A.; MacKay, J.L.; Kundu, K.; Kumar, S.; Murthy, N. A fluorescent peroxidase probe increases the sensitivity of commercial ELISAs by two orders of magnitude. *Chem. Commun.* **2013**, *49*, 10379-10381. doi:10.1039/C3CC44783A
25. Suri, S.; Lehman, S.M.; Selvam, S.; Reddie, K.; Maity, S.; Murthy, N.; García, A.J. In vivo fluorescence imaging of a biomaterial-associated inflammation and infection in a minimally invasive manner. *J. Biomed. Mater. Res. A.* **2015**, *103*, 76-83. doi:10.1002/jbm.a.35162
26. Kim, J.Y.; Choi, W.I.; Kim, Y.H.; Tae, G. Highly selective in vivo imaging of tumor as an inflammation site by ROS detection using hydrocyanine-conjugated, functional nano-carriers. *J. Control. Release.* **2011**, *156*, 398-405. doi:10.1016/j.jconrel.2011.07.017
27. Frangioni, J.V. In vivo near-infrared fluorescence imaging. *Curr. Opin. Chem. Biol.* **2003**, *7*, 626-634. doi:10.1016/j.cbpa.2003.08.007
28. Proulx, S.T.; Luciani, P.; Christiansen, A.; Karaman, S.; Blum, K.S.; Rinderknecht, M.; Leroux, J.-C.; Detmar, M. Use of a PEG-conjugated bright near-infrared dye for functional imaging of rerouting of tumor lymphatic drainage after sentinel lymph node metastasis. *Biomaterials*. **2013**, *34*, 5128-5137. doi:10.1016/j.biomaterials.2013.03.034
29. Kvach, M.V.; Ustinov, A.V.; Stepanova, I.A.; Malakhov, A.D.; Skorobogatyl, M.V.; Shmanai, V.V.; Korshun, V.A. A convenient synthesis of cyanine dyes: reagents for the labeling of biomolecules. *Eur. J. Org. Chem.* **2008**, 2107-2117. doi:10.1002/ejoc.200701190
30. Andina, D.; Brambilla, D.; Munzinger, N.; Frei, J.; Zivko, C.; Leroux, J.-C.; Luciani, P. Development of a modular ratiometric fluorescent probe for the detection of extracellular superoxide. *Chem. Eur. J.* **2017**, *23*, 4765-4769. doi:10.1002/chem.201700563
31. Larrañeta, E.; Lutton, R.E.M.; Brady, A.J.; Vicente-Pérez, E.M.; Woolfson, A.D.; Thakur, R.R.S.; Donnelly, R.F. Microwave-assisted preparation of hydrogel-forming microneedle arrays for transdermal drug delivery applications. *Macromol. Mater. Eng.* **2015**, *300*, 586-595. doi:10.1002/mame.201500016
32. Sangster, J. Octanol-water partition coefficients of simple organic compounds. *J. Phys. Chem. Ref. Data.* **1989**, *18*, 1111-1227. doi:10.1063/1.555833
33. Kumar, V.; Kalonia, D.S. Removal of peroxides in polyethylene glycols by vacuum drying: implications in the stability of biotech and pharmaceutical formulations. *AAPS PharmSciTech*. **2006**, *7*, 47-53. doi:10.1208/pt070362

34. Walling, C.; El-Taliawi, G.M.; Johnson, R.A. Fenton's reagent. IV. Structure and reactivity relations in the reactions of hydroxyl radicals and the redox reactions of radicals. *J. Am. Chem. Soc.* **1974**, *96*, 133-139. doi:10.1021/ja00808a022
35. Walling, C. Fenton's reagent revisited. *Acc. Chem. Res.* **1975**, *8*, 125-131. doi:10.1021/ar50088a003
36. Sadlowski, C.M.; Maity, S.; Kundu, K.; Murthy, N. Hydrocyanines: a versatile family of probes for imaging radical oxidants in vitro and in vivo. *Mol. Syst. Des. Eng.* **2017**, *2*, 191-200. doi:10.1039/c7me00014f
37. Wasylaschuk, W.R.; Harmon, P.A.; Wagner, G.; Harman, A.B.; Templeton, A.C.; Xu, H.; Reed, R.A. Evaluation of hydroperoxides in common pharmaceutical excipients. *J. Pharm. Sci.* **2007**, *96*, 106-116. doi:10.1002/jps.20726
38. Ashraf-Khorassani, M.; Taylor, L.T.; Waterman, K.C.; Narayan, P.; Brannegan, D.R.; Reid, G.L. Purification of pharmaceutical excipients with supercritical fluid extraction. *Pharm. Dev. Technol.* **2005**, *10*, 507-516. doi:10.1080/10837450500299958
39. Haaf, F.; Sanner, A.; Straub, F. Polymers of N-vinylpyrrolidone: synthesis, characterization and uses. *Polym. J.* **1985**, *17*, 143-152. doi:10.1295/polymj.17.143
40. Brough, C.; Miller, D.A.; Keen, J.M.; Kucera, S.A.; Williams, R.O. Use of polyvinyl alcohol as a solubility-enhancing polymer for poorly water-soluble drug delivery. *AAPS PharmSciTech.* **2016**, *17*, 167-179. doi:10.1208/s12249-015-0458-y
41. Liu, S.; Jin, M.N.; Quan, Y.S.; Kamiyama, F.; Katsumi, H.; Sakane, T.; Yamamoto, A. The development and characteristics of novel microneedle arrays fabricated from hyaluronic acid, and their application in the transdermal delivery of insulin. *J. Control. Release.* **2012**, *161*, 933-941. doi:10.1016/j.jconrel.2012.05.030
42. Davis, S.P.; Landis, B.J.; Adams, Z.H.; Allen, M.G.; Prausnitz, M.R. Insertion of microneedles into skin: measurement and prediction of insertion force and needle fracture force. *J. Biomech.* **2004**, *37*, 1155-1163. doi:10.1016/j.jbiomech.2003.12.010
43. Donnelly, R.F.; Garland, M.J.; Morrow, D.I.; Migalska, K.; Singh, T.R.; Majithiya, R.; Woolfson, A.D. Optical coherence tomography is a valuable tool in the study of the effects of microneedle geometry on skin penetration characteristics and in-skin dissolution. *J. Control. Release.* **2010**, *147*, 333-341. doi:10.1016/j.conrel.2010.08.008
44. van der Maaden, K.; Sekerdag, E.; Jiskoot, W.; Bouwstra, J. Impact-insertion applicator improves reliability of skin penetration by solid microneedle arrays. *AAPS J.* **2014**, *16*, 681-684. doi:10.1208/s12248-014-9606-7

45. Zhang, D.; Das, D.B.; Rielly, C.D. Microneedle assisted micro-particle delivery from gene guns: experimentals using skin-mimicking agarose gel. *J. Pharm Sci.* **2014**, *103*, 613-627. doi:10.1002/jps.23835
46. Koelmans, W.W.; Krishnamoorthy, G.; Heskamp, A.; Wissink, J.; Misra, S.; Tas, N. Microneedle characterization using a double-layer skin simulant. *Mech. Eng. Res.* **2013**, *3*, 51-63. doi:10.5539/mer.v3n2p51

2.8. Supporting Information

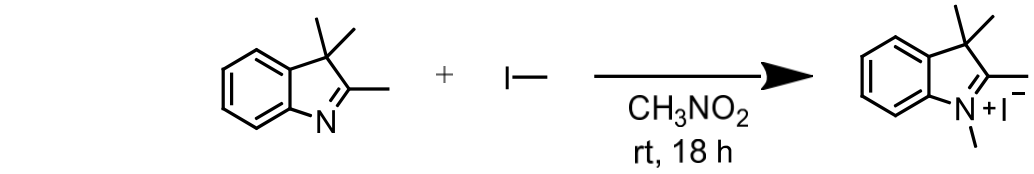

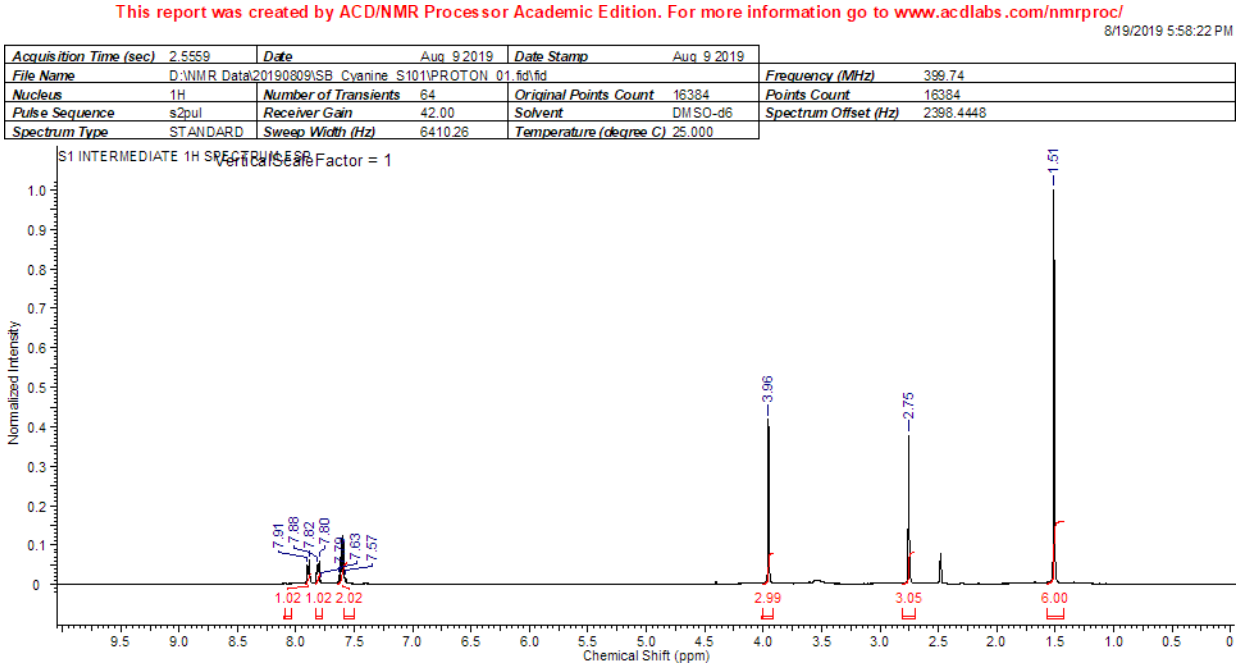

Figure 2.S1: Reaction scheme and ^{1}H NMR spectrum for Intermediate **S1**.

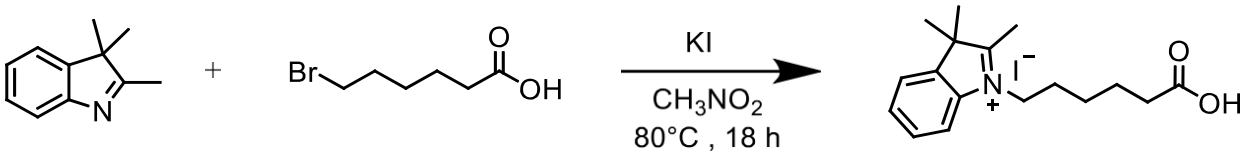

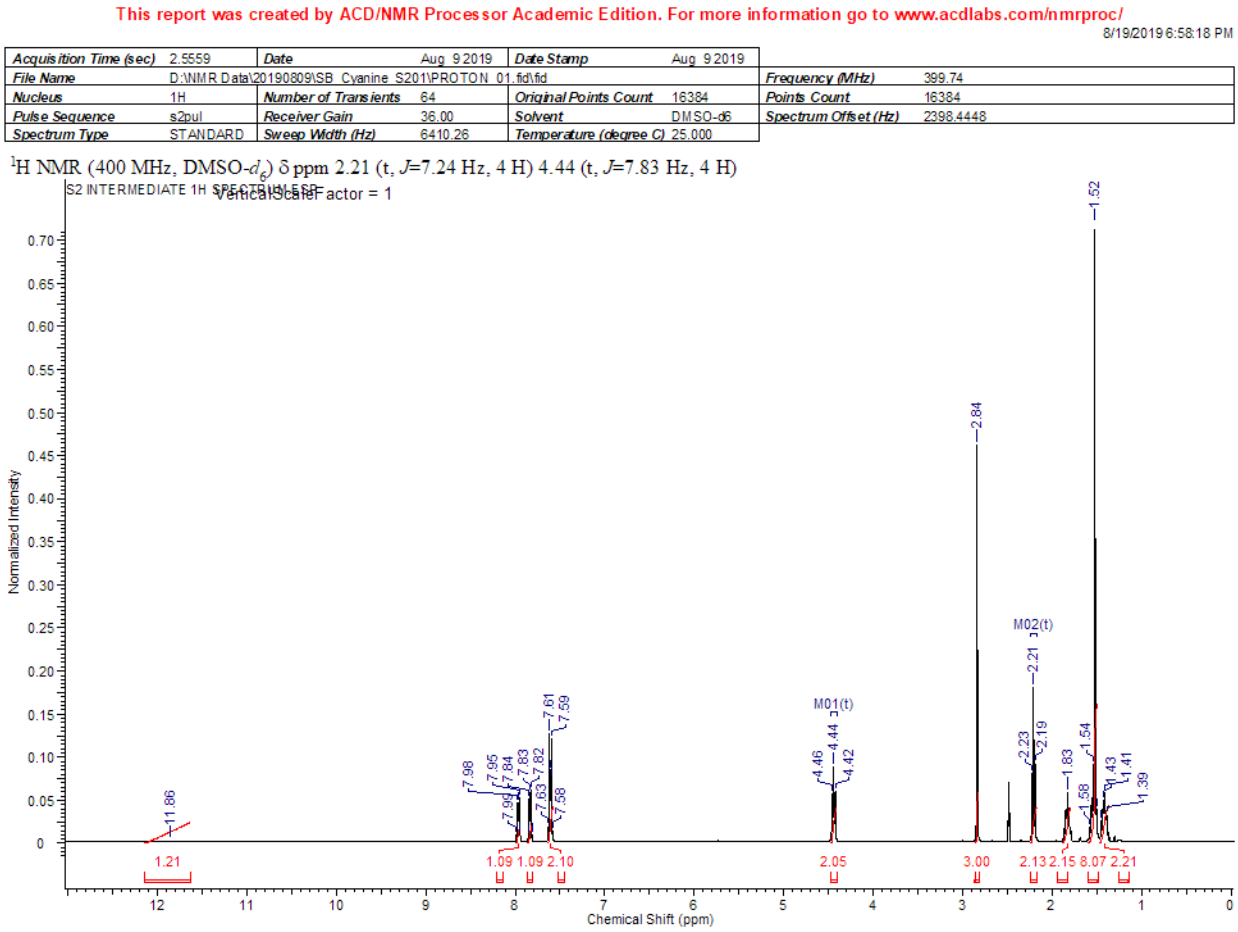

Figure 2.S2: Reaction scheme and ^{1}H NMR spectrum for Intermediate **S2**.

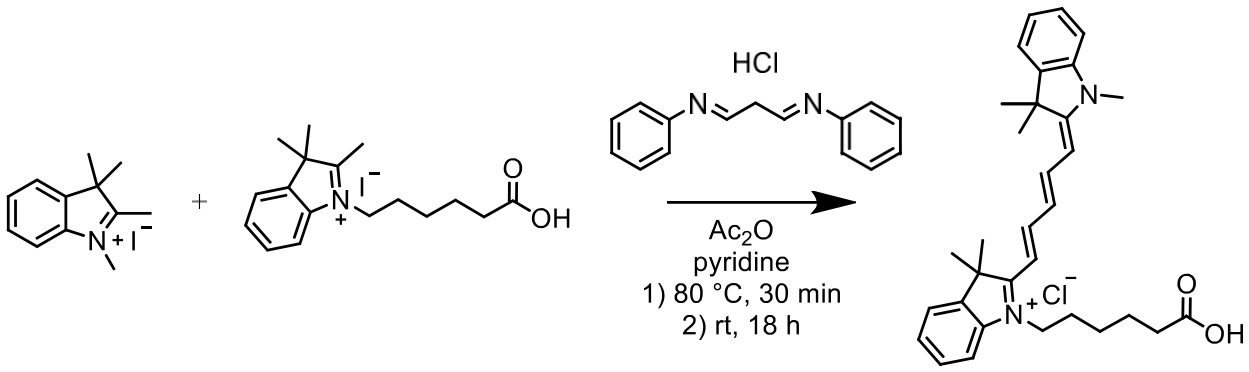

8/19/2019 6:56:49 PM

Acquisition Time (sec)	2.5559	*Date*	Aug 9 2019	*Date Stamp*	Aug 9 2019		
File Name	D:\NMR Data\20190809\SB_Cy301\PROTON_01.fid\fid					*Frequency (MHz)*	399.74
Nucleus	1H	*Number of Transients*	64	*Original Points Count*	16384	*Points Count*	16384
Pulse Sequence	s2pul	*Receiver Gain*	42.00	*Solvent*	DMSO-d6	*Spectrum Offset (Hz)*	2398.4448
Spectrum Type	STANDARD	*Sweep Width (Hz)*	6410.26	*Temperature (degree C)*	25.000		

^{1}H NMR (400 MHz, DMSO-d_6) δ ppm 2.18 (t, *J*=7.24 Hz, 1 H) 2.28 (t, *J*=7.24 Hz, 1 H) 4.07 (t, *J*=7.04 Hz, 2 H) 6.27 (dd, *J*=16.82, 14.09 Hz, 2 H) 6.55 (t, *J*=12.33 Hz, 1 H) 7.60 (d, *J*=7.43 Hz, 2 H) 8.32 (t, *J*=13.11 Hz, 2 H)

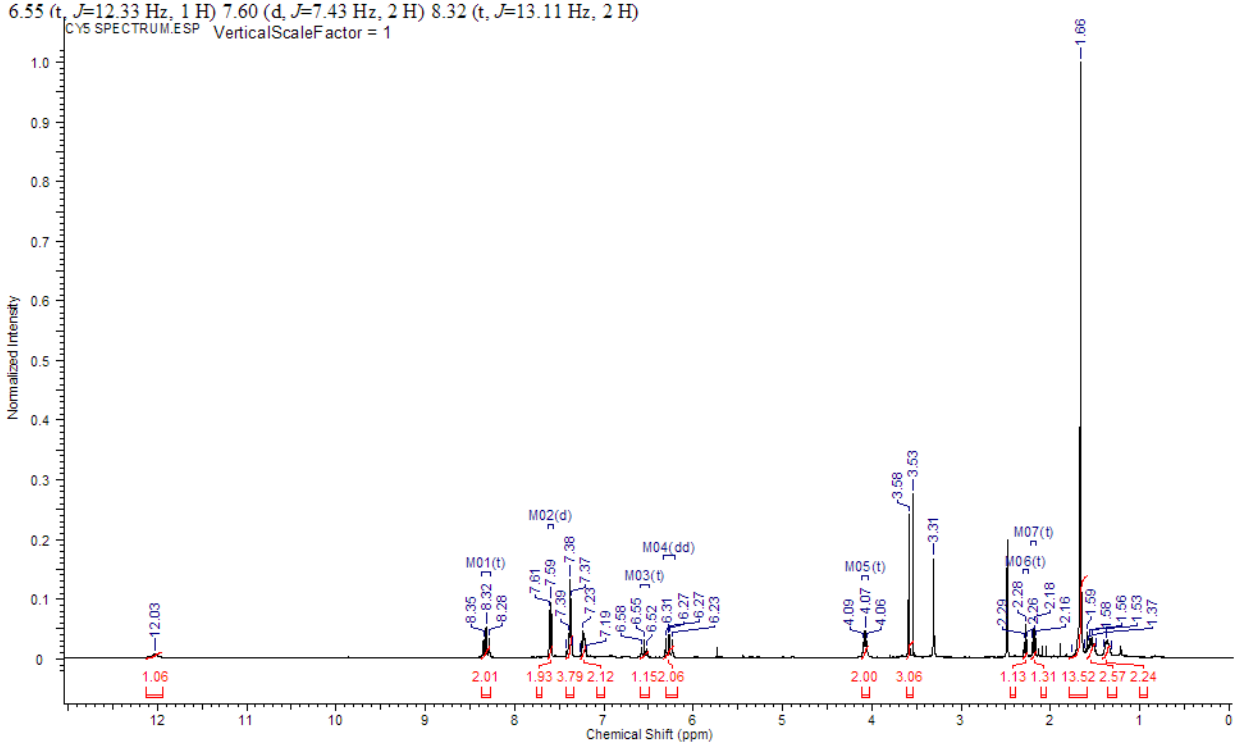

Figure 2.S3: Reaction scheme and ^{1}H NMR spectrum for **Cy5**.

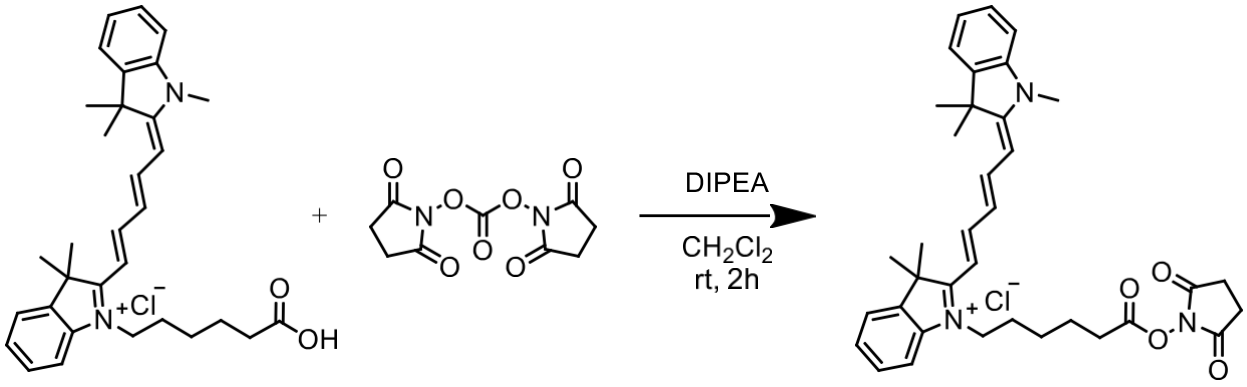

Figure 2.S4: Reaction scheme for synthesis of **Cy5-NHS**.

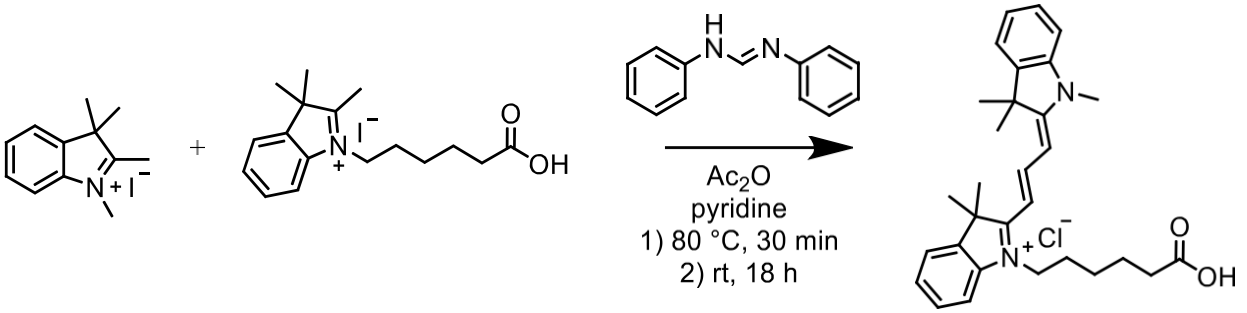

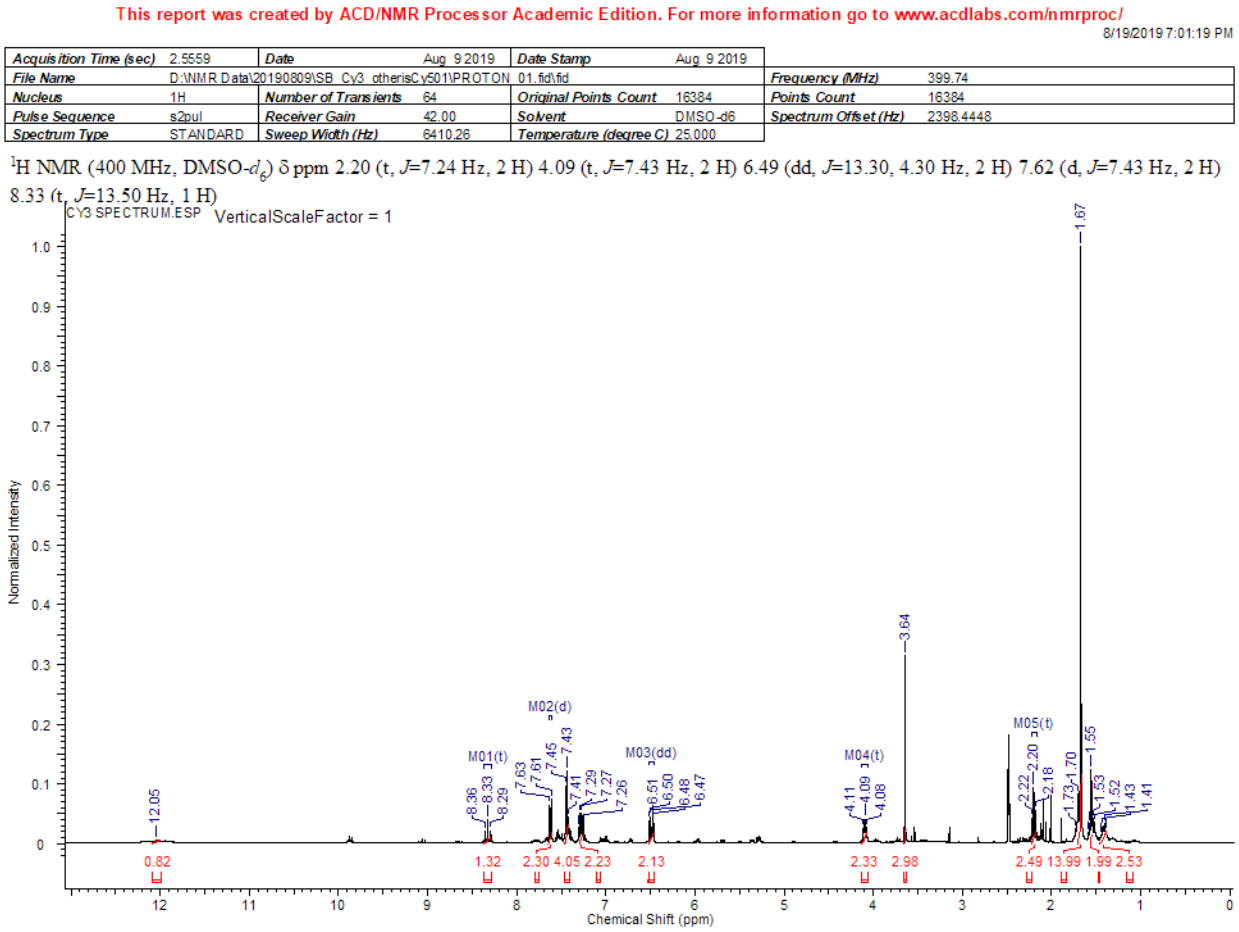

Figure 2.S5: Reaction scheme for synthesis of **Cy3**.

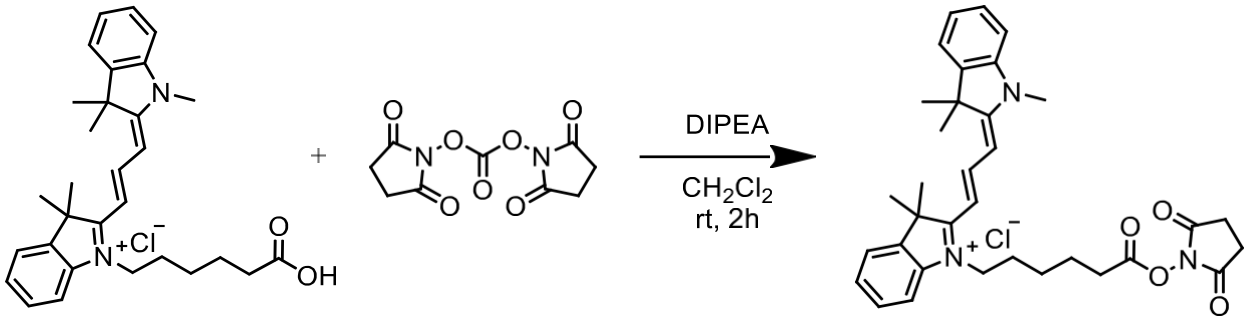

Figure 2.S6: Reaction scheme for synthesis of **Cy3-NHS**.

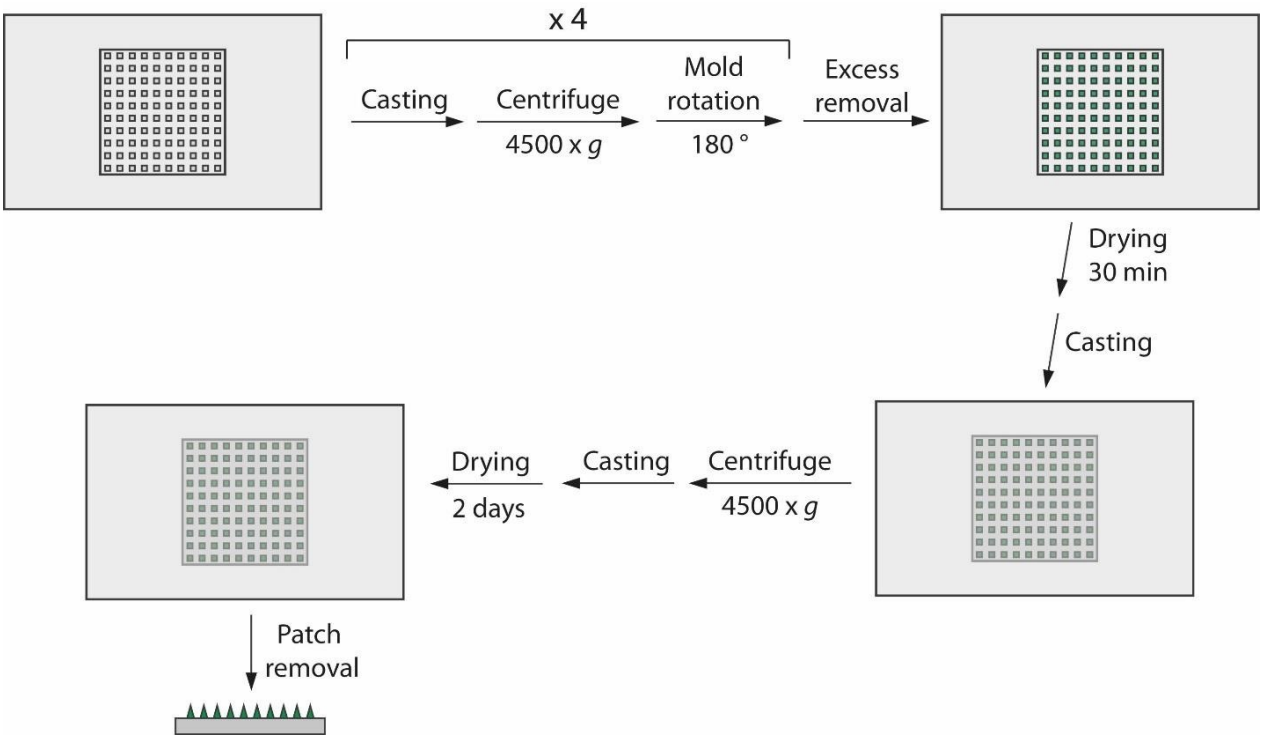

Figure 2.S7: Solvent-casting method for fabrication of dissolving polymeric MNs.

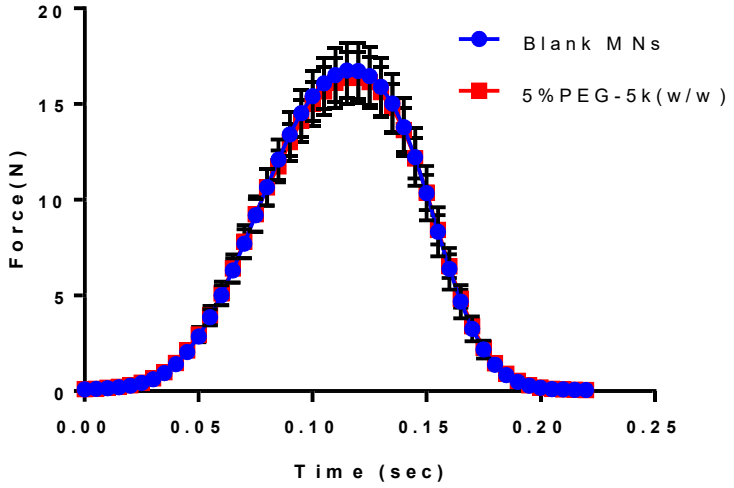

Figure 2.S8: Force-time curve of failure force of MNs. Force required for deflection of MNs over time, demonstrating their suitable mechanical strength. Mean ± SD (n = 6).

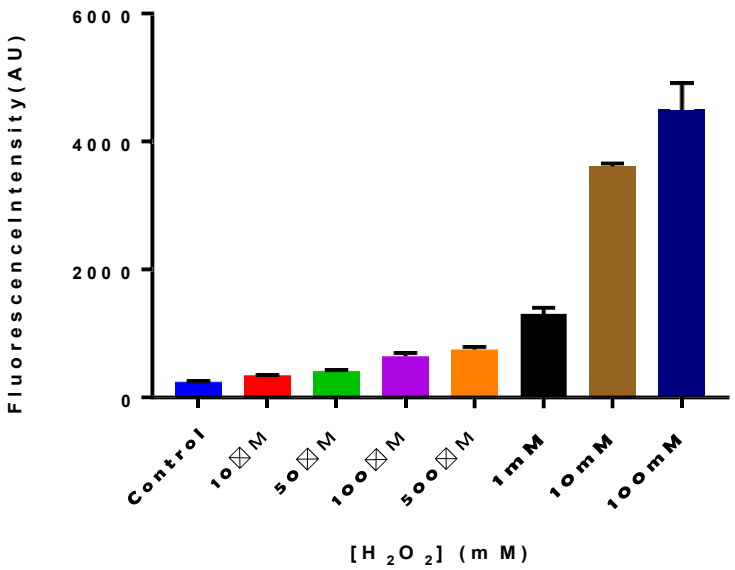

Figure 2.S9: Re-oxidation of H-Cy5 using H_2O_2. When exposed to H_2O_2, the magnitude of the increase in fluorescence of H-Cy5 is greatly reduced, and only occurs at high concentrations (≥ 1 mM). Mean ± SD (n = 3).

Chapter 3

Aside from the delivery of functional sensors, MNs have previously been described for the delivery of an inert NIR fluorescent dye for imaging and monitoring lymphatic drainage. This method of lymphatic monitoring displays important advantages over existing methods, notably the potential for at-home or point-of-care monitoring without the need for specially trained personnel. The previously described MN-based system suffers from limitations relating to the fluorescent dye used (ICG) and its relatively poor solubility, stability, and selectivity, which limit its potential *in vivo*. Here, an alternative NIR fluorescent dye — optimized for specific lymphatic drainage — is synthesized and characterized, and paired with an improved dissolving polymeric MN delivery system. These MNs are tested *in vivo* and found to be compatible with a recently described portable fluorescence detection system. Further, the *tattoo* delivered by these MNs is shown to be capable of discriminating between situations of lymphatic drainage and lack of lymphatic drainage *in vivo* using rat models. Finally, the discrimination potential of the MN *tattoo* is improved by tuning the length and spatial location of the NIR fluorescent dye within the MNs in order to limit the amount of dye retained in the skin. Overall, this system shows potential for improving the point-of-care monitoring of normal or impaired lymphatic drainage.

Development of a fluorescent microneedle tattoo for non-invasive monitoring of lymphatic function

Samuel Babity[1], Anna Polomska[2], Frederic Couture[3], Mattias Bonmarin[4], Daniel Fehr[4], Michael Detmar[2] and Davide Brambilla[1]

[1] Faculté de Pharmacie, Université de Montréal, C.P. 6128, Succursale Centre-ville, Montréal, Québec H3C 3J7, Canada;

[2] Swiss Federal Institute of Technology (ETH Zürich), Department of Mechanical and Process Engineering, Leonhardstrasse 21, 8092 Zürich, Switzerland;

[3] Institut TransBioTech, 201 Rue Monseigneur-Bourget, Lévis, Québec, G6V 6Z9, Canada;

[4] Zurich University of Applied Sciences, School of Engineering, Technikumstrasse 9, 8401 Winterthur, Switzerland.

Corresponding author: davide.brambilla@umontreal.ca

3.1. Abstract

The monitoring of lymphatic drainage is of great importance, particularly in the context of the early detection and diagnosis of lymphedema. Existing methods of imaging and monitoring lymphatic drainage can be costly and require trained personnel, posing problems for at-home or point-of-care monitoring. Recently, an alternative approach has been proposed, consisting of using MNs to deliver an NIR-fluorescent *tattoo* to the skin, which can be monitored with traditional or portable fluorescence monitoring equipment. However, this system retains limitations, particularly relating to the fluorescent dye used for the *tattoo* (ICG). In this work, we present further development of this approach, using a specifically designed NIR-fluorescent probe and optimization of MN length and spatial location of the NIR dye within the MNs. This method was demonstrated to be compatible with portable fluorescence measurement and discriminate between drainage and lack of drainage *in vivo* in rats.

Keywords: microneedles, monitoring, tattoo, diagnostics, lymphatics

3.2. Introduction

The lymphatic system consists of a network of vessels and nodes that spread throughout the body, playing an essential role in tissue homeostasis and immune response.[1,2] It is now known that a variety of pathological conditions are associated with altered lymphatic function, most notably lymphedema. This disease, affecting approximately 3 million people in the United States, is characterized by an accumulation of interstitial fluid in the extremities due to impaired lymphatic drainage.[3,4] In the developed world, lymphedema occurs most commonly as a complication of breast cancer treatment, primarily resulting from the removal of axillary lymph nodes.[5,6] Because of the significant impact to quality of life caused by this disorder, as well as the improved outcomes associated with rapid treatment, the early detection of lymphedema is considered to be of critical importance.[7]

While lymphatic imaging techniques remain less developed than those used for imaging the circulatory system, a variety of methods exist, including magnetic resonance[8], computed tomography[9], and lymphoscintigraphy-based techniques.[10] However, there remains significant drawbacks associated with the cost and complexity of these imaging strategies, which has led to the emergence of near-infrared (NIR) fluorescence imaging as an alternative means of visualizing the lymphatic system.[11] This technique has emerged as a candidate due to its high sensitivity and spatial resolution, owing to the minimal tissue autofluorescence observed at NIR wavelengths (>750 nm), which enables a non-invasive assessment of lymphatic structure and function.[12] In these initial studies, the NIR-fluorescent dye used was indocyanine green (ICG)[13,14], a tricarbocyanine dye that can be excited around 780 nm, with peak fluorescence emission around 813 nm.[15] Despite its improved sensitivity relative to other methods of lymphatic imaging, the delivery of ICG remains an invasive procedure, requiring subcutaneous or intradermal injection to reach lymphatically vascularized tissue. A proposed solution to this issue has been the delivery of ICG using microneedles (MNs).[16] Consisting of miniaturized needles with lengths below 1 mm, often assembled into an array, MNs are long enough to pierce the skin's outer barrier — the *stratum corneum* — but short enough to avoid activating pain-sensing neurons found deeper in the tissue.[17,18] While initially proposed for the delivery of therapeutics, in recent years MNs have been increasingly studied for their potential diagnostic applications.[19] In the aforementioned study, dissolving polymeric MNs made from poly(*N*-vinylpyrrolidone) (PVP) were shown in mice to be able to effectively deliver ICG across the *stratum corneum*, allowing the visualization of lymphatic vessels.[16] The soluble polymeric MNs used in this study offer several advantages over other described classes (*e.g.* solid metal MNs or hollow silicon MNs), due to their simple manufacturing process and the ability to incorporate a fluorescent dye directly into the structure of the MN, allowing release upon dissolution in the skin.

In all of the previous works on lymphatic imaging, the NIR dye selected was ICG, likely based on its FDA-approved status and long history of clinical use, dating to 1959.[20] However, ICG poses important

limitations for use *in vivo* due to its rapid degradation, poor solubility (resulting in fluorescence quenching), and low quantum yield.[15,21,22] Further, as a small molecule, ICG shows limited selectivity for drainage *via* the lymphatic system and can also be drained through blood vessels, drastically limiting the selectivity and clinical utility of this imaging technique.[23] A potential solution these issues is the use of PEGylated conjugates, which have been shown to promote selective lymphatic targeting in the context of drug delivery.[24-26] This strategy has also been applied to other NIR dyes, which have subsequently displayed improved solubility, as well as much higher selectivity for drainage through lymphatic vessels.[23] Specifically, it was found that a 20 kDa PEG chain resulted in excellent selectivity for lymphatic drainage while remaining small enough to easily diffuse through the skin. However, these conjugates were still delivered through intradermal injection, necessitating trained personnel, generating sharp waste, and requiring that analysis be performed in a hospital setting.

Taking advantage on the non-invasive nature of MNs, and the improved solubility and lymphatic selectivity of PEGylated NIR tracers, we have described the design of a dissolving polymeric MN patch loaded with a PEG (20kDa) conjugate of Cy7.5, a NIR fluorescent probe. By optimizing dye concentration, MN length and composition, and location of the dye within the MNs, it was found that lymphatic drainage function could be reliably followed using *in vivo* models of mice and rats. Specifically, it was determined that the spatial location of the fluorescent tracer within the MN patch is critical, to limit the high levels of background signal occurring when the dye is not drained from the application site. Additionally, it was demonstrated that this system could be paired with a portable detection technology, allowing simpler, less invasive monitoring of lymphatic drainage.[27] Importantly, we highlighted the importance of MN length optimization, which could have important implications for the transdermal delivery of other macromolecules through dissolving polymeric MN systems.

3.3. Experimental

3.3.1. Materials

Poly(*N*-vinylpyrrolidone) (PVP) K-12 was kindly provided by BASF (Ludwigshafen, Germany). Poly(vinyl alcohol) (PVA) was purchased from Sigma-Aldrich (St. Louis, MO). Indocyanine green (ICG, IR125, laser grade) and dimethyl sulfoxide (DMSO) were purchased from Acros Organics (Morris Plains, NJ). Cyanine 7.5 NHS ester (Cy7.5-NHS) was purchased from Lumiprobe (Hunt Valley, MD). Poly(ethylene glycol) amine (PEG-NH_2) (20 kDa) was purchased from JenKem Technologies (Plano, TX). Sephadex G-15 was purchased from GE Life Sciences (Mississauga, ON). Square pyramidal female MN moulds made of room temperature vulcanizing silicone, 10 × 10 array, 250 μm × 250 μm × 800 μm (W ×

L × H) and 15 × 15 array, 250 µm × 250 µm × 600 µm (W × L × H) with peak to peak spacing of 500 µm were purchased from Micropoint Technologies Pte. Ltd. (Singapore).

3.3.2. Synthesis of Cy7.5-PEG

Cy7.5-PEG was synthesized by adapting a previously described procedure.[23] Briefly, Cy7.5-NHS (6.0 mg, 7.2 µmol, 1 eq) and MeO-PEG-NH_2 (MW = 20,000 g/mol) (144 mg, 7.2 µmol, 1 eq) were dissolved in 2 mL of anhydrous DMSO, and the mixture was stirred in the dark for 18 – 24 h. Following this, the mixture was diluted in 40 mL of milli-Q H_2O and lyophilized. The resulting residue was dissolved in 1 mL of 180 mM NaCl and purified on G-15 Sephadex. The fractions were combined and lyophilized, yielding Cy7.5-PEG as a light green solid (95 mg, 4.5 µmol, 63% yield). The purity of the product was confirmed by HPLC-MS analysis (**Figure 3.S1**).

3.3.3. Preparation of Cy7.5-PEG-loaded MNs

MNs were manufactured by adapting a previously described solvent casting method.[12] Briefly, to 2 mL of distilled H_2O, PVP K-12 (0.800 g) and PVA (0.800 g) were added and mixed thoroughly. The mixture was heated for 30 – 40 mins in a 75 °C oven and centrifuged (Sorvall ST 16R, ThermoFisher Scientific, Waltham, MA) for 5 mins at 4700 *g*. Cy7.5-PEG was added, resulting in a final concentration of 720 µM. Using a 1 mL syringe, roughly 100 µL of this solution was cast into PDMS moulds (Micropoint Technologies Pte. Ltd., Singapore) and these moulds were secured with tape in 6-well cell culture plates (Sarstedt AG & Co., Nümbrecht, Germany). The plates were covered, secured with parafilm, and centrifuged for 5 mins at 2300 *g*. After centrifugation, polymer solution was re-applied, and the plates were rotated 180° and centrifuged again. This process was repeated a total of four times. After the final centrifugation, any excess polymer solution was removed from the molds using a spatula, and they were placed in a vacuum chamber at 150 mbar for 30 minutes. Roughly 100 µL of dye-free polymer solution was added to each mold, and they were allowed to dry for 18 – 24 h at 25 °C and 60 % humidity, after which the MNs were removed from the moulds. For the modified solvent-casting procedure, after removal of excess polymer solution from the moulds, a spatula was used to further remove dye-loaded polymer from the MN tips, followed by a fifth and final centrifugation using dye-free polymer.

3.3.4. Characterization of mechanical properties of MNs

The failure force of the MNs was evaluated using a TA.XT-Plus Texture Analyser (Stable Micro Systems, Surrey, UK) in compression mode. MNs were prepared as previously described, without addition of dye, and with or without addition of PEG-NH_2 (20 kDa). MNs were placed on an aluminum plate and a cylindrical stainless-steel probe (6 mm diameter) was moved towards the MNs. The probe moved at 1.2

$mm \cdot s^{-1}$ with a maximum travel distance of 300 µm (sufficient to induce MN deflection). The MN failure force was measured as the maximum of the force-time curve.[28]

3.3.5. Application of Cy7.5-PEG MNs in vivo to mice

Animals

Mice were kept under specific pathogen–free conditions until imaging. FVB mice were bred in-house. All experiments were carried out in strict accordance with the animal protocols approved by Kantonales Veterinaramt Zurich (protocol: 237/2013).

***In vivo* imaging**

The IVIS Spectrum imaging system and the custom portable device were used simultaneously for the *in vivo* clearance assay in the back skin of mice. Six 19-week-old male FVB mice were used for the assay. Mice were anesthetized with 2% isoflurane, and fur was removed from the back skin in an area of approximately 3 cm in diameter using an electric shaver followed by depilating cream (Nair, Church & Dwight, Ewing, NJ). MNs were applied under anesthesia using a commercially available spring-loaded applicator generating an impact rate of 2 $m \cdot s^{-1}$, an impact force of 1.6 N, and with a spring constant of 1 $N \cdot mm^{-1}$ (values provided by the manufacturer, Micropoint Technologies Pte. Ltd., Singapore) with a prolonged contact for 3 minutes for each application. Animals were kept away from direct light between imaging sessions.

Animals were imaged in an IVIS Lumina XR (Caliper Sciences, Hopkinton, MA) in fluorescence mode using a field of view of 6.6 cm × 6.6 cm (FOV D) with an exposure time of 1.5 seconds, lens aperture (fstop) of f/16 and pixel binning set to 8. Excitation lamp was set to high with the 745 nm excitation filter and the ICG emission filter (810 – 875 nm). The average fluorescence intensity in a circular ROI (3 cm in diameter) was analyzed using Living Image Software. Simultaneously, measurements were performed with the custom portable device. After tracer injection, the circular area (3 cm in diameter) around the application site was marked. The device was moved slightly around the marked injection area until the region of highest intensity was detected. Six measurements were then recorded, and the average of the 3 highest values were used for the data analysis. After subtracting the background readout, the values obtained by each instrument were normalized to the time 0 measurement and plotted against time.

3.3.6. Application of Cy7.5-PEG MNs in vivo to rats

Animals

Female Sprague-Dawley rats (Charles River, Senneville, QC) with weights ranging from 400 – 500 g were fed with Alfalfa-free rodent diet (Envigo RMS Inc., Lachine, QC) for 3 weeks prior to experimentation. Experiments were conducted under an ethical protocol approved by the Animal Care Committee of the Faculty of Pharmacy at the University of Montreal (protocol: 19-002).

***In vivo* imaging**

Rat dorsal skin was shaved and depilated under isoflurane-induced anesthesia using an electric razor and depilating cream (Nair, Church & Dwight, Ewing, NJ) the day before experimentation. For dead animals, rats were euthanized under anesthesia by cervical dislocation using cutting pliers. Carcasses were kept away from light between scans and kept at 4 °C for the overnight incubation. For living animals, MNs were applied under anesthesia using a commercially available spring-loaded applicator generating an impact rate of 2 $m \cdot s^{-1}$, an impact force of 1.6 N, and with a spring constant of 1 $N \cdot mm^{-1}$ (values provided by the manufacturer, Micropoint Technologies Pte. Ltd., Singapore) with a prolonged contact for 3 minutes for each application. Animals were kept away from direct light between imaging sessions.

Animals were imaged in an IVIS Lumina XR (Caliper Sciences, Hopkinton, MA) in fluorescence mode using a field of view of 12.5 cm × 12.5 cm (FOV D) with exposure time set to auto-compensated, lens aperture (fstop) of f/16 and pixel binning set to 8. Excitation lamp was set to high with the 745 nm excitation filter and the ICG emission filter (810 – 875 nm). Quantitative data were obtained by drawing square (with constant area) areas of interest around the MN application site to measure fluorescence efficiencies (in %) which correspond to the quotient of emitted light divided by the excitation light (both in photons/second).

3.3.7. Histological Analysis

The skin area was harvested and frozen at –80 °C in Optimal Cutting Temperature (OCT)-sucrose compound. Sections of 50 µm were cut and chilled by dry ice and stored at -80 °C until imaging for ICG signal with a fluorescence stereomicroscope (AxioZoom.V16, Zeiss, Oberkochen, Germany) equipped with NIR settings (Excelitas Technologies X-Cite® Xylis light source; Photometrics® Prime™ 95B camera) using a Cy7 long pass filter set (λ_{ex} = 675 nm, $\lambda_{em} \geq$ 730 nm). Sections were then stained with hematoxylin and eosin, and the same regions were imaged under white light excitation (exposure time: 75 and 100 ms for mice and rat skin, respectively).

3.4. Results

3.4.1. Synthesis and Characterization of Cy7.5-PEG

As a result of the limitations posed by ICG, namely its aggregation and non-specific drainage, Cyanine-7.5 (Cy7.5) was selected as an alternative NIR dye candidate for imaging lymphatic drainage. Displaying comparable excitation and emission wavelengths to ICG (λ_{ex} = 788 nm, λ_{em} = 808 nm for Cy7.5; λ_{ex} = 788 nm, λ_{em} = 813 nm for ICG) this dye should be similarly well-suited for *in vivo* imaging. However, unconjugated Cy7.5 exhibits relatively poor water solubility (potentially leading to aggregation and cellular uptake)[21,22], and as a small molecule, is susceptible to the same non-specific drainage observed with ICG.[16,27] To address both of these issues, Cy7.5 was conjugated to a 20 kDa PEG polymer through amine coupling, using an activated NHS ester of Cy7.5, as this length was found to be optimal for promoting selective lymphatic drainage (**Figure 3.1. A**)[23]. As expected, the resulting conjugate (Cy7.5-PEG) was observed to be highly water soluble and was too large and hydrophilic to be taken up into dermal cells. Further, previous studies have shown that 20 kDa PEGylated dyes are large enough to be selectively drained through lymphatic vessels while remaining small enough to diffuse away from the delivery site in the dermis.[23-25] The excitation and emission spectra of Cy7.5-PEG were also examined relative to the unconjugated Cy7.5-NHS ester and no difference was observed, highlighting that the fluorescence properties of the dye are retained after PEGylation (**Figure 3.1. B**).

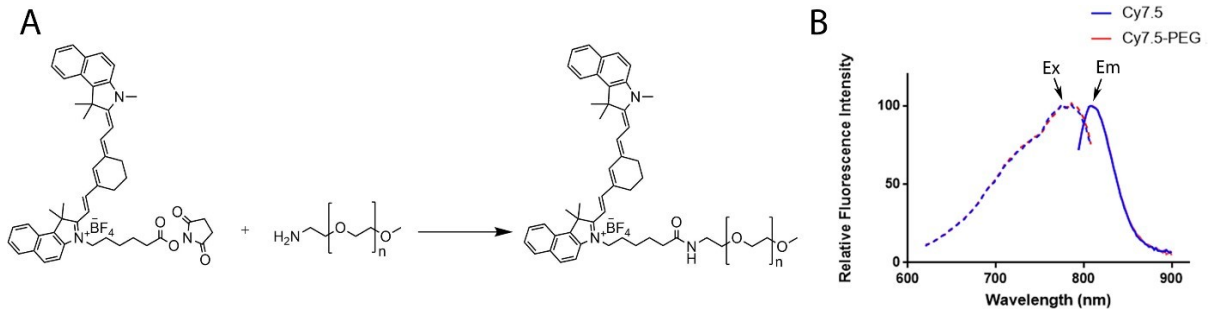

Figure 3.1. Synthesis and characterization of Cy7.5-PEG: A) Synthesis of Cy7.5-PEG; B) Excitation and emission spectra of Cy7.5 and Cy7.5-PEG

3.4.2. Preparation and Characterization of Dissolving Polymeric MNs

While earlier studies utilized MNs composed of pure poly(*N*-vinylpyrrolidone) (M_w = 3,500 – 7,000 Da) (PVP K-12), this polymer was found to require long drying times (> 3 days) and was associated with fluorophore degradation.[16] Further, it was observed that MNs prepared from PVP K-12 alone were very hygroscopic and required delicate storage conditions to preserve their structure. To address this, MNs were prepared from a 1:1 mixture of PVP K-12 and poly(vinyl alcohol) (M_w = 10,000 Da) (PVA) — both injectable polymers commonly used for dissolving MNs[29-31] — using a solvent casting method in PDMS moulds.[32] The resulting MNs were found to dry within 24 – 48 hours under ambient conditions and produced sharp, uniform MNs, highlighting the suitability of the polymer blend. Under bright-field

microscopy, the MNs appeared as a 15 × 15 array of square pyramidal projections with average lengths of 479 ± 13 µm and widths of 248 ± 6 µm × 248 ± 6 µm at the base (**Figure 3.2. A**). While the base dimensions of the MNs were in agreement with those of the PDMS moulds (250 µm × 250 µm), the lengths were significantly shorter than the nominal lengths of the moulds (600 µm), likely due to water loss during the drying process, as has been previously described (**Figure 3.S2**).[33]

The solvent casting process outlined in previous work allowed a dye to be dispersed throughout the solid structure of the MNs, including the tips and the backing layer. However, when using the MNs for dermal delivery, only the tips dissolve and release their payload, meaning that any dye in the backing layer is wasted. More significantly, dye towards the base of the MN tips would primarily be delivered to the *stratum corneum* and would thus not be drained from the skin. To resolve this limitation, the solvent casting method was modified to allow dye to be incorporated only in the tips of the MNs, with the backing layer composed of dye-free polymer. This was accomplished by preparing two polymer matrix solutions (PMS), one with Cy7.5-PEG and one with no dye. The dye-containing PMS was used for the initial centrifugation steps, after which any excess PMS not localized in the tips of the moulds was removed. At this point, a backing layer of dye-free polymer was applied and the MNs were allowed to dry, yielding MNs with Cy7.5-PEG only in the tips. Under fluorescence stereomicroscopy, clear Cy7.5 fluorescence could be observed exclusively in the tips of the MNs, with no apparent diffusion into the backing layer (**Figure 3.2. B**). The dye-containing MNs were also examined using scanning electron microscopy (SEM), which revealed smooth, sharp MNs with tips diameters significantly below 10 µm (**Figure 3.2. C**).

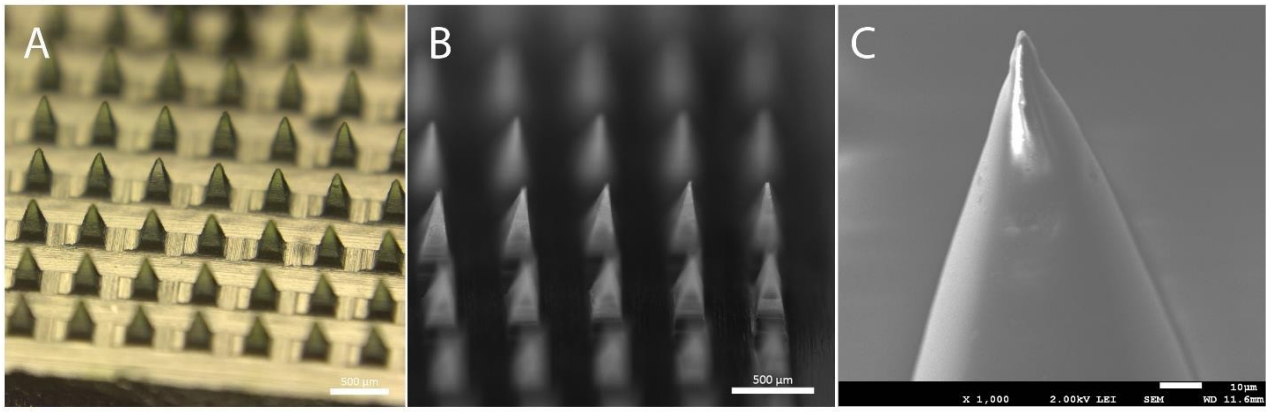

Figure 3.2. Structure of Cy7.5-PEG-containing polymeric MNs: A) Brightfield image of PVP/PVA (1:1) MNs with Cy7.5-PEG in the tips; B) Fluorescent image of Cy7.5-PEG localized within MN tips; C) SEM image of PVP/PVA MNs.

When developing dissolving polymeric MNs, it is essential to ensure that their mechanical strength is sufficient to pierce the skin without experiencing deformation or failure. Because of the relatively high concentration of PEGylated dye to be included in the MN matrix, it was necessary to

ensure that the strength of the MNs was preserved, even when large amounts of PEG were present. To do so, increasing concentrations of PEG-NH_2 (20 kDa) were incorporated into the MNs and the compression force required to induce structural failure was measured. Ultimately, no significant relationship was observed between failure force and the concentration of PEG-NH_2 (20 kDa), indicating that the concentrations of PEGylated dye used in our experiments should not negatively impact the mechanical properties of the MNs (**Figure 3.3. A**). Collectively, the MNs tested displayed an average failure force of 9.6 ± 1.8 N, well above the force required to penetrate human skin (between 0.1N and 3 N), indicating their suitability for use *in vivo*.[34] The MNs were examined under brightfield microscopy, where it was found that the most common mode of failure was 90° deflection without breakage of the MN tip (**Figure 3.S3**).

After confirming that the PVP/PVA MNs possessed the required mechanical strength to breach the skin, their ability to release PEGylated dye within the skin was investigated. To accomplish this, repeated applications of Cy7.5-PEG MNs to mouse skin were performed in order to determine optimal application time; the minimum time required for full release of the dye from the MN tips. After testing applications of 2, 5, and 10 minutes, it was found that there was no significant difference in the amount of dye delivered, suggesting that a 2 minute application was sufficient for full dissolution of the MN tips and delivery of the maximum possible amount of dye (**Figure 3.3. B**).

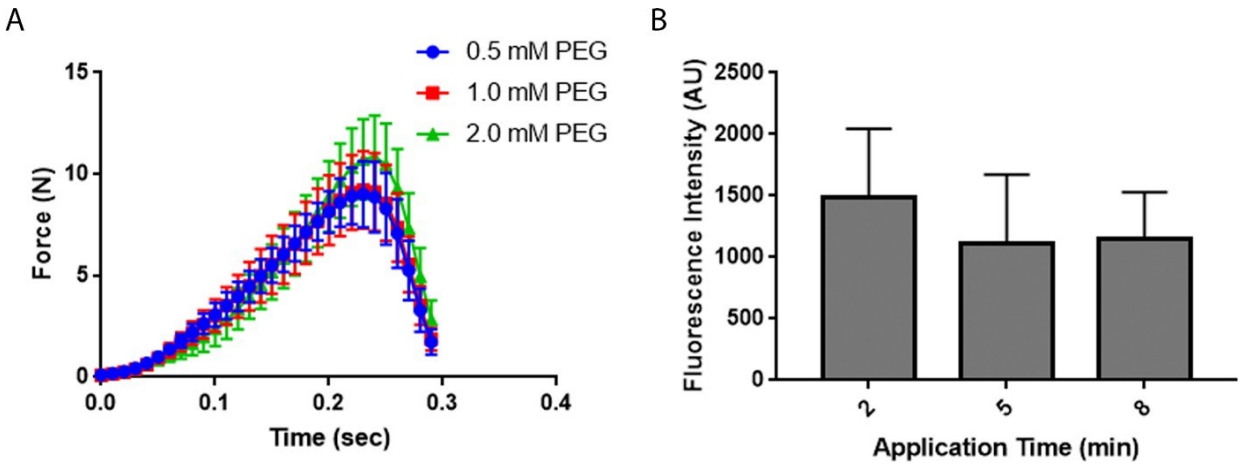

Figure 3.3. Characterization of mechanical and delivery properties of Cy7.5-PEG MNs: A) Mechanical properties of PVP/PVA (1:1) MNs with increasing concentrations of PEH-NH_2 (20 kDa). Mean ± SD (n = 4); B) Effect of application time on delivery of Cy7.5-PEG to mouse skin ex vivo, Mean ± SD (n = 3).

To further validate the use of Cy7.5-PEG as an alternative to ICG, MNs were prepared with high concentrations (720 μM) of either ICG or Cy7.5-PEG in the tips. After drying, the MN arrays were

examined under fluorescence stereomicroscopy and the fluorescence intensities of individual MNs from each array were compared, with Cy7.5-PEG MNs displaying an average increase in fluorescence of 33.4 ± 4.5% relative to their ICG-containing counterparts (**Figure 3.4. A**). This observed difference in fluorescence (despite the same concentration) could result from greater quenching within the ICG-containing MNs, or a higher quantum yield of Cy7.5-PEG. MNs of each type were also applied to mouse skin, to compare the intensities of the resulting tattoos (**Figure 3.S4**). In the skin, the average fluorescence intensity of a Cy7.5-PEG tattoo was found to be 126 ± 41% greater than the average signal of an ICG tattoo (**Figure 3.4. B**). This relatively greater increase in fluorescence could be explained by aggregation caused by the relatively poor solubility of ICG in the aqueous environment of the skin, relative to the hydrophilic Cy7.5-PEG. Overall, this serves to highlight the advantages of a highly water-soluble PEGylated probe relative to a less soluble alternative such as ICG.

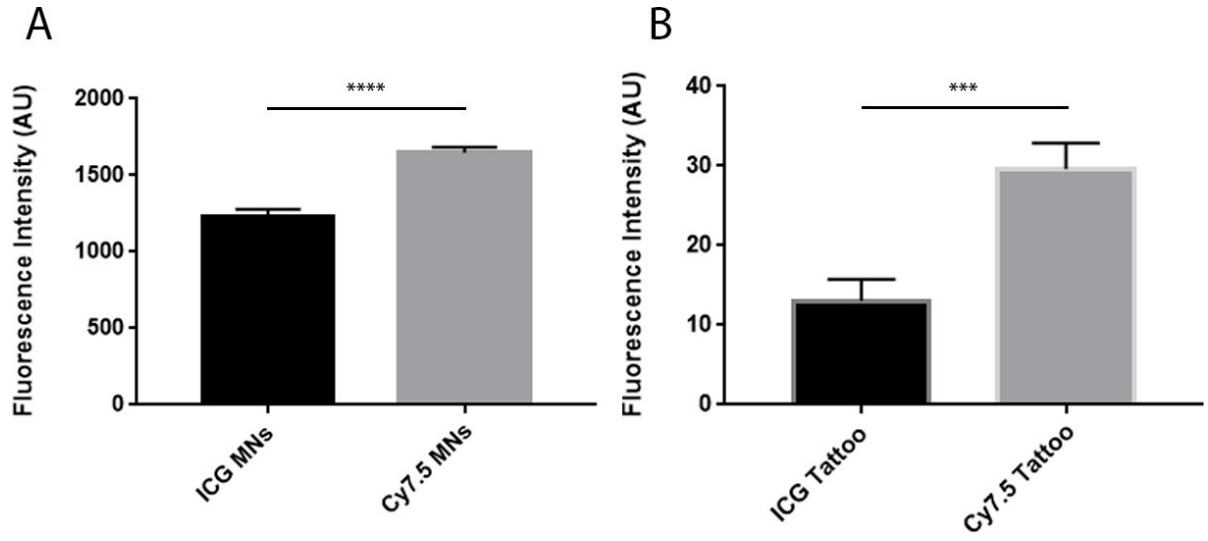

Figure 3.4. Fluorescence properties of dye-loaded MNs and their tattoos: A) Fluorescence intensity of MNs containing ICG or Cy7.5-PEG, Mean ± SD (n = 8), $p < 0.0001$; B) Fluorescence intensity of ICG or Cy7.5-PEG MN tattoos, Mean ± SD (n =4), $p \leq 0.0005$.

3.4.3. In vivo experiments in mice

Following *ex vivo* optimization of dye delivery, tests were performed *in vivo* to determine whether MN-delivered Cy7.5-PEG could successfully be used to monitor lymphatic drainage in mice. To do this, MNs were applied to the backs of shaved mice, and the resulting fluorescence signal was followed using an IVIS and a recently developed portable NIR fluorescence detector.[27] The signal was followed over 24 h (**Figure 3.5.A**), with a clear decrease in signal observed, following first-order decay kinetics, indicating that the dye was being drained from the application site. The signal initially displayed a steep decline, gradually leveling

off into a plateau between T = 6 h and T = 24 h at 40 ± 10% of the initial signal (IVIS) and 32 ± 11% of the initial signal (portable device).

To quantify this, the relative fluorescence of each MN tattoo was plotted as a function of time and the area under the curve (AUC) was measured for each run (**Figure 3.5. B**). This allowed comparison of the total amount of dye drained for each application, which could ultimately be used to quantitatively differentiate between normal lymphatic drainage, and impaired lymphatic drainage in the context of diseases of the lymphatic system. Comparison of the fluorescence measurements collected by the IVIS and the portable fluorescence detector revealed that there was no significant difference between the drainage measurement by either instrument ($p > 0.05$), validating the use of the portable detector for this application (**Figure 3.5. C**). This finding is notable, as portable monitoring of lymphatic drainage could have meaningful clinical implications, particularly given the expensive and bulky nature of other forms of NIR fluorescence monitoring.[27] However, when comparing the half-life ($t_{1/2}$) values (corresponding to the speed of drainage from the application site), a slight significant difference was observed, though this could be due to differences in instrument sensitivity (**Figure 3.5. D**).

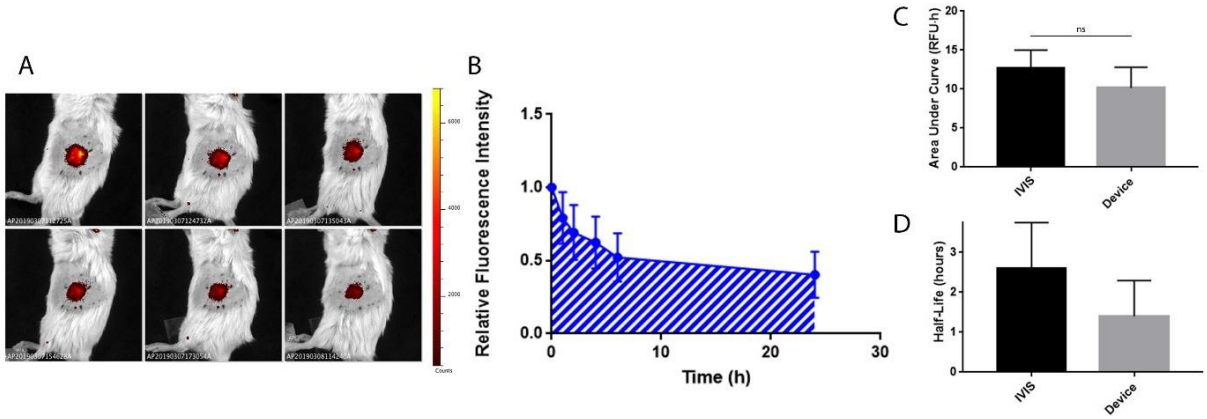

Figure 3.5. In vivo experiments in mice (IVIS vs portable device): A) IVIS fluorescence image of MN tattoo in mouse at t = 1, 2, 4, 6, 24 h; B) Example AUC plot of relative fluorescence intensity of Cy7.5-PEG in skin, measured using IVIS; C) Comparison between AUCs of measurements performed using IVIS and portable fluorescence detector; D) Comparison between half-life values of Cy7.5-PEG drainage using IVIS and portable fluorescence detector. Mean ± SD (n = 7).

3.4.4. In vivo experiments in rats

Following initial results in mice, further *in vivo* studies were conducted in rats, as their skin is known to be a much better model for human skin, owing to its similar thickness.[35] Specifically, the thickness of rat dorsal (back) skin was reported to be approximately 2 mm, comparable to or greater than many regions of the human body, including back, neck, and notably arm skin (a common location of lymphedema).[36] Cy7.5-PEG-containing MNs of the same geometry and concentration used in mice were applied to the backs of

shaved rats, and the resulting fluorescence signal was followed for 24 hours using an IVIS. To mimic conditions of impaired lymphatic drainage, MNs were also applied to the backs of shaved dead rats, as lymphedema models in rats are complex, and primarily affect the extremities, where reproducible MN application is impractical.[37,38] This should allow determination of the portion of signal loss caused by diffusion or degradation of the dye rather than drainage, and identify the discrimination potential of the MN tattoo. Similar to mice, an initial steep decrease in signal was observed in living rats, with a plateau occurring between T = 6 h and T = 24 h (**Figure 3.6. A**). However, this plateau occurred at a significantly higher fluorescence intensity than in mice, with 63 ± 8 % of the initial signal remaining after 24 hours, suggesting that less Cy7.5-PEG was drained from the application site. This could be due to the increased thickness of the non-viable epidermis (*stratum corneum*) in rats relative to mice, resulting in more dye remaining trapped in this non-drained region of the skin.[35] This was significantly different from the results observed in dead rats, where no drainage was observed, and the average T = 24 h fluorescence intensity corresponded to 85 ± 19 % of the initial signal (**Figure 3.6. A**). This is reasonable, as no lymphatic drainage was expected in dead rats, and the signal decrease observed was likely due to diffusion or degradation of the dye, also explaining the high variability. Upon comparison of the AUC values between living (15.71 ± 0.67 RFU·h) and dead rats (20.58 ± 1.94 RFU·h), a significant difference was o bserved ($p < 0.05$), suggesting that this MN tattoo is capable of discrimination between lymphatic drainage and simple degradation or diffusion of dye (**Figure 3.6. B**). This p-value, corresponding to the statistical difference between the change in fluorescence in the presence or absence of lymphatic drainage, reflects the discrimination potential of the MN tattoo, with lower values indicating a greater potential to discriminate between normal and impaired lymphatic drainage. Histological examination of rat skin after MN application revealed significant Cy7.5-PEG fluorescence present in the outer epidermis, with no signal visible deeper in the dermis (**Figure 3.6. C, D**). This further supports the notion that while dye delivered to the dermis or viable epidermis is readily drained through lymphatic vessels, any dye delivered to the outer epidermis remains trapped due to its size and hydrophilicity, resulting in the strong fluorescence after 24 hours.[39,40]

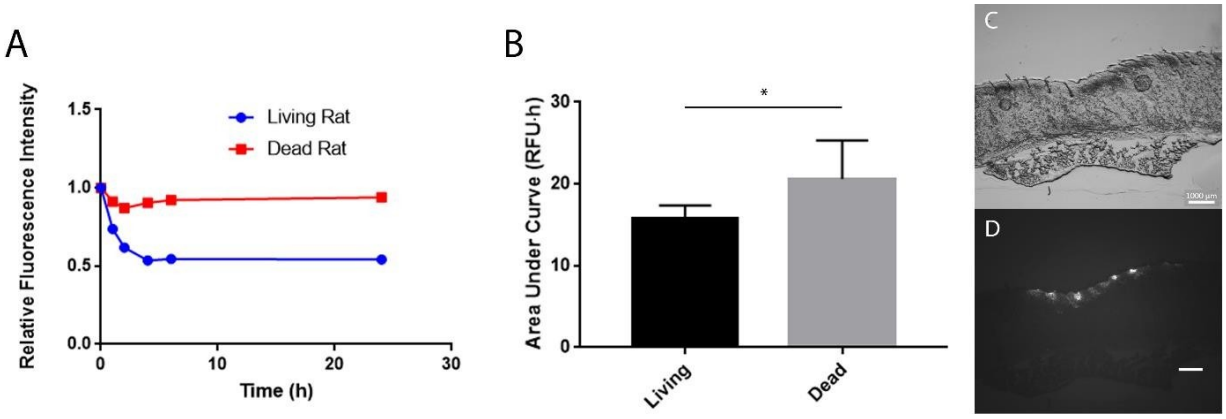

Figure 3.6. Preliminary in vivo MN applications in rats: A) Example of relative fluorescence decrease resulting from Cy7.5-PEG drainage in living and dead rats; B) Comparison between AUCs of Cy7.5-PEG drainage curves in living and dead rats; C) Brightfield microscopy image of histology of rat skin after Cy7.5-PEG MN application; D) Fluorescence microscopy image of histology of rat skin showing dye remaining trapped in outer epidermis. Mean ± SD (n = 6).

3.4.5. MN optimization for in vivo monitoring of lymphatic drainage

To address the issue of dye remaining trapped in the outer epidermis, and to improve the discrimination potential of the system, modifications were made to the MN preparation process, beginning with the solvent-casting method. By more specifically delivering the dye to the deeper, lymphatically drained tissue, the final fluorescence value is lowered, thereby improving the discrimination factor of the MN tattoo. After the initial centrifugation steps with the Cy7.5-PEG-containing PMS, a spatula was scraped along the base of the MN moulds to remove some of the dye-loaded polymer from the base of the MNs. This was followed by a centrifugation using dye-free polymer before addition of the backing layer, resulting in MNs with dye more localized towards the tip (**Figure 3.7. A**). Specifically, when prepared using the standard method, the average height of dye within the MNs was measured as 368 ± 18 µm, corresponding to 76.8% of the total length of the MNs (479 ± 13 µm). When prepared using the modified method, Cy7.5-PEG was found to be present up to an average height of 286 ± 19 µm, or 59.8% of the total MN length. Another modification to the process was made by using longer MNs prepared in moulds with a nominal height of 800 µm (actual MN height measured as 651 ± 27 µm). When MNs of this length were prepared using the modified casting process, the presence of dye was observed up to a height of 304 ± 11 µm, only 46.7% of the total MN length (**Figure 3.7. A**).

These modified MNs were also tested *in vivo* in rats, and the decrease in fluorescence was monitored by IVIS, as previously described. For the 600 µm (nominal) MNs prepared using the modified method, drainage appeared very similar to previous tests, with an initial decline followed by a slow plateau to 60.7 ± 6.9 % of initial fluorescence. For the 800 µm (nominal) MNs, however, initial drainage appeared

steeper, before gradually reaching an average T = 24 h fluorescence signal of 50.3 ± 6.7% of the initial signal, lower than previously observed (**Figure 3.7. B**). The MNs were also applied to dead rats, yielding results similar to previous tests (84.3 ± 9.2 % for 600 µm, 91 ± 22 % for 800 µm), with no drainage and mild diffusion of degradation of the fluorescence signal observed after 24 hours (**Figure 3.7. C**).

After application of both lengths of MN to living and dead rats, the AUCs were compared for each MN type, to quantitatively assess their performance. For the shorter MNs prepared with the modified method, AUCs were very similar to those previously observed, with 15.56 ± 0.56 RFU·h for living rats and 21.04 ± 0.924 RFU·h for dead rats, though the discrimination potential was greater ($p \leq 0.0005$) due to less signal variability between applications (**Figure 3.7. D**). For the longer MNs, the difference was more pronounced, with the average AUC in living rats measured as 13.71 ± 0.41 RFU·h, compared to 23 ± 2 RFU·h in dead rats (**Figure 3.7. E**). This discrimination potential ($p < 0.0001$) was much greater than any previously observed, and coupled with the overall greater drainage observed, suggests that longer MNs allow for meaningfully better monitoring of impaired lymphatic drainage and result in less dye trapped in the outer epidermis.

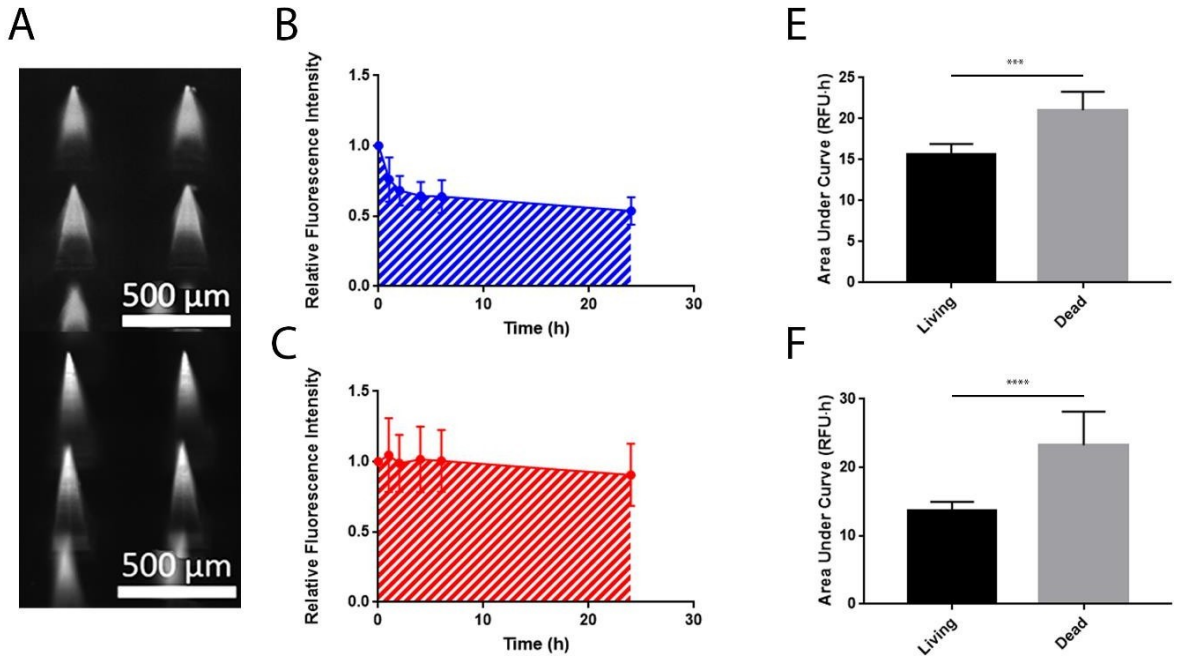

Figure 3.7. Optimization of MNs for in vivo tests: A) Fluorescence microscopy images of (top to bottom) 600 µm MNs prepared using the modified method, and 800 µm MNs prepared using the modified method; B) AUC plot of relative fluorescence decrease in living rat skin of Cy7.5-PEG delivered using longer MNs. Mean ± SD (n = 9); C) AUC plot of fluorescence in dead rat skin of Cy7.5-PEG delivered using longer MNs. Mean ± SD (n = 6); D) Comparison between AUCs of Cy7.5-PEG drainage curves in living and dead rats using shorter MNs. Mean ± SD (n = 6); F) Comparison between AUCs of Cy7.5-PEG drainage curves in living and dead rats using shorter MNs. Mean ± SD (n = 6).

3.5. Conclusions & Outlook

Lymphatic monitoring technology is a rapidly developing field, and the system developed in this study represents a step towards a viable MN-based method of lymphatic monitoring. It was found that by utilizing a PEGylated NIR dye such as Cy7.5-PEG, rather than ICG, it was possible to deliver a significantly brighter MN tattoo to the skin, while avoiding aggregation of dye. By optimizing the composition of the dissolving polymeric MNs, it was possible to create strong, uniform MNs compatible with the chosen NIR dye and able to dissolve readily in the skin to release the probe. Notably, the *in vivo* studies conducted in mice served to further validate the use of portable fluorescence detection technology, based on the comparable data obtained relative to standard IVIS measurements. This is significant, as portable measurement would constitute an important clinical advantage for NIR fluorescence imaging of lymphatic drainage, opening the door to at-home and point-of-care monitoring without the need for bulky and expensive detection equipment and trained personnel.

The results obtained in this study also revealed important considerations that should be taken into account for future studies using dissolving polymeric MNs. Most importantly, it was found that upon dissolution of the MNs, much of the dye is released into the outer epidermis or *stratum corneum*, where it cannot effectively be drained through the lymphatic system.[39,40] This has implications for diagnostic applications of dissolving polymeric MNs, as care should be taken to deliver as much dye or sensor as possible to lymphatically drained layers of the skin, to avoid background signal. This should also be a consideration for drug delivery studies, as larger therapeutic compounds could remain similarly trapped in the skin, decreasing the total dose delivered systemically. A potential solution to this could lie in the optimization of MN lengths, as it was observed that a greater portion of dye was drained when delivered using the longer 800 μm MNs, increasing the discrimination potential of the system. With this in mind, it will be important to evaluate and optimize MN length and delivery in human skin for the eventual clinical translation of this technology. Given the differences observed between mice and rats, it will be important to select a MN length that is ideal for delivery to lymphatically drained skin layers in humans.

3.6. Acknowledgements

The authors kindly acknowledge Zineb Benkhachan. S.B., and D.B. gratefully acknowledge financial support from the Faculty of Pharmacy at the Université de Montréal, Natural Sciences and Engineering Research Council of Canada, the Canada Foundation for Innovation, and the Canadian Generic Pharmaceutical Association and Biosimilars Canada.

3.7. References

1. Swartz, M.A. The physiology of the lymphatic system. *Adv. Drug Deliv. Rev.* **2001**, *50*, 3-20. doi:10.1016/S0169-409X(01)00150-8
2. Randolph, G.J.; Ivanov, S.; Zinselmeyer, B.H.; Scallan, J.P. The lymphatic system: Integral roles in immunity. *Annu. Rev. Immunol.* **2017**, *35*, 31-52. doi:10.1146/annurev-immunol-041015-055354
3. Grada, A.A.; Phillips, T.J. Lymphedema: pathophysiology and clinical manifestations. *J. Am. Acad. Dermatol.* **2017**, *77*, 1009-1020. doi:10.1016/j.jaad.2017.03.022
4. Rockson, S.G.; Rivera, K.K. Estimating the population burden of lymphedema. *Ann. N.Y. Acad. Sci.* **2008**, *1131*, 147-154. doi:10.1196/annals.1413.014
5. Clark, B.; Sitzia, J.; Harlow, W. Incidence and risk of arm oedema following treatment for breast cancer: a three-year follow-up study. *QJM*. **2005**, *98*, 343-348. doi:10.1093/qjmed/hci053
6. Hayes, S.C.; Janda, M.; Cornish, B.; Battistutta, D.; Newman, B. Lymphedema after breast cancer: incidence, risk factors, and effect on upper body function. *J. Clin. Oncol.* **2008**, *26*, 3536-3542. doi:10.1200/JCO.2007.14.4899
7. Shah, C.; Arthur, D.W.; Wazer, D.; Khan, A.; Ridner, S.; Vicini, F. The impact of early detection and intervention of breast cancer-related lymphedema: a systematic review. *Cancer Med.* **2016**, *5*, 1154-1162. doi:10.1002/cam4.691
8. Misselwitz, B.; Schmitt-Willich, H.; Michaelis, M.; Oellinger, J.J. Interstitial magnetic resonance lymphography using a polymeric T1 contrast agent. *Invest. Radiol.* **2002**, *37*, 146-151. doi:10.1097/00004424-200203000-00007
9. Mancuso, A.A.; Harnsberger H.R.; Muraki, A.S.; Stevens, M.H. Computed tomography of cervical and retropharyngeal lymph nodes: normal anatomy, variants of normal, and applications in staging head and neck cancer. *Radiology*. **1983**, *148*, 715-723. doi:10.1148/radiology.148.3.6878692
10. Szuba, A.; Shin, W.S.; Strauss, H.W.; Rockson, S. The third circulation: radionuclide lymphoscintigraphy in the evaluation of lymphedema. *J. Nucl. Med.* **2003**, *44*, 43-57.
11. Rasmussen, J.C.; Tan, I.-C.; Marshall, M.V.; Fife, C.E.; Sevick-Muraca, E.M. Lymphatic imaging in humans with near-infrared fluorescence. *Curr. Opin. Biotechnol.* **2009**, *20*, 74-82. doi:10.1016/j.copbio.2009.01.009
12. Mihara, M.; Hara, H.; Araki, J.; Kikuchi, K.; Narushima, M.; Yamamoto, T.; Iida, T.; Yoshimatsu, H.; Murai, N.; Mitsui, K.; Okitsu, T.; Koshima, I. Indocyanine green (ICG) lymphography is superior to lymphoscintigraphy for diagnostic imaging of early lymphedema of the upper limbs. *PLoS One*. **2012**, *7*, e38182. doi:10.1371/journal.pone.0038182

13. Unno, N.; Inuzuka, K.; Suzuki, M.; Yamamoto, N.; Sagara, D.; Nishiyama, M.; Konno, H. Preliminary experience with a novel fluorescence lymphography using indocyanine green in patients with secondary lymphedema. *J. Vasc. Surg.* **2007**, *45*, 1016-1021. doi:10.1016/j.jvs.2007.01.023
14. Sevick-Muraca, E.M.; Sharma, R.; Rasmussen, J.C.; Marshall, M.V.; Wendt, J.A.; Pham, H.Q.; Bonefas, E.; Houston, J.P.; Sampath, L.; Adams, K.E.; Blanchard, D.K.; Fisher, R.E.; Chiang, S.B.; Elledge, R.; Mawad, M.E. Imaging of lymph flow in breast cancer patients after microdose administration of a near-infrared fluorophore: feasibility study. *Radiology*. **2008**, *246*, 734-741. doi:10.1148/radiol.2463070962
15. Philip, R.; Penzkofer, A.; Bäumler, W.; Szeimes, R.M.; Abels, C. Absorption and spectroscopic investigation of indocyanine green. *J. Photochem. Photobiol. A Chem.* **1996**, *96*, 137-148. doi:10.1016/1010-6030(95)04292-x
16. Brambilla, D.; Proulx, S.T.; Marschalkova, P.; Detmar, M.; Leroux, J.-C. Microneedles for the noninvasive structural and functional assessment of dermal lymphatic vessels. *Small*. **2016**, *12*, 1053-1061. doi:10.1002/smll.201503093
17. Kaushik, S.; Hord, A.H.; Denson, D.D.; McAllister, D.V.; Smitra, S.; Allen, M.G.; Prausnitz, M.R. Lack of pain associated with microfabricated microneedles. *Anesth. Analg.* **2001**, *92*, 502-504. doi:10.1097/00000539-200102000-00041
18. Jeong, H.-R.; Lee, H.-S.; Choi, I.-J.; Park, J.-H. Considerations in the use of microneedles: pain, convenience, anxiety and safety. *J. Drug Target.* **2016**, *25*, 29-40. doi:10.1080/1061186x.2016.1200589
19. Babity, S.; Roohnikan, M.; Brambilla, D. Advances in the design of transdermal microneedles for diagnostic and monitoring applications. *Small*. **2018**, *14*, 1803186. doi:10.1002/smll.201803186
20. Cherrick, G.R.; Stein, S.W.; Leevy, C.M.; Davidson, C.S. Indocyanine green: observations on its physical properties, plasma decay, and hepatic extraction. *J. Clin. Invest.* **1959**, *39*, 592-600. doi:10.1172/JCI104072
21. Zhou, F.Z.; Chin, M.P.; Schafer, S.A. Aggregation and degradation of indocyanine green. In *Proc. SPIE 2128, Laser Surgery: Advanced Characterization, Therapeutics, and Systems IV*. Loas Angeles, CA, 7 September 1994. Anderson, R.R., Ed. doi:10.1117/12.184936
22. Saxena, V.; Sadoqi, M.; Shao, J. Degradation kinetics of indocyanine green in aqueous solution. *J. Pharm. Sci.* **2003**, *92*, 2090-2097. doi:10.1002/jps.10470
23. Proulx, S.T.; Luciani, P.; Christiansen, A.; Karaman, S.; Blum, K.S.; Rinderknecht, M.; Leroux, J.-C.; Detmar, M. Use of a PEG-conjugated bright near-infrared dye for functional imaging of

rerouting of tumour lymphatic drainage after sentinel lymph node metastasis. *Biomaterials*. **2013**, *34*, 5128-5137. doi:10.1016/j.biomaterials.2013.03.034

24. Kaminskas, L.M.; Ascher, D.B.; McLeod, V.M.; Herold, M.J.; Le, C.P.; Sloan, E.K.; Porter, C.J. PEGylation of interferon α2 improves lymphatic exposure after subcutaneous and intravenous administration and improves antitumour efficacy against lymphatic breast cancer metastases. *J. Control. Release.* **2013**, *168*, 200-208. doi:10.1016/j.jconrel.2013.03.006
25. Trevaskis, N.L.; Kaminskas, L.M.; Porter, C.J. From sewer to savior – targeting the lymphatic system to promote drug exposure and activity. *Nat. Rev. Drug Discov.* **2015**, *14*, 781-803. doi:10.1038/nrd4608
26. Chan, L.J.; Ascher, D.B.; Yadav, R.; Bulitta, J.B.; Williams, C.C.; Porter, C.J.; Landersdorfer, C.B.; Kaminskas, L.M. Conjugation of a 10 kDa linear PEG onto trastuzumab Fab' is sufficient to significantly enhance lymphatic exposure while preserving in vitro biological activity. *Mol. Pharm.* **2016**, *13*, 1229-1241. doi:10.1021/acs.molpharmaceut.5b00749
27. Polomska, A.K.; Proulx, S.T.; Brambilla, D.; Fehr, D.; Bonmarin, M.; Brändli, S.; Meboldt, M.; Steuer, C.; Vasileva, T.; Reinke, N.; Leroux, J.-C.; Detmar, M. Minimally invasive method for the point-of-care quantification of lymphatic vessel function. *JCI Insight*. **2019**, *4*, 126515. doi:10.1172/jci.insight.126515
28. Larrañeta, E.; Lutton, R.E.M.; Brady, A.J.; Vicente-Pérez, E.M.; Woolfson, A.D.; Thakur, R.R.S.; Donnelly, R.F. Microwave-assisted preparation of hydrogel-forming microneedle arrays for transdermal drug delivery applications. *Macromol. Mater. Eng.* **2015**, *300*, 586-595. doi:10.1002/mame.201500016
29. Chu, L.Y.; Prausnitz, M.R. Separable arrowhead microneedles. *J. Control. Release.* **2011**, *149*, 242-249. doi:10.1016/j.jconrel.2010.10.033
30. Lee, I.-C.; He, J.-S.; Tsai, M.-T.; Lin, K.-C. Fabrication of a novel partially dissolving polymer microneedle patch for transdermal drug delivery. *J. Mater. Chem. B.* **2015**, *3*, 276-285. doi:10.1039/C4TB01555J
31. Wang, M.; Hu, L.; Xu, C. Recent advances in the design of polymeric microneedles for transdermal drug delivery and biosensing. *Lab Chip.* **2017**, *17*, 1373-1387. doi:10.1039/C7LC00016B
32. Indermun, S.; Luttge, R.; Choonara, Y.E.; Kumar, P.; du Toit, L.C.; Modi, G.; Pillay, V. Current advances in the fabrication of microneedles for transdermal delivery. *J. Control. Release.* **2014**, *185*, 130-138. doi:10.1016/j.jconrel.2014.04.052
33. Yang, S.; Feng, Y.; Zhang, L.; Chen, N.; Yuan, W.; Jin, T. A scalable fabrication process of polymer microneedles. *Int. J. Nanomed.* **2012**, *7*, 1415-1422. doi:10.2147/IJN.S28511

34. Davis, S.P.; Landis, B.J.; Adams, Z.H.; Allen, M.G.; Prausnitz, M.R. Insertion of microneedles into skin: measurement and prediction of insertion force and needle fracture force. *J. Biomech.* **2004**, *37*, 1155-1163. doi:10.1016/j.jbiomech.2003.12.010
35. Monteiro-Riviere, N.A.; Bristol, D.G.; Manning, T.O.; Rogers, R.A.; Riviere, J.E. Interspecies and interregional analysis of the comparative histologic thickness and laser Doppler blood flow measurements at five cutaneous sites in nice species. *J. Invest. Dermatol.* **1990**, *95*, 582-586. doi:10.1111/1523-1747.ep12505567
36. Lee, Y.; Hwang, K. Skin thickness of Korean adults. *Surg. Radiol. Anat.* **2002**, *24*, 183-189. doi:10.1007/s00276-002-0034-5
37. Wang, G.Y.; Zhong, S.Z. A model of experimental lymphedema in rats' limbs. *Microsurgery.* **1985**, *6*, 204-210. doi:10.1002/micr.1920060404
38. Serizawa, F.; Ito, K.; Matsubara, M.; Sato, A.; Shimokawa, H.; Satomi, S. Extracorporeal shock wave therapy induces therapeutic lymphangiogenesis in a rat model of secondary lymphoedema. *Eur. J. Vasc. Endovasc. Surg.* **2011**, *42*, 254-260. doi:10.1016/j.ejvs.2011.02.029
39. Bos, J.D.; Meinardi, M.M. The 500 Dalton rule for the skin penetration of chemical compounds and drugs. *Exp. Dermatol.* **2000**, *9*, 165-169. doi:10.1034/j.1600-0625.2000.009003165.x
40. Palmer, B.C.; DeLousie, L.A. Nanoparticle-enabled transdermal drug delivery systems for enhanced dose control and tissue targeting. *Molecules.* **2016**, *21*, 1719-1735. doi:10.3390/molecules21121719

3.7. Supporting Information

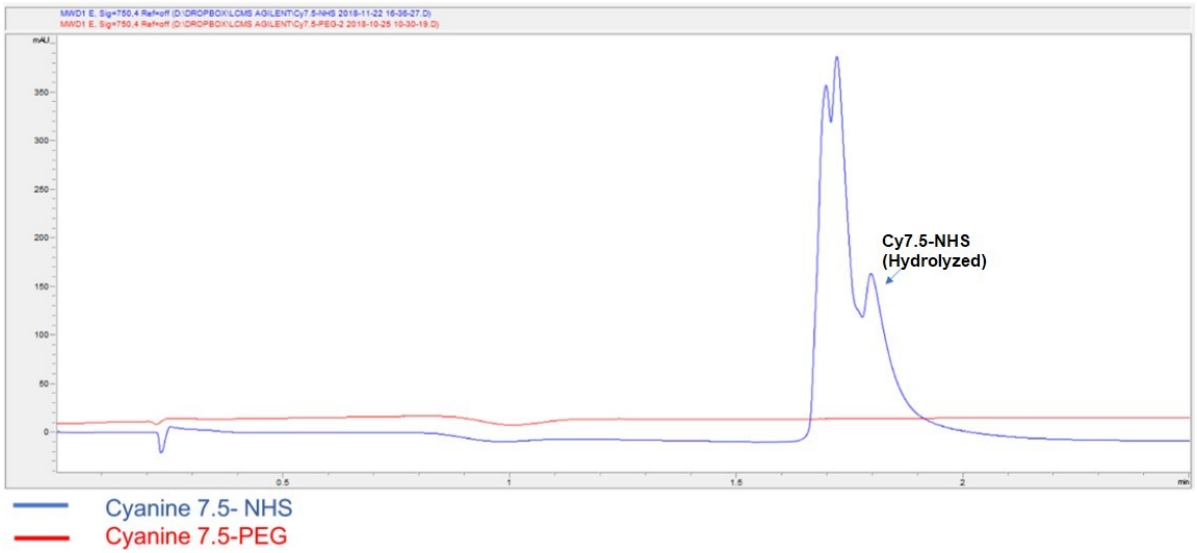

Figure 3.S1: LC-MS Chromatogram highlighting the absence of free Cy7.5-NHS after purification of Cy7.5-PEG.

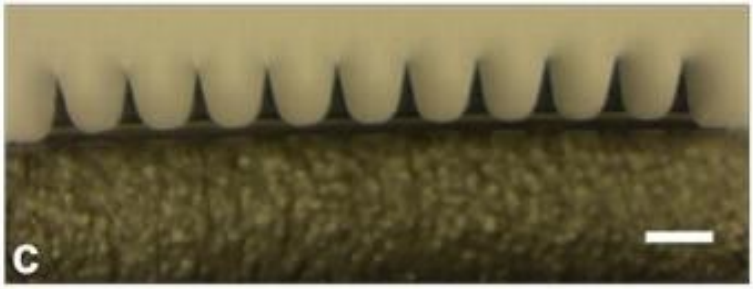

Figure 3.S2: MNs are straight and of a uniform length, shrinking during the drying process. Scale bar = 500 µm

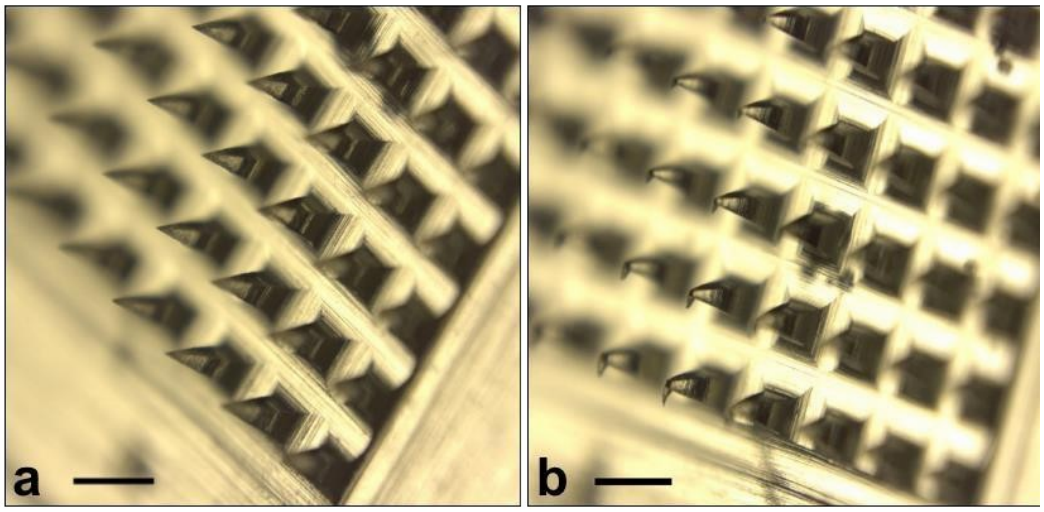

Figure 3.S3: a) PVP/PVA (1:1) MNs before mechanical properties test; b) Same MNs after deflection when testing mechanical properties, highlighting mode of failure (90 ° deflection without breakage). Scale bar = 500 μm

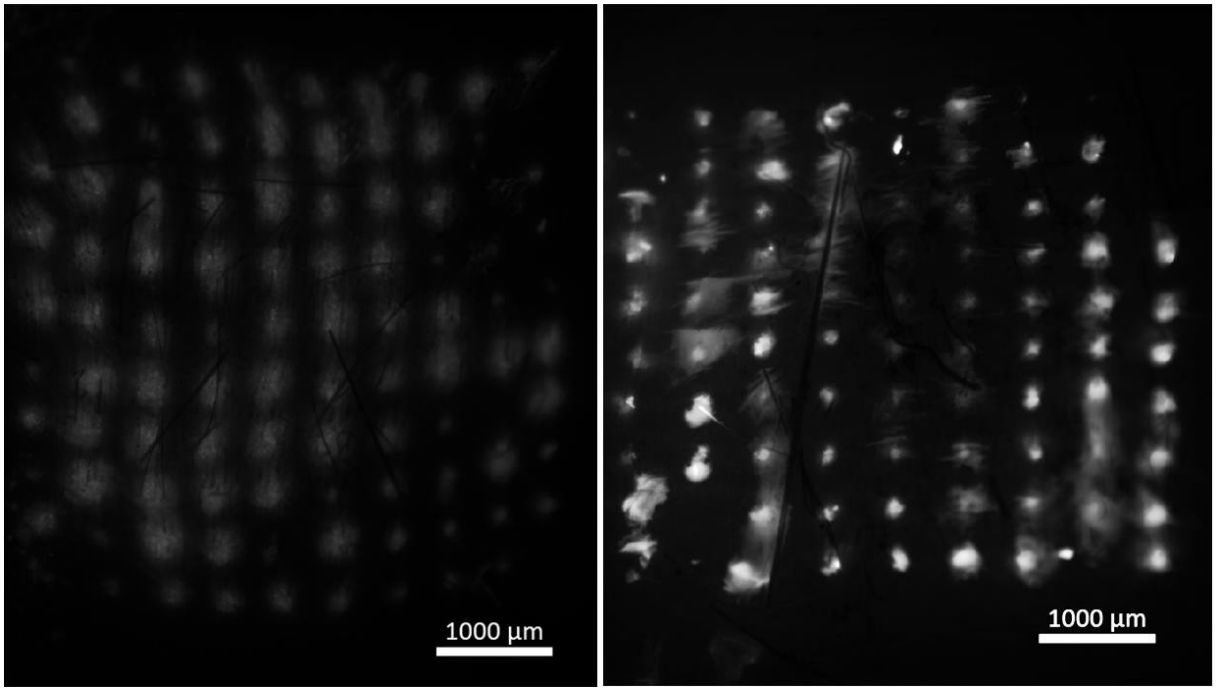

Figure 3.S4: A) PVP/PVA (1:1) MN tattoo of ICG in rat skin; b) PVP/PVA (1:1) MN tattoo of Cy7.5-PEG in rat skin.

General Discussion

Taken together, these works serve to demonstrate the potential of dissolving polymeric microneedles as a means to deliver sensors and diagnostic agents to the skin for real-time *in situ* monitoring, while also highlighting the inherent limitations of such a newly developed technology. This section serves to address these limitations, as well as any topics not fully explored in the preceding articles. Overall, the optimization of sensors compatible with incorporation into polymeric MNs, as well as the specifics of their delivery *in vivo*, are topics that merit further investigation.

4.1 MNs for the delivery of H-Cy5-PEG

Among the principal challenges associated with incorporation of H-Cy5-PEG into polymeric MNs, and its subsequent delivery into the skin, is the tendency of the dye by factors other than the intended ROS. While hydrocyanines have been reported as having increased stability relative to earlier classes of ROS sensors, it was observed that they remain susceptible to oxidation by atmospheric O_2 and light, especially when stored at high concentration in aqueous solution.[1] While efforts were taken to limit this during MN preparation, such as storing polymer solutions away from light as much as possible and limiting exposure of the solutions to air, the high concentrations of H-Cy5-PEG used during MN preparation (250 μM) resulted in a degree of oxidation of the sensor in the dried MNs. This was likely a contributing factor to the significantly reduced sensitivity of the final MN tattoo relative to H-Cy5-PEG in solution.

Another limiting factor is the relatively low amount of dye able to be delivered through the MNs, owing to their small volume and the solubility of H-Cy5-PEG in polymer solution. The low amount of dye delivered by the MNs was likely a contributing factor in the relatively weak signal observed using the fluorescence stereomicroscope. It was observed that the brightness of re-oxidized H-Cy5-PEG was significantly lower than an equivalent concentration of Cy5-PEG, indicating that even under ideal circumstances, not all of the H-Cy5-PEG is effectively converted into the fluorescent Cy5-PEG form by ROS. In fact, a solution of re-oxidized H-Cy5-PEG was observed to display around 10 % of the fluorescence of a solution of an equivalent concentration of Cy5-PEG.[1] This means that in MNs containing 250 μM of H-Cy5-PEG, the effective concentration of dye that can be converted into fluorescent Cy5-PEG was approximately 2.5 μM. Because of the relatively high molecular weight of the PEGylated dye (> 5,000 Da), concentrations above 250 μM displayed limited solubility in the polymer solutions used to prepare the MNs, thereby limiting the amount of dye able to be delivered. This posed a particular problem when tests were conducted *ex vivo* in excised porcine skin. Even following the addition of Fenton's reagent, the signal from the MN tattoo in skin was too weak to give a quantifiable signal on the fluorescence stereomicroscope. This

serves to highlight the likely need for further optimization of the ROS sensor to perform tests in actual models of skin.

4.2 MNs for the delivery of Cy7.5-PEG

When delivering the NIR sensor for the monitoring of lymphatic drainage, visibility of the dye proved less problematic, as Cy7.5-PEG was delivered in its oxidized form. Additionally, due to the less significant fluorescence background of skin at NIR wavelengths, greater contrast was observed using the fluorescence stereomicroscope.[2]

The main limitation in this study was the observation that a significant portion of dye remains trapped in the outer epidermis, not drained by the lymphatic system, resulting in the plateaus of fluorescence signal observed in this study. While this was partially mitigated by optimization of the MN length and structure, it highlights that unless dye were specifically localized to the very tip of the MNs, dissolving polymeric MNs will release their loaded sensor at a gradient in the skin, from the outer epidermis into the dermis.

This demonstrates the need for further studies, particularly concerning the depth of penetration of the MNs into the skin, to better discern where sensors should be placed within the MN for optimal delivery to a desired depth. Such a study would also be of value for future drug delivery studies using dissolving polymeric MNs (particularly for high molecular weight compounds), as any drug remaining trapped in the outer epidermis would be incapable of reaching its target.

Conclusions & Outlook

Overall, dissolving polymeric MNs appear to present a viable avenue for real-time *in situ* monitoring of physiological data, provided that the technology continues to be developed. Interest in the diagnostic applications of MNs appears to be strong, and many groups are currently investigating new MN-based diagnostic devices.[3-5] This is particularly true of polymeric MNs, with many examples seen within the past 5 years — either for sampling or delivery — likely due to their simple and inexpensive manufacturing process.[6,7] In particular, the use of dissolving polymeric MNs for the delivery of diagnostic agents seems to hold much untapped potential, with current examples seemingly limited to simple devices for antigen delivery (*e.g.* allergy testing) and the delivery of inert lymphatic tracers.[2,8,9] Ultimately, as evidenced by the technologies described in this thesis, this could be expanded to allow access to a far greater variety of health-related information in a non-invasive manner.

The delivery of H-Cy5-PEG for the detection of dermal ROS, while showing initial promise, was ultimately limited by the low brightness and amount of dye delivered, and limitations of the available detection equipment. Nonetheless, the results observed in agarose gels clearly indicate that the activity of the sensor is preserved after incorporation into the dissolving polymeric MNs and delivery to the gel. In this sense, the work serves as a valuable proof-of-concept for the delivery of functional sensors through similar dissolving MN systems. By selecting a brighter sensor that could be potentially delivered at a higher concentration, the concept of a functional MN tattoo could prove much more viable.

Further, studying the delivery of Cy7.5-PEG for monitoring the lymphatic system has provided a great deal of valuable information on lymphatic drainage as well as MN-assisted delivery to the skin. The MN tattoo itself demonstrated high discrimination potential between animals displaying lymphatic drainage and those in which no drainage occurred, suggesting its diagnostic potential for lymphedema. Perhaps of equal note were the findings on the MN-based delivery of the PEGylated fluorescent tracer. When a similar PEGylated dye was previously delivered through intradermal injection (at a uniform depth), it was observed to diffuse freely through the dermis.[10] However, when Cy7.5-PEG was delivered using the dissolving MNs, the dye delivered to deeper portions of the skin was drained through the lymphatic vessels, while dye delivered to the upper regions of the skin (particularly the *stratum cornuem*) was not drained. This finding highlights the importance of fine-tuning the depth of delivery when developing a MN tattoo, and surely merits further investigation, both in the context of diagnostics and drug delivery.

5.1 References

1. Kundu, K.; Knight, S.F.; Willett, N.; Lee, S.; Taylor, W.R.; Murthy, N. Hydrocyanines: a class of fluorescent sensors that can image reactive oxygen species in cell culture, tissue, and in vivo. *Angew Chem. Int. Ed. Engl.* **2009**, *48*, 299-303. doi:10.1002/anie.200804851
2. Brambilla, D.; Proulx, S.T.; Marschalkova, P.; Detmar, M.; Leroux, J.-C. Microneedles for the noninvasive structural and functional assessment of dermal lymphatic vessels. *Small*. **2016**, *12*, 1053-1061. doi:10.1002/smll.201503093
3. Samant, P.P.; Prausnitz, M.R. Mechanisms of sampling interstitial fluid from skin using a microneedle patch. *Proc. Natl. Acad. Sci. U. S. A.* **2018**, *115*, 4583-4588. doi:10.1073/pnas.1716772115
4. Pei, W.; Zhang, H.; Wang, Y.; Guo, X.; Xing, X.; Huang, Y.; Xie, Y.; Yang, X.; Chen, H. Skin-potential variation insensitive dry electrodes for ECG recording. *IEEE Trans. Biomed. Eng.* **2017**, *64*, 463-470. doi:10.1109/TBME.2016.2562702
5. Ranamukhaarachchi, S.A.; Padeste, C.; Häfeli, U.O.; Stoeber, B.; Cadarso, V.J. Design considerations of a hollow microneedle-optofluidic biosensing platform incorporating enzyme-linked assays. *J. Micromech. Microeng.* **2018**, *28*. doi:10.1088/1361-6439/aa9c9c
6. Chang, H.; Zheng, M.; Yu, X.; Than, A.; Seeni, R.Z.; Kang, R.; Tian, J.; Khanh, D.P.; Liu, L.; Chen, P.; Xu, C. A swellable microneedle patch to rapidly extract skin interstitial fluid for timely metabolic analysis. *Adv. Mater.* **2017**, *29*. doi:10.1002/adma.201702243
7. Yu, J.; Zhang, Y.; Ye, Y.; DiSanto, R.; Sun, W.; Ranson, D.; Ligler, F.S.; Buse, J.B.; Gu, Z. Microneedle-array patches loaded with hypoxia-sensitive vesicles provide fast glucose-responsive insulin delivery. *Proc. Natl. Acad. Sci. U. S. A.* **2015**, *112*, 8260-8265. doi:10.1073/pnas.1505405112
8. Bollinger, A.; Amann-Vesti, B.R. Fluorescence microlymphography: diagnostic potential in lymphedema and basis for the measurement of lymphatic pressure and flow velocity. *Lymphology* **2007**, *40*, 52-62.
9. Sun, W.; Araci, Z.; Inayathullah, M.; Manickam, S.; Zhang, X.; Bruce, M.A.; Marinkovich, M.P.; Lane, A.T. Milla, C.; Rajadas, J.; Butte, M.J. Polyvinylpyrrolidone microneedles enable delivery of intact proteins for diagnostic and therapeutic applications. *Acta Biomater.* **2013**, *9*, 7767-7774. doi:10.1016/j.actbio.2013.04.045
10. Proulx, S.T.; Luciani, P.; Christiansen, A.; Karaman, S.; Blum, K.S.; Rinderknecht, M.; Leroux, J.-C.; Detmar, M. Use of a PEG-conjugated bright near-infrared dye for functional imaging of rerouting of tumour lymphatic drainage after sentinel lymph node metastasis. *Biomaterials*. **2013**, *34*, 5128-5137. doi:10.1016/j.biomaterials.2013.03.034